

Design and development of a downstream separation process for ethylene recovery within the e-Refinery framework

Casper Snoeks



Design and development of a downstream separation process for ethylene recovery within the e-Refinery framework

by

Casper Snoeks

to obtain the degree of Master of Science
at the Delft University of Technology,
to be defended publicly on Monday March 1, 2021 at 11:00 AM.

Student number:	4385098	
Project duration:	April, 2020 – March, 2021	
Thesis committee:	Prof. ir. A. E. M. Huesman,	TU Delft
	Dr. H. B. Eral,	TU Delft, supervisor
	Dr. R. Kortlever,	TU Delft
	Dr. T. E. Burdyny,	TU Delft

An electronic version of this thesis is available at <http://repository.tudelft.nl/>.

Abstract

Electroreduction of CO₂ into high-valued chemicals is a promising way to reduce CO₂ emissions while simultaneously producing bulk chemicals currently produced from fossil-fuel feedstocks. The downside of this process is that conversion rates are low, meaning the resulting product stream is a complex gas mixture consisting primarily of reactants and by-products and a relatively small amount of product. This study focuses on the development of a new downstream separation process to capture ethylene from a mock-up reaction mixture (mole fractions C₂H₄/CO₂/CO/H₂/H₂O : 20/55/15/15/5), based on low driving forces and suitable for application in a 100kW test case within the e-Refinery. An extensive literature study of numerous separation techniques for gases was conducted and adsorption was chosen as the most suitable option. After screening of various adsorbents, active carbon was selected as the most potential sorbent. Based on a selectivity analysis, the primary focus was on the behaviour of C₂H₄/CO₂ on active carbon. Using a simple, custom-build set-up, transient breakthrough experiments were performed for this gas mixture and the resulting selectivity for an equivolume feed, yielded a lower separation performance than expected based on the ideal adsorption solution theory, respectively a selectivity of 1.5–1.7 versus 3.2–3.5. Additionally a theoretical model was developed using MATLAB, which described the velocity profile inside the adsorber column and could qualitatively predict breakthrough behaviour. Further analysis led to the conclusion that for a more accurate quantitative match between experimental and numerical results, isotherm parameters should be obtained from the same type of active carbon. Ultimately this technique could be used to increase the ethylene content in a CO₂-bearing stream and pave the way for a new, energy-efficient method to obtain hydrocarbons, ethylene in this case, from an electrolyzer cell.

Keywords: Adsorption, ethylene capture, breakthrough times, activated carbon, separation technology, e-Refinery, numerical model, velocity variation

Acknowledgements

Over the past months I have had the honour to be a part of the e-Refinery initiative and help in their efforts to work towards a carbon circular and energy neutral world. Within this project I had the honourable and ambitious task to initiate a new separation process that can ultimately be implemented to recover fuels and chemical building blocks from electrochemicals cells.

The first person I would like to be grateful to is Burak Eral to take me into his group and to assist me during my thesis. At the time of my thesis the Covid-19 pandemic raged in the world and therefore physical contact was not possible for the majority of the project duration. Instead Burak and I spoke extensively via videochat in which he was always encouraging and motivating me. Secondly I would like to thank Ruud Kortlever, Tom Burdyny and Monique van der Veen for their advice, guidance and knowledge to obtain the best result possible. Thirdly I would like to thank Johan Padding to have the time to discuss my model and give valuable input and advice which ultimately led to a satisfactory result. And finally I would like to thank Ruud, Tom and Adrie Huesman to be part of my defence committee.

This project was however not possible without the help of technician Michel van den Brink, I would like to thank him personally for the time he spend helping me with me set up and answering my question. Further I would like to thank Parsa Habibi and especially Fred Marques Penha to have me in their office and keep me company during coffee breaks and during lunch. Further I would like to thank everybody else in the P&E group who keep the group running and make sure everybody feels welcome.

What is sincerely liked in this project was the freedom Burak gave me to develop the project in the way I thought was the best option. I think this is what makes this project different compared to other theses and from which I learned a lot. This makes you consider every decision you make, which I expected is a skill that very valuable in later stages in life. Also the combination of experimental and numerical work, supplemented with an extensive literature study made this project very all-round and from which I gained a lot of new knowledge.

Of course doing a significant portion of work from home meant I had to work more than ever side-to-side with my roommates, Joris, Michiel, Guido and Victor. Our fruitful discussions on paper and on the refrigerator door, helped me make this a successful project. And finally I would like to thank my girlfriend, Christa and my family, Elly and Wim and Koen to always stand by side and support me during this project.

This report is something I am genuinely proud of and I hope the people who read it find it joyful as well as enlightening.

*Casper Snoeks
Rotterdam, February 2021*

Contents

Abstract	iii
Acknowledgements	v
Nomenclature	xi
List of Figures	xii
List of Tables	xiii
1 Introduction	1
1.1 CO ₂ reduction in the world	1
1.2 Carbon cycle and e-Refinery	1
1.3 Industrial Separations	2
1.4 Alternative Production Route	2
1.5 Goals and research question	2
2 Literature research and theory	4
2.1 Introduction & Physical properties	4
2.2 Selection criteria	5
2.3 Absorption	5
2.3.1 Physical absorption	5
2.3.2 Chemical absorption	5
2.3.3 Ionic liquids	6
2.3.4 Conclusion on absorption based technologies	7
2.4 Cryogenic separation techniques	7
2.4.1 Cryogenic Distillation	8
2.4.2 Stirling coolers	8
2.4.3 Cryogenic Packed Bed	8
2.4.4 Controlled Freeze Zone	9
2.4.5 Alternative cryogenic methods	9
2.4.6 Conclusion on cryogenic separation methods	10
2.5 Adsorption	10
2.5.1 Finding an ethylene selective handle	11
2.5.2 Comparison to the fruit industry	12
2.5.3 Effect of activated carbon on other species	12
2.5.4 Effect of π -complexation and examples	12
2.5.5 Conclusion on adsorbent technologies	13
2.6 Membrane Technology	14
2.6.1 Polymeric Membranes	15
2.6.2 Inorganic membranes	15
2.6.3 Facilitated transport membranes	15
2.6.4 Pilot scale OCM processes	15
2.6.5 Olefin/paraffin separations	16
2.6.6 Metal-organic framework membranes	16
2.6.7 Conclusion on membranes	16
2.7 Other technologies	17
2.7.1 Reactive separation	17
2.7.2 High temperature looping	17
2.7.3 Hybrid technologies	18

2.8	Selection process	18
2.8.1	Selection criteria	18
2.8.2	TRL explanation	18
2.8.3	TRL Table	19
2.9	Result	20
3	Adsorption Theory, Screening and Selection	21
3.1	Fundamentals of adsorber design	21
3.2	Adsorbent Screening	21
3.2.1	General Adsorbents	22
3.2.2	Zeolites	22
3.2.3	Metal Organic Frameworks	23
3.2.4	Overview of screened sorbent materials	23
3.2.5	Uninvestigated Options	25
3.3	Adsorbent Selection	25
3.4	Adsorption Equilibria	25
3.4.1	Classification of Isotherms	25
3.4.2	Isotherm Models	26
3.4.3	Error analysis	28
3.4.4	Model selecting criteria	28
3.5	Isotherm data and parameter estimation	29
3.5.1	Activated carbon isotherm data	29
3.5.2	Results of data fitting and parameter estimation	29
3.6	Selectivity analysis	29
3.6.1	Ideal Adsorbed Solution Theory (IAST)	29
3.6.2	Binary selectivities	31
3.6.3	Limitations and extensions to IAST	31
3.6.4	Effect of water vapour on AC	32
3.7	Kinetics	33
3.7.1	Governing kinetics of gases in activated carbon	33
3.7.2	Modelling of kinetics	33
3.8	Pressure Drop/Fixed bed dynamics	34
3.9	Application review and Process design	34
4	Experimental Procedure	35
4.1	Introduction	35
4.2	Adsorber bed design	35
4.2.1	Geometrics of the column	35
4.2.2	Adsorbent properties	35
4.2.3	Other factors	36
4.3	Chemicals	36
4.4	Experimental set-up	37
4.4.1	Framework	37
4.4.2	Column	37
4.4.3	Loading of the column	37
4.4.4	Fraction collection	37
4.4.5	Micro Gas Chromatograph	37
4.4.6	Limitations of set up	38
4.5	Column heating	39
4.6	Numerical analysis of breakthrough times	39
4.6.1	Mass balance	39
4.6.2	Accuracy of numerical analysis	41
5	Experimental Results	43
5.1	Unary breakthrough analysis	43
5.2	Error analysis of the system	44
5.2.1	Types of errors	44
5.2.2	Propagation of error and calculation	46

5.3	Binary breakthrough experiments	46
5.3.1	Experimental results	46
5.3.2	Comparison to IAST methodology	47
5.3.3	Effect of temperature variation	49
5.3.4	Conclusion on binary breakthrough experiments	49
5.4	Desorption experiments	49
5.5	Summarising the experimental results	50
6	Modelling and Simulation Results	52
6.1	Introduction	52
6.2	Assumptions	53
6.3	Model equations	53
6.3.1	Axial dispersion model	53
6.3.2	Mass transfer coefficient	54
6.3.3	Boundary Conditions	55
6.4	Solving method	55
6.5	Discretisation	55
6.6	Model validation	56
6.7	Transient breakthrough simulations	56
6.7.1	System parameters	56
6.7.2	Simulation Results	58
6.7.3	Effect of variable velocity on breakthrough behaviour	58
6.7.4	Velocity behaviour inside the fixed bed	60
6.7.5	Model and isotherms parameters	60
6.7.6	Conclusion on the theoretical model	62
7	Conclusions and Recommendations	64
7.1	Conclusions	64
7.2	Recommendations and Outlook	65
A	Active Carbon Isotherm Data	74
A.1	Hwang et al CO ₂ /CO	74
A.2	Reich et al C ₂ H ₄ /CO ₂	75
A.3	Osterkamp C ₂ H ₄ /CO ₂	76
A.4	Choi et al C ₂ H ₄ /H ₂	77
A.5	Grande et al CO ₂ /CO/H ₂	78
A.6	Lopes et al CO ₂ /CO/H ₂	79
A.7	Park et al CO ₂ /CO/N ₂ /H ₂	81
A.8	Al-Janabi et al CO ₂ /N ₂	81
B	System error analysis of microGC	84
B.1	Procedure	84
B.2	Results	84
C	Experimental Set-up	85

Nomenclature

Acronyms

AC	Active Carbon
IAST	Ideal Adsorbed Solution Theory
LDF	Linear Driving Force
micro GC	micro Gas chromatograph
MoL	Method of Lines
MTZ	Mass Transfer Zone
PDE	Partial Differential Equation
RAST	Real Adsorbed Solution Theory

Dimensionless Relations

Fo	Fourier number
Re	Reynolds number
Sc	Schmidt number

Greek Symbols

π	Spreading pressure	N m^{-1}
Ψ	Adsorption Potential	mol kg^{-1}
ψ	Particle shape factor	—
ρ_g	Density of the gas in bulk phase	kg m^{-3}
τ_p	tortuosity	—
ε_b	porosity of the packed bed	—
ε_p	porosity of the adsorbent particle	—
ζ_i	Diffusion volume of specie i	$\text{cm}^3 \text{mol}^{-1}$

Roman Symbols

c_t	Total molar concentration of gas mixture	mol m^{-3}
d_p	Diameter of particles in the packed bed	m
d_{pore}	Pore diameter of adsorbent particle	m
k_{LDF}	Mass transfer coefficient used in the linear driving force model	m s^{-1}
L	Length of the adsorber bed	m
m	Mass	kg
M_i	Molecular weight of specie i	g mol^{-1}

Nomenclature		xi
m_{ads}	Mass of adsorbent in the column	kg
n	Number of species in the mixture	–
P	Pressure	bar
Q	Volumetric flow rate	$\text{m}^3 \text{s}^{-1}$
q_i	Molar loading of component i	mol kg^{-1}
R	Universal gas constant	$8.314 \text{ J mol}^{-1} \text{ K}^{-1}$
S_{ij}	Selectivity in favour of component i with respect to component j	–
T	Absolute temperature	K
t	Time	s
u	Interstitial velocity in the packed bed	m s^{-1}
x_i	Mole fraction of i in the solid adsorbent phase	–
y_i	Mole fraction of i in the bulk gas phase	–
z	Adsorber length	m
\mathcal{D}_{ax}	Axial dispersion coefficient	$\text{m}^2 \text{s}^{-1}$
\mathcal{D}_{eff}	Effective diffusion coefficient	$\text{m}^2 \text{s}^{-1}$
$\mathcal{D}_{k,i}$	Knudsen diffusion coefficient of specie i	$\text{m}^2 \text{s}^{-1}$
$\mathcal{D}_{m,i}$	Molecular diffusion coefficient of specie i	$\text{m}^2 \text{s}^{-1}$
iso-nSTD	Normalised standard deviation to determine the fit quality of isotherm parameters	%
nSTD	Normalised standard deviation	%
Superscript		
0	Referring to pure component property	–
Subscript		
i, j	Referring to component i or j	–

List of Figures

2.1	Vapour liquid equilibria for binary ethylene and carbon dioxide mixture	7
2.2	Schematic representation of an olefin binding with transition metal Ag^+	13
2.3	Ethylene/ethane separation performance for various types of membranes	14
3.1	Structure and positions of cations in zeolite prisms	23
3.2	IUPAC classification of adsorption isotherms	26
3.3	IAST selectivities for five binary mixtures	32
4.1	Dependence of particle sphericity and packing density on bed voidage	36
4.2	Flow chart of the experimental set up	38
4.3a	Plot of an analytical sigmoid function for increasing α	41
4.3b	Monte Carlo analysis of the Simpson and Trapezoid approximation for a sigmoid function	41
5.1	Unary breakthrough diagrams	44
5.2	Transient breakthrough experiments for $\text{C}_2\text{H}_4/\text{CO}_2$ gas mixtures for various temperatures	47
5.3	Comparison of theoretical IAST calculations with experiments for binary $\text{C}_2\text{H}_4/\text{CO}_2$ mixture	48
5.4	Transient desorption experiments for $\text{C}_2\text{H}_4/\text{CO}_2$ gas mixtures	51
6.1	Velocity deviation of different models describing CO_2 adsorption on AC	52
6.2	Validation of the model with experimental transient breakthrough data	57
6.3	Comparison of numerical simulations versus the breakthrough experiments	59
6.4	Effect of model having variable velocity and constant velocity	59
6.5	Velocity behaviour inside a fixed-bed column	61
6.6	Comparison of two different sets of isotherm parameters on breakthrough behaviour	62
A.1	Hwang isotherm data for CO_2 and CO	74
A.2	Reich isotherm data for C_2H_4 and CO_2	75
A.3	Osterkamp isotherm data for C_2H_4 and CO_2	76
A.4	Choi isotherm data for CO_2 and CO	77
A.5	Grande isotherm data for CO_2, CO and H_2	78
A.6	Lopes isotherm data for CO_2, CO and H_2	80
A.7	Park isotherm data for $\text{CO}_2, \text{CO}, \text{N}_2$ and H_2	82
C.1	Experimental set-up used for the transient breakthrough experiments	85

List of Tables

2.1	Physical property data	4
2.2	Loading of various compounds onto different active carbon types at 298K and 1 bar . . .	12
2.3	Overview of Technology Readiness Levels	19
2.4	Overview of the screened technologies	19
3.1	Screening of adsorbents for selective ethylene capture	23
3.2	Selection of the most common used adsorption isotherms	27
3.3	Overview of different sources of isotherm data for active carbon	30
4.1	Overview of applicable heating times in the adsorber bed	39
5.1	Loading, volume feed fraction and selectivity for transient breakthrough experiments . . .	48
6.1	Initial and boundary conditions for an open-open fixed bed column	55
6.2	Column properties and input parameters	57
6.3	Diffusion volumes for various simple molecules	57
6.4	Comparison of selectivities found using various methods	62
A.1	Hwang isotherm parameter fits for CO ₂ and CO	74
A.2	Reich isotherm parameter fits for C ₂ H ₄ and CO ₂	75
A.3	Osterkamp isotherm parameter fits for C ₂ H ₄ and CO ₂	76
A.4	Choi isotherm parameter fits for C ₂ H ₄ and H ₂	77
A.5	Grande isotherm parameter fits for CO ₂ , CO and H ₂	78
A.6	Lopes isotherm parameter fits for CO ₂ , CO and H ₂	79
A.7	Park isotherm parameter fits for CO ₂ , CO, N ₂ and H ₂	81
A.8	Al-Janabi isotherm parameter fits for CO ₂ and N ₂	81
B.1	Analysis of micro-GC accuracy	84

1

Introduction

1.1. CO₂ reduction in the world

We are living in a world where CO₂ or carbon dioxide and its influence is mentioned daily in newspapers, social media, scientific journals etc. and even though its global effects on climate change are subject of discussion. It is measured that CO₂ concentrations in the atmosphere have increased that over the last 30 years at 1% per year, with a decline seen in Q1 of 2020 due to decreased energy demand in China and mild weather conditions on the northern hemisphere [1], [2]. At the time this thesis was written, the COVID-19 pandemic raged over the world and the forced confinement imposed by many governments is estimated to decrease global emissions by -4% (-2 to -7%) for low estimates and up to -7% (-3 to -13%) if restrictions are continued until the end of 2021 [2]. The effects of this decrease will last for years and gives us a another good motivation to rethink current emission patterns. This, combined with the new strategies of the European Union of CO₂ utilisation and increasing carbon dioxide taxes could be good incentives for us to look into a new direction [3].

1.2. Carbon cycle and e-Refinery

In a techno-economical study by Fernández-Dacosta et al. a prospective assessment is made where 10% CO₂ is captured off an industrial hydrogen unit and used for commercial-scale polyol production. The authors mention that CO₂ utilisation in this form has "limited potential" for full scale operation on an industrial level, however has a 23% reduction in "climate change potential" with respect to the base case, in which no CO₂-capture system is implemented [4]. This illustrates how Carbon Capture and Utilisation (CCU) uses flue gas and is converted into re-usable bulk chemicals, in contrast to Carbon Capture and Storage (CCS), where CO₂ is only stored. The complex process of commercial scale CO₂ utilisation faces huge challenges which need to be identified and understood. The capture and processing required for CCU will not necessarily result in the lowest climate change potential, since the the environmental trade-off is more complex compared to CCS [4], [5]. Nevertheless the prospect of closing the carbon cycle is a great step towards a carbon neutral future.

To achieve this feat we would have to reconsider the concept that the bulk of the worlds chemicals is retrieved from fossil fuel-derived feedstocks and look into alternatives. Electroreduction of CO₂ offers a potential route towards the production of gaseous carbons, such as the aforementioned polyols or methane and ethylene [6], [7], alcohols [8], [9] and oxygenates [9], [10]. Advances in this field has led to more workable productivity, selectivity and efficiency, as well as more durable and more efficient catalysts [6], [11]. Combining electroreduction with renewable energy sources creates a useful bridge between emissions and fossil fuels, while simultaneously creating a method to store (long times, e.g. seasonal storage) electrical into chemical energy. This is why the the e-Refinery incentive was launched in 2018 at the TU Delft. This consortium has the goal to "electrify and decarbonise the chemical and energy industries with its unique integrated approach, ranging from materials to processes and their upscaling" [12].

1.3. Industrial Separations

Inherent within the e-Refinery, identical to the classical, fossil-based refineries, separation processes account for a huge portion of the energy consumption. To illustrate the vastness of energy required, David S. Sholl and Ryan P. Lively mention seven industrial separations to change the world. Three of seven, e.g. splitting of alkanes and alkenes, capture dilute emissions from flue gases and hydrocarbons from crude oil, are related to the e-Refinery in some way. To further stress the need for improvement the authors state that approximately 32% of the energy in the United States is used for industrial purposes, of which 45-55% is used for separation processes [13].

The first industrial separation mentioned, the splitting of alkanes and alkenes, is of particular interest. Ethylene, and in general olefins, are fundamental feedstocks for a wide range of chemical products. Global production of ethylene was 116 million tonnes in 2005 [14] and exceeded 200 million tons in 2016 [13], this is almost 30 kilograms for every person on earth per year and is one of the most produced organic compounds in the world. In industry, the olefin/paraffin separation is typically done using high-pressure cryogenic distillation and the huge amount of production, combined with the STP boiling point of ethylene at -107.3 degrees Celsius accounts for 0.3% of the worlds energy use [13]. As mentioned, ethylene is also a potential product of electroreduction of CO_2 , and even though production using this technique is nowhere near industrially relevant quantities, the previous statements on current ethylene cryo-based separation, emphasise the need for a less energy demanding separation process.

The second method mentioned, capturing of CO_2 in flue gas, is important since it is the obvious feedstock in CO_2 -reduction. Capturing this gas efficiently will reduce the amount of CO_2 emitted into the atmosphere, while simultaneously reducing raw material costs. Eventually such an alternative production method would eliminate the need for the third industrial separation mentioned.

1.4. Alternative Production Route

Contrary to other common, binary gas mixtures, such as $\text{CH}_4/\text{C}_2\text{H}_4$ [14], [15] CH_4/CO_2 [15]–[17], $\text{C}_2\text{H}_4/\text{C}_2\text{H}_6$ [15], [18]–[21], the $\text{C}_2\text{H}_4/\text{CO}_2$ -mixture is significantly less studied. A good example where the $\text{C}_2\text{H}_4/\text{CO}_2$ -mixture plays an essential role, is in the effluent of the Oxidative Coupling of Methane (OCM) reaction. This is another pathway that is used for producing ethylene in a more sustainable way and it is based on pyrolysing CH_4 into ethylene with side products ethane, carbon monoxide and hydrogen. The motivation for using methane feedstock is that it can be obtained through a variety of renewable options, such as biogas from organic waste [22] or landfills [23]. This process is interesting to compare to the CO_2 reduction pathway as both are upcoming technologies and both have issues to be proved in industry because of poor ethylene conversion and selectivity, as well as limited catalyst lifetime [6], [24], [25]. Two important differences between the renewable synthesis routes can be observed. Firstly, OCM depends on a constant supply of biogas and production can be controversial, as land used for agriculture could be replaced for chemicals production. Secondly, OCM reactor effluent contains two more light hydrocarbon gases (neglecting minor side products), i.e. methane and ethane [26]. Because of the low conversion, over 70% of methane is still present in the gas mixture after reaction as well as ethane as side product. The resulting mixture is challenging to separate using conventional scrubbing and distillation methods, because large amounts of methane and other products need to be recycled to minimise waste streams and conserve carbon in the process, making this process economically unfeasible for now [26]. The advantage of using CO_2 electrolyzer from a separation perspective is substantial, as the gas-phase reactor effluent is free of methane and ethane.

1.5. Goals and research question

Focus of this thesis and its research question is finding a downstream separation process of CO_2 -reduction cell, which captures ethylene, while using minimal energy resources and yields high purity product. To help answer this question this thesis is subdivided into various chapters. In Chapter 2 a thorough literature of various separation techniques and its relation to the mock-up reactor effluent is described and aims to find the one with most potential. In chapter 3 the chosen separation technique,

adsorption, will be examined further and various sorbent materials are screened for their separation capabilities. Chapter 4 discusses an experimental set-up to determine breakthrough times and chapter 5 will cover experimental work where the chosen material is used in transient breakthrough experiments and the behaviour of binary C_2H_4/CO_2 mixture on active carbon is investigated. Chapter 6 will provide a theoretical model of the experiments which can be used in a later stadium for improving the adsorption based separation process. This thesis will finish by giving the conclusions found in this work and the recommendations to further design and develop a downstream separation process.

2

Literature research and theory

2.1. Introduction & Physical properties

Selection of a suitable and efficient separation process is essential in making any process successful. This chapter is dedicated to evaluating current separation strategies and discusses their potential for the mock-up reactor effluent. Possible options that are investigated include absorption, cryogenic methodologies, membrane technologies, surface separations and more are all discussed in the upcoming sections. The low conversion rates of CO₂ to C₂-products, due to the high kinetic barrier of the C-C coupling step, will increase the amount of reactants and products in the gas mixture, making the separation process more complex [10]. Additionally the desire to focus on low driving force technologies makes finding a solution a challenging task.

In Table 2.1 the physical properties of the gas-phase components of the electrolyzer are given and upon inspection of the kinetic diameter, normal boiling point, polarizability, dipole and quadrupole moments, it is hard to identify a clear handle which can easily be exploited. Ideally ethylene can be separated from the mixture in a single unit operation, simultaneously recycling CO₂ and H₂, while purging water and CO. Capturing of a specific gas in similar mixtures is possible if the target gas has a suitable handle, this could be the Lewis acidity of CO₂ or the distinctive kinetic diameter of H₂ or the dipole moment of H₂O [28]. Performing such an operation with ethylene as target gas in a mixture of gases with similar physical properties, while also adhering to the low driving force goal, is something that has not been accomplished before.

Another complication lies in the large amount of ethylene and CO₂ in the gas mixture, accounting together for roughly 75% of the mixture, meaning their characteristics are of major importance when choosing the separation system. Both gases have low boiling points, do not differ a lot in size, have high polarizability and no dipole moment.

Table 2.1: Physical property data [27]

Compound	molecular weight [g/mol]	Kinetic diameter (Å)	Normal boiling point (K)	Polarizability × [10 ²⁵ cm ³]	Dipole moment [10 ¹⁸ per (esu · cm)]	Quadrupole moment [10 ²⁶ per (esu · cm ²)]
C ₂ H ₄	28.05	4.16	169.42	42.52	-	1.5
CO ₂	44.01	3.30	216.55	26.5	-	4.3
CO	28.02	3.69	81.66	19.5	0.110	2.5
H ₂ O	18.01	2.65	373.15	14.5	1.855	-
H ₂	2.02	2.89	20.27	8.0	-	0.662

2.2. Selection criteria

Having mentioned this lack of a suitable handle, this chapter will focus on highlighting various types of separation techniques to determine the most promising one, while fulfilling the highest percentage of process requisites. Before embarking into a huge campaign to identify all possible separation schemes for the full mixture, they are accessed based upon a few criteria to efficiently choose the most auspicious candidate. Those include:

- A considerable amount of information should be available in literature concerning the material and/or process.
- The technology should be ethylene selective for the given reactor effluent
- Experimental testing can be performed on a small scale and can be upscaled for application in a 100kW electrolyzer cell.
- The process should operate at low driving forces, in other words energy requirements should be low.

Besides these criteria, the system is preferably able to deal with water vapor, however due to the complication of water vapor present for most systems, it is assumed water can be removed using a condenser. Goal is not to design or synthesise new materials, nor to go on an extensive experimental campaign to test the separation capacity of unproven materials, but rather to focus on methods that are (partially) proven for (a part of) the mock-up reactor effluent.

In the following section some well-known separation techniques as absorption, distillation, adsorption and membranes technologies as well as more unproven options will be explained and their potential is discussed.

2.3. Absorption

Absorption based separation is based on relative solubility's of individual components in the mixture in liquid phase, meaning some components get enriched in the bulk aqueous phase, while the remainder stays in the gas phase, creating a split. Within absorption three types are commonly described: e.g. physical, chemical and ionic liquid absorption.

2.3.1. Physical absorption

Physical absorption is based on the principles of Henry's law, meaning that equilibrium concentration is a function of partial pressure and temperature and does not react with the solvent [29]. Because uptake is higher at high partial pressures, pressurising or heating of the feed is one of the main energy consumers, making physical absorption generally uneconomical when absorbate feed concentration is under 15% [30]. To regenerate the absorbent heat is applied, pressure is reduced or a combination of both.

Commercial processes include the Rectisol process with methanol as sorbent and over 100+ plants in operation, the UOP selexol process, which uses dimethyl ether and ethylene glycol blend as sorbent and has over 110 operational plants worldwide. Other processes are the Purisol, Morysorb and Shell Sulinol processes [31], [32]. These processes have in common that they are mainly used to remove acid gases (CO_2 , SO_2 , COS) to upgrade natural gas, purify Fischer-Tropsch effluent or biogas.

2.3.2. Chemical absorption

Chemical absorption is characterised by a chemical reaction between the absorbent and the gas phase component to form a weakly bonded intermediate. The solvent is chosen in a way that the equilibrium favours the formation of this intermediate and is therefore often preferred when absorbate concentration in the feed is low or partial pressures are low. Within chemical absorption two types can be identified; reversible and irreversible absorption. In reversible absorption the solvent can be regenerated using heat or pressure changes, in the second case the bonded intermediate is essentially irreversible and is

commonly applied when the amount to be adsorbed is small and requires marginal exit concentrations [29].

Both chemical and physical absorption is usually performed in counter-current columns, where the solvent is fed at the top and gas flows from the bottom and is absorbed by the lean solvent. The saturated solvent leaves from the bottom and is (often thermally) regenerated in the stripper, the absorbate is now recovered and removed while the adsorbent is cycled back to the absorbing column [31].

Chemical absorption is extensively used for CO₂ capture, therefore a very mature technology and has been commercialised for many decades. Arguably the most important industrial application is the removal of CO₂ using alkanolamines, this includes primary, secondary, and tertiary amines containing a hydroxyl group, for example Monoethanolamine (MEA), diethanolamine (DEA) or more complex multi- or cyclic amines [31], [33]. The MEA process is exploited by numerous suppliers, such as CB&I, Caloric Anlagenbau and Randall Gas Technologies [32].

2.3.3. Ionic liquids

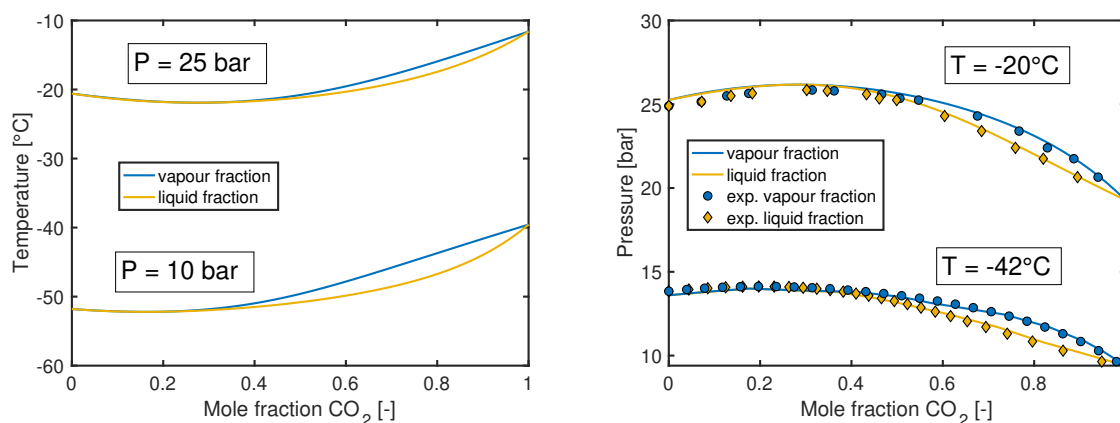
Ionic Liquids (ILs) are salt solutions that are in liquid form under an arbitrary temperature, for example 100°C, and consist mainly of ions and short lived electron pairs. Main advantages of ILs are their low vapor pressure, high polarity, wide liquid region, good thermal stability and non-toxicity [31], [34]. ILs are used in many applications in various fields however limited amount of solvents have made it to commercialisation, the same is observed for separation applications of ILs [35].

ILs can both be used as a chemical and physical absorbent. For physical absorption main factors in the solubility are the free volume and the size of ILs, as well as used cations and anions [31]. Anthony et al. measured the effect of various ILs, e.g. [bmim][BF₄] and [bmim][Tf₂N]¹ on the solubility of CO₂, ethylene and various other gases. They concluded that cations do not play a significant role on CO₂-solubility and anions do play a role, where for the [Tf₂N] anion the highest solubility was reported. Additionally it was reported that gases with large dipole or quadrupole moments and molecules able to form other bonds (i.e. hydrogen bonds) have the highest affinity with the IL and finally other non-polar gases related accurately with their polarizability. This results, in decaying order of solubility, for the mock-up reactor effluent in: H₂O > CO₂ > C₂H₄ > CO > H₂ [36].

Chemical absorption in ILs for CO₂-capture is reported by Bates et al., who created a task specific ionic liquid (TSIL), which is a IL tailor-made for specific characteristics. Using this technique they created a IL able to absorb CO₂ with similar efficiency as existing absorbent solutions. Downside of this technique is that as CO₂ is absorbed, the viscosity of the fluid increases and flow becomes increasingly more difficult [37]. Alternatively to this problem Camper et al. mixed commercially available alkanolamines (MEA, DEA) with the room temperature IL. This way the absorbent mixture could be tuned to more effectively capture CO₂ in various conditions and processes. Advantageous of these amine-IL solutions is that they possess similar CO₂ uptake capabilities and behaviour, but lack the disadvantages of TSIL (high viscosity) and pure alkanolamines solutions (high vapor pressure, low CO₂ loading, solvent degradation, corrosion) [38].

Alternatively, options may lie in the olefin/paraffin separations as huge gains are also to be made in this section as mentioned in the introduction. The unsaturated bonds of olefins have the capability of donating π -electrons, contrary to saturated paraffins whose electrons are confined in the bond orbitals. This makes olefins essentially Lewis acids which are able to interact with transition metal cations, for example Ag⁺ and Cu⁺ [20]. Sun et al. investigated a novel copper(I)-based supported ionic liquid membrane (SILM). This SILM is a polyvinylidene fluoride microporous membrane impregnated by a IL consisting of CuCl and 1-butyl-3-methylimidazolium chloride ([Bmim][Cl]). The result showed that ethylene permeability and permselectivity could be controlled by varying the CuCl/[Bmim][Cl] ratio, for a ratio of two the highest permeability and permselectivity were reported [39]. Similar research is reported for polysulfone (PSf) asymmetrical porous hollow fibers with solvents consisting of silver salts

¹[bmim][BF₄] = 1-n-butyl-3-methyl imidazolium tetrafluoroborate, [bmim][Tf₂N] = 1-n-butyl-3-methyl imidazolium bis(trifluoromethylsulfonyl) imide



(a) T-xy diagram

(b) P-xy diagram. Experimental data obtained from Nagahama et al. [44]

Figure 2.1: Vapour liquid equilibria for binary ethylene and carbon dioxide mixture. The equilibria were estimated with the Peng Robinson equation of state using Aspen Plus software.

(AgNO₃ and AgBF₄) solutions in various IL with imidazolium and phosphonium cations. In this case 37% of the original ethylene in a 80:20 ethylene:ethane ratio was recovered after 8 hours [40].

2.3.4. Conclusion on absorption based technologies

Numerous examples were given of industrial scrubbing installations using physical or chemical absorption for CO₂-removal strategies, however non of them met the criteria of one-step ethylene capture. Of course this does not mean that one-step ethylene capture using absorption is impossible, however in the light of our goal to not embark on an experimental endeavour, it is considered out of scope to continue in this field and search for a suitable solvent. An alternative would be to consider two-step process, where CO₂ is removed using absorption from of the reaction mixture, resulting in a mixture from which ethylene can more easily be isolated.

Also for ionic liquids substantial amount of research is conducted on CO₂-capture. Interesting for our specific gas mixture are the solubilities of various gases in ILs reported by Anthony et al., seen here was that solubility of ethylene is simple intermediate with respect to the other components in our mixture and therefore does not provide us with the desired handle for the one-step capture.

Ionic liquids provide us with a paradigm, as there are a million simple ionic liquids [35], which can be used binary or ternary systems giving us respectively 10¹² and 10¹⁸ possible combinations between them, one could argue that one of them provides a good option for this process, however finding it, is not the scope of thesis.

2.4. Cryogenic separation techniques

No exact definition exists when the cryogenic temperature range begins, but the cryogenic range begins when so-called permanent gases (N₂, O₂ etc.) start to liquefy around -150°C. The reason to chill gases to these low temperatures is that phase changes start occurring and separation can be performed based on differences in condensation and sublimation point. Based on this principle high purity oxygen and nitrogen (> 99.9%) are obtained in air separation [41] or CO₂ can be captured from flue gases with 99.99% purity and recovery [42], these examples indicate the possibilities to obtain high quality product. Cryogenic separation methods are not limited to just distillation, other options include; the cryogenic packed bed, anti-sublimation process, Controlled Freeze Zone process, CryoCell process or implementation of stirling coolers. [43].

2.4.1. Cryogenic Distillation

The first method that comes to mind when separating at cryogenic temperatures is cryogenic distillation. Its principle is based on the relative volatilities of the components in the mixture and the goal is use the effective vapor pressures to extract one or several components from the mixture. The advantages of (cryogenic) distillation are well-known and is therefore extensively used in industry, some include: high maturity of the process, no need to introduce additional components and the ability to produce high purity products combined with minimal losses of product [29]. It is currently also the dominant separation technique for the splitting of hydrocarbons [14].

Inspecting the standard boiling points of all components in Table 2.1, it is immediately clear that ethylene has the middle boiling point and therefore does not provide an easily accessible handle for 1-step capture of ethylene. Additionally the vapour-liquid equilibria of $\text{CO}_2/\text{C}_2\text{H}_4$ are given in Figure 2.1. Reviewing these diagrams it is seen that for low CO_2 fractions the difference in boiling point is minimal, making it energy intensive to obtain a high purity ethylene fraction, additionally the azeotrope will increase the process complexity. Stünkel et al. report a process scheme for the removal of ethylene in a OCM reaction mixture (see section 1.4) and the process consists of a purification and separation section. In the purification section CO_2 is removed using a MEA-based absorption unit and in the separation stage one or multiple distillation columns are used to capture methane and ethylene [45]. To reduce the energy requirements, Salerno et al. use a technique called feed-splitting, where gas and liquid fractions are split in a decanter and subsequently fed at different trays in ethane/ethylene column, the result is a 16% drop in refrigerant costs [25]. Alternatively Dutta et al. modelled the economic feasibility of using LNG as cold source for the distillation of the OCM reactor effluent and showed that no other external cooling was required. However because of the relative high price of LNG with respect to NG, this method is only favorable when LNG-cold energy is obtained as side product from another process [46].

Despite all of the previously mentioned processes the huge stand-in-the-way for this method to be implemented in the e-Refinery is still the considerable energy demand necessary to bring down the gas mixture to a point where components start condensing. It is not uncommon that cooling accounts for 50% of operating costs [43]. To reduce this amount, energy efficient solutions, for example multistage compression and cooling [47], increasingly synergistic process flow diagrams [25] or process intensification. The latter even reported that using their optimised and intensified cryogenic network a profit gain of over 69% could be reached [48]. An important sidenote is the required use of the ethylene product, preferably product is used locally or transported through high pressure pipelines, besides this it is not uncommon for ethylene to be stored in surface refrigerated tanks, in this case ethylene is required at cryogenic temperatures, making the economic case stronger for cryogenic separation methods [14].

2.4.2. Stirling coolers

The basic principle of Stirling Coolers is based on the reversible Stirling cycle and allows for gases to be cooled to very low temperatures. Its basic operation is based on four phases being repeated in a cycle, the phases are described by Song et al. as: 1. expansion under an isothermal condition, 2. refrigeration under a constant volume condition, 3. compression under an isothermal condition, and 4. heating under a constant volume condition. Advantages of the coolers are their high reliability, high efficiency, small size and they are only reliable on electrical power [49]. The mechanical cooler is in itself not a separation method, but a tool that can be used to cool gases to cryogenic levels. Song et al. proposed a CO_2 -capture process based on Stirling Coolers combined with heat integration to find an efficient method to desublimation and capture CO_2 [50]. Downside is that this concept has only been proven on lab scale using binary mixtures (N_2 and CO_2) and no pilot scale or industrial applications have been reported [43].

2.4.3. Cryogenic Packed Bed

Tuinier et al. proposed a post-combustion CO_2 capture process, which effectively freezes out CO_2 and water and captures the permanent gases. This packed bed consists of a steel monolith structure which is cooled using excess cold duty that is available at liquefied natural gas regasification sites [51]. This concept is based on the desublimation and freezing of CO_2 and H_2O , where different fronts of firstly condensing H_2O create the equilibrium temperature and subsequently a second front of desublimat-

ing CO₂ forms and creates the second equilibrium temperature. The authors mention that amount of condensation and desublimations reaches a maximum, depending on the amount of cold energy in the bed, this prevents plugging or unacceptable pressure drop in the bed during a capture cycle [51]². This concept proved to be successful for a mixture of N₂, CO₂ and H₂O. Major advantage of this process is that water is removed in the same unit operation, removing the need for an additional drying section. Additionally H₂S has been added to the mixture and the total mixture had more capture potential than the MEA based absorption process or a VPSA separation process [52].

Although this method removes water and carbon dioxide from the gas mixture, simplifying the original gas mixture, it does not provide a single unit operation which captures ethylene and a second unit operation step would be required. Another downside of this method is that is reliable on the availability of LNG gas, when this is not the case a refrigerating system is required, substantially increasing energy consumption [52]. Additionally this process has not been proven in industry and has only be shown in small scale experiments, making the cryogenic packed bed not a viable option.

2.4.4. Controlled Freeze Zone

The Controlled Freeze Zone (CFZ) technology is originally intended to deal with very sour natural gas reserves, which may contain up to 70% CO₂ and 5% H₂S and must be removed to make it suitable for transportation and combustion [43]. This large amount of CO₂ and H₂S makes normal distillation difficult as CO₂ is very prone to freezing and blocking the column. As a solution ExxonMobil proposed the idea to dedicate a specific zone in the column where CO₂ is allowed to freeze out and falls down to a melt tray and capture the acidic gases in a single separation step. This melt tray is kept above the solidification temperature by feeding heat through warm vapor coming from the stripping section of the column [53], [54]. This idea could be extended to multi-component mixtures, where multiple components are frozen out [55]. The high CO₂ content in the proposed reactor effluent, make this type of distillation interesting. Downside however of this method is that it was originally intended for methane separation and Northrop et al. mention that higher concentrations of heavier hydrocarbons (C₂+) will end up in the CO₂-stream and thus making a second separation step inevitable [53].

2.4.5. Alternative cryogenic methods

As alternative to the previously mentioned methods the following methods are described for flue gas CO₂ capture of coal fired power plant and were investigated as viable ethylene capture options.

Anti-sublimation (AnSu) process

This method, described by Clodic et al. is based on the similar physical principle as the cryogenic packed bed, that is the desublimation of CO₂. Difference is however that CO₂ is freezing directly to the heat exchanger with as main advantage that the heat of fusion can be recovered [56]. This process consists of five stages. In the first stage moisture is removed and the mixture is cooled to -40°C, in the second stage cold energy is retrieved from the outflowing streams using a heat exchanger, in the third stage the gas mixture is further cooled using a integrated refrigeration cascade. Stage four consists of the actual CO₂ heat exchangers where the CO₂ is desublimated. In the fifth stage the CO₂ is recovered. In this system water should be removed to prevent unacceptable rise in pressure drop in the fourth stage, this in contrast with the cryogenic packed bed, where different moving fronts prevent substantial pressure drop differences. Another complication is that the build-up of CO₂ on the heat exchanger limits the amount of heat transfer to the gas mixture negatively affecting efficiency. An extra complication is that the freezing temperature of CO₂ is dependent on its partial pressure in the gas mixture, the lower the desired final concentration of CO₂ the lower the temperature of the heat exchanger should be and the more energy is required.

CryoCell process

In the CryoCell process flue gas is dehydrated, cooled using outflowing gas and further cooled to the CO₂ freezing point. In the next step it is expanded using a Joule-Thomson valve and enters the special

²For detailed information on the process, the reader is referred to the original paper by Tuinier and coworkers [51].

designed CryoCell column as a three phase system. The solid CO₂ is recovered at the bottom of the column, heated by the reboiler and removed as a liquid. At the top methane is recovered and compressed to storage or sale specifications [57].

Both processes are intended and designed for CO₂ recovery from flue gases or upgrading of biogas, and could prove useful when reducing the CO₂ amount in the mock-up reactor effluent or when high purity CO₂ need to be recycled. The implementation would however not provide the desired handle for ethylene capture.

2.4.6. Conclusion on cryogenic separation methods

The advantages of cryogenic distillation are the high recovery and purity of products, the maturity of the technology, makes it a viable option for this separation process. Simulations of the separation process of the OCM reactor effluent show that cryogenic distillation can be efficiently applied for a more complex reaction mixture (mock-up mixture including methane and ethane) and using methods as feedsplitting, synergistic schemes, process intensification or using more unproven options such as stirling coolers, energy demands can be decreased.

Alternatively CO₂ freezing or sublimation methods are considered, the applicability of these methods ranged between lab scale and pilot scale and were mainly designed for the capture of CO₂. These methods would reduce the amount of CO₂ in the mixture and would make separation easier, non of them provided perspective of obtaining high purity ethylene, in other words, all of them would require additional separation steps.

Main issue with cryogenic distillation is the inherent need for cooling and the auxiliary equipment costs and one could wonder if this fits the green character of the e-Refinery. The normal boiling point of ethylene with respect to the mixture does not allow for a one-step capture of ethylene, meaning multiple columns are required for product retrieval. An important side note needs to be made, if at the process implementation site cold energy is available, for example the expansion of LNG which can efficiently be captured, operational costs would decrease substantially. This differs of course per location and therefore it is assumed in this thesis, that such cold energy is not available and the reactor effluent needs to be cooled in its entirety.

2.5. Adsorption

Adsorption is the natural tendency of molecules to collect at the surface of a solid material. This binding strength is unique for every adsorbent-adsorbate combination and can therefore be used as a separation technique. Most of the time, the binding is weaker than chemical bonds and be reversed by a relative mild adaptation in process conditions [29]. This reversibility is the basis of two fundamental stages, first the adsorption phase, where a mixture of gases (in this case) is fed and the more strongly adsorbed species is captured by the adsorbate and the second stage where this adsorbate is released by a change in pressure (pressure swing adsorption) or temperature (temperature swing adsorption) and the adsorbent bed is regenerated. The first industrial applications of adsorption were reported for N₂/O₂ splitting, air drying or in hydrogen purification. Nowadays adsorption is seen in more and bigger processes, with the largest hydrogen purification units in the petroleum industry having production rates up to 100 tonnes per day [58]. Other applications that are currently used on industrial scale are carbon dioxide recovery or natural gas purification. For example the Molecular Gate adsorbents of Guild Associates Inc. are in operation with over 40 units today. These units are used for the upgrading of landfill gas, digester gas, coalbed methane and natural gas and are able to deal with water saturated stream containing 3 to 40% CO₂ levels [32].

Similar to absorption, two types of adsorption typically occur. Physical adsorption, which is based on weak Van der Waals-attraction forces and are characterised by low enthalpy values, typically around 20 kJ/mole. This type of sorption is reversible and molecules are not bounded to a single adsorbent molecule, but are free to travel over the surface. Chemical bonding between adsorbate and adsorbent is identified by a much stronger bonds, such as covalent or electrostatic bonds, and have a high enthalpy bond around 200 kJ/mole and are irreversible [59]. This irreversibility is a major disadvantage

when used for bulk separations, as the adsorbent will need replacement very regularly, disrupting the process and increasing the operational costs. The next sections will focus on finding a method to effectively capture ethylene.

2.5.1. Finding an ethylene selective handle

Materials often used as adsorbent include activated carbon, metal-organic frameworks, silica gel, activated alumina, zeolites [29], [58]. The amount of dispersion forces a molecule “feels” towards the adsorbent is dependent on molecular weight, presence of functional groups, such as double bonds or halogens, polarizability and the micropores of the solid. Inspecting Table 2.1 it can be observed that ethylene and CO₂ both are non-polar molecules with large quadrupole moments, where CO₂ > ethylene. Using surface modifications or locally introduced charges in cation exchanged zeolites or open metal sites in MOFs, the adsorbent structure can be adapted in such a way that the electrical field can act on the quadrupole moment of ethylene or CO₂ and create a potential separation handle [60]. Difficulty lies in finding a suitable network that is able to selectively capture ethylene without co-capturing CO₂ or other species in the mixture.

For example García et al. reported the dynamic adsorption experiments using a zeolite 5A Molecular Sieve (MS) on a mini-plant scale for the separation process for the OCM reactor effluent. The uptake of ethylene, CO₂ and other species in the mixture were reported and it was observed that adsorption of both C₂H₄ and CO₂ was significant, in other words no suitable handle for ethylene capture was found. To obtain a good ethylene/CO₂ split the authors proposed to use amine based absorption to remove CO₂ [61].

Alternatively Bachman et al. sought to find a handle by using porous, highly tuneable metal organic frameworks. Their idea was to use a framework with open metal sites that “involves balancing the electropositivity and π -backbonding ability of the coordinating metal site for achieving selectivity” [26]. In this context the authors found of the investigated materials, e.g. M₂(*m*-dobdc) (M = Mg, Mn, Fe, Co, Ni)³, that Mn₂(*m*-dobdc) did not exhibit a particularly large affinity towards different species in the mixture, however did have the relative largest affinity towards ethylene. The calculated binary ethylene/CO₂ selectivity for this compound was around 8. For Fe₂(*m*-dobdc) an even higher selectivity of 11 was reported, however ethylene/CO selectivity was a factor 10 lower compared to Mn₂(*m*-dobdc), being approximately 10 and 100 respectively. These calculations were verified in breakthrough experiments and simulations and proved that Mn₂(*m*-dobdc) is capable of high selective ethylene capture [26].

Disadvantage of the previously mentioned adsorbents is that they are not commercially available, limiting up-scaling capabilities. Zandvoort et al. recently investigated the same mixture of gases and screened commercially available adsorbents for selective ethylene capture in CO₂ bearing mixtures. In their research the authors examined cation exchanged zeolites (13X, CaX, NaY, 5A, 4A) and activated carbon (AC) to test adsorption capabilities. Using ideal adsorption solution theory (IAST) predictions (see section 3.6.1) the selectivity of the binary mixture C₂H₄/CO₂ was determined for all adsorbents, from these results it was observed that zeolites 4A and 13X were CO₂ selective and AC was ethylene selective, the remainder showed no significant extra adsorption of either species. These calculations were verified in transient breakthrough experiments and simulations using the binary mixture in various ratios. For a C₂H₄/CO₂ ratio of three a breakthrough time of 15 minutes for ethylene was observed compared to 6 minutes for CO₂, indicating the preferable adsorption of ethylene on AC in agreement with the calculations.

Desorption was investigated using N₂ carrier gas at normal pressure, observed was that CO₂ desorption was substantially faster than ethylene desorption, the authors state that for a C₂H₄/CO₂ ratio of 0.5, comparable ratio as the mock-up reactor effluent, after 12 minutes a nearly pure ethylene stream could be obtained. No experiments with hydrogen or carbon monoxide were performed by the authors.

³*m*-dobdc⁴⁻ = 4,6-dioxido-1,3-benzenedicarboxylate

2.5.2. Comparison to the fruit industry

In an extensive review Keller et al. describe ethylene as the natural ripening agent in plants, and has therefore significant effect on growth and development as well as the storage life. Since low concentrations already have influence, controlling ethylene concentrations in storage can prevent major product losses and insure a fresh product. The most widely used technology is the use of potassium permanganate-based scrubbers, which oxidizes ethylene into carbon dioxide and water. Also among other methods, the use of zeolites and carbon based adsorbents is suggested to reduce ethylene concentrations. Of the reported zeolites, mordenite Na was the most favorable as a cyclic adsorbent and could be regenerated using micro-wave heated water. Ethylene uptake was about half compared to the oxidation capacity of the potassium permanganate-based scrubbers (20 versus 37 mmol/kg), but could be regenerated [62]. Additionally Bailén et al. describe the use of carbon-based adsorbents for ethylene control and could, depending on the conditions (partial pressures of CO₂, O₂ and other gases, temperature, humidity) obtain similar ethylene uptake as permanganate-based scrubbers [62], [63]. The involvement of ethylene in fruit ripening and in the reactor effluent make it interesting to compare both and the possibility to use AC as adsorbent is investigated further in the next section.

2.5.3. Effect of activated carbon on other species

To further investigate the possibility of AC as adsorbent the theoretical IAST separation factor of ethylene and the other various species in the mixture was determined. Naturally AC is a hydrophobic adsorbent, however adsorption effects of water vapor on AC can be significant. This effect can be explained by the presence of functional groups on the surface or edges which can act as nucleating sites. Depending on the amount of functional groups or the concentration of water vapor in the feed, this effect can compete and disrupt adsorption of the originally targeted species [64].

Experimental adsorption equilibria of pure hydrogen and carbon monoxide on activated carbon were investigated to relate their uptake to ethylene and CO₂, these results are given in Table 2.2. The experimental data have been extracted from the original paper using the Data Thief tool [65] and have been fitted using a temperature dependent, dual site Langmuir model (see section 3.4.2) to quantitatively compare their uptake. Observed is that for similar conditions, different types of AC yield a range of uptakes for the same specie, this effect can be explained by the differences in pore size, specific surface area and surface chemistry [66]. A similar feat is observed by Zandvoort et al. who attempted to model breakthrough experiments on zeolites and AC. Contrary to zeolites, they were unable to match simulations with experiments and they explained this poor quantitative match because isotherms for the simulations were obtained from a different kind of AC than the type used in breakthrough experiments [67]. Nevertheless can it be observed that for the given AC types hydrogen uptake is limited and most likely has limited effect on ethylene uptake. Carbon monoxide uptake is more substantial and its effect on ethylene capture should be investigated.

2.5.4. Effect of π -complexation and examples

π -complexation or π -back bonding is a special kind of bond in which the π -orbitals of a metal line-up with a ligand and are able to release (e.g. back donation) electrons from a filled d-orbital of the metal to an antibonding orbital of the ligand and is for example seen in transition metal-olefin complexes [72]. In Figure 2.2 this is graphically displayed, seen is how the 5s orbital of a silver atom binds with π^* -orbital. Because of the relatively diffuse π -orbitals of olefins, adsorbents containing metals capable of π -back

q [mol kg ⁻¹]				AC type/supplier	Ref.
C ₂ H ₄	CO ₂	CO	H ₂		
	2	0.35		Norit B4	[68]
2.6*	1.5*			Type BPL, 6/16 mesh	[69]
2.9*			0.02*	Calgon Co	[70]
	2.4*	0.9*	0.03*	'Commercial'	[71]

Table 2.2: Loading of various compounds onto different active carbon types at 298K and 1 bar. (*) are calculated using the dualsite, temperature dependent Langmuir model.

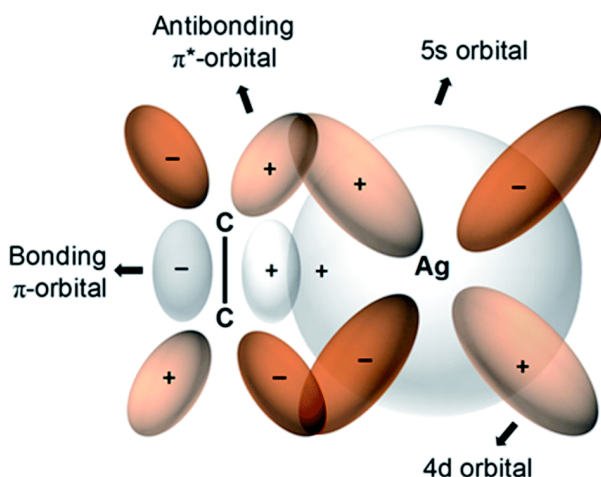


Figure 2.2: Schematic representation of an olefin binding with transition metal Ag^+ . First the outside s-orbital binds with the bonding orbital of the metal, second the π -bond consisting of the outside electrons in 4d orbital bind with the empty antibonding π^* orbital of ethylene [19].

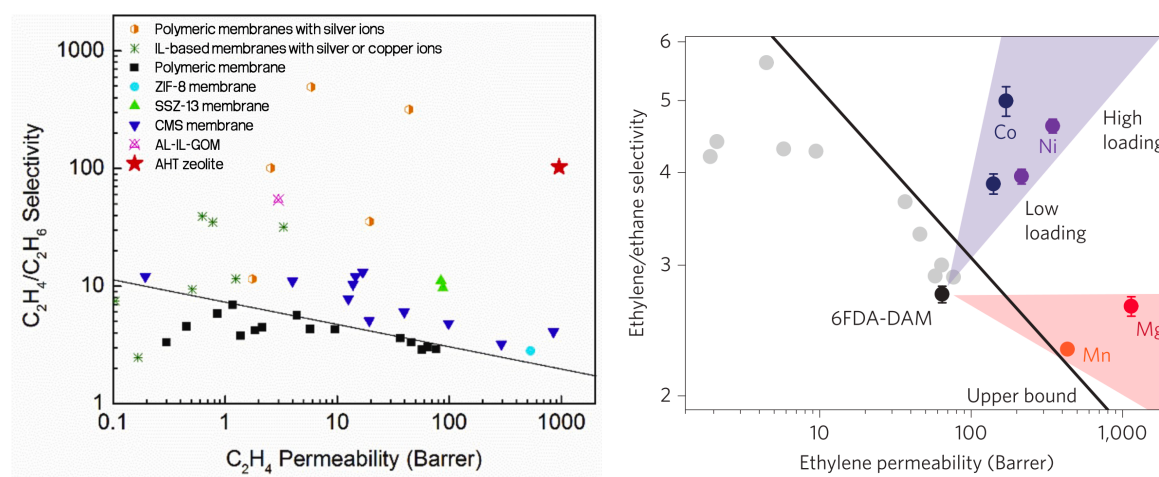
bonding are commonly investigated in olefin/paraffin separations. Reported metals that provide good selectivity for olefin capture include Cu^+ or Ag^+ , when incorporated in an adsorbent framework it can result in adsorption enthalpies of over 100 kJ/mol. Downside of this strong bond is that regeneration may prove to be quite challenging [73]. This affinity towards ethylene can also be exploited in ethylene/carbon dioxide mixtures, two examples are given below.

Zhou et al. studied the deep removal of ethylene of a carbon dioxide stream (approx. 1% (V) C_2H_4 in CO_2) comparing NaY and HY zeolites with AgNO_3 -Modified Y-Zeolites. They reported the presence of two types of adsorption sites for the modified zeolites, the weak sites that were also found in the unmodified zeolites and the strong sites, which are the newly introduced Ag^+ active sites. For the weak adsorption sites strong competition exists between ethylene and CO_2 and therefore ethylene particles are primarily captured by the strong, more selective adsorption sites. Also desorption for the weaker sites occurs at around 100 °C, while for the strong sites desorption is at 240 °C. Using temperature-programmed desorption the authors were able to selectively capture ethylene [74]. For the opposite mixture (1% (V) $\text{CO}_2/\text{C}_2\text{H}_4$) He et al. reported the metal-organic framework named Qc-5-Cu (fabricated by copper tetrafluoroborate and quinoline-5-carboxylic acid), which was able to capture CO_2 with great selectivity (IAST calculations showed selectivity of almost 40). In density functional theory (DFT) calculations it was observed that binding occurs through $\pi-\pi$ interactions between the molecules and the framework, and that in this case the high selectivity can be explained because the quinoline ring makes it difficult for ethylene to conjugate with the framework [18]. These examples indicate that with proper use of metal complexes, adsorbents can be tuned to specifically target ethylene (or CO_2 , interesting for the upgrade towards high-grade ethylene).

2.5.5. Conclusion on adsorbent technologies

Finding a suitable adsorbent capable of selectively capturing ethylene is not straightforward, however the potential advantages are clear; simple equipment, process operation at moderate conditions and low energy requirements. Possible adsorbent options include activated carbon, silica gel, zeolites and metal-organic frameworks, which can be tailored to meet specific needs. The similar properties (polarity, quadrupole moment, dipole moment) of ethylene and carbon dioxide make the need for a custom adsorbent seem evident. $\text{Mn}_2(m\text{-dobdc})$ and $\text{Fe}_2(m\text{-dobdc})$ were reported to have good selectivity's towards ethylene, being 8 and 11 respectively, where $\text{Mn}_2(m\text{-dobdc})$ also has large $\text{C}_2\text{H}_4/\text{CO}$ selectivity of approximately 100. Additionally transition metals Cu^+ and Ag^+ are reported to have good π -back bonding capabilities with ethylene, these capabilities are used create a selective handle towards ethylene and CO_2

Besides these MOFs and zeolites, active carbon was also reported as adsorbent with favorable equilibrium towards ethylene in a range of $\text{C}_2\text{H}_4/\text{CO}_2$ (0.5-3) mixtures, having a calculated IAST selectivity of 3 to 4. This is not as high as the custom made adsorbents, however does have the advantage of being widely available and cheap, being advantageous when larger scale set-up are build. Additionally the



(a) Xu et al. provide an overview of carbon molecular sieves, zeolite, polymeric and silver/copper based membranes [77]. (b) Bachman et al. report membranes incorporated with various loadings of $M_2(\text{dobdc})$ nanocrystals. Grey dots represent polymeric membranes [28].

Figure 2.3: Ethylene/ethane separation performance for various types of membranes. The black lines in both figures indicates the upper bound for polymeric molecules.

transient desorption experiments of a binary C_2H_4/CO_2 mixture indicate that CO_2 desorption is faster than ethylene desorption, meaning that after all CO_2 has desorped a stream of nearly pure ethylene can be recovered. Interestingly a similar feat is currently seen in the plant conservation industry, where the organophilicity of AC is used to effectively capture ethylene and could be regenerated after use.

2.6. Membrane Technology

Membrane separation is based on the relative permeability of a individual gases through a membrane based on the physical or chemical properties of the gas. The main driving force in gas-membrane separation is the pressure difference that is present across the membrane and based on the gaseous solubility and permeability, the permeable molecules (permeate) diffuse through and the non-permeable molecules (retentate) stay on the feed stream side. The specific kind of membrane that is used, is of great importance in the design of a membrane-separation unit as it will hugely effect the performance [75], [76].

Industrial applications of membranes include for example the UOP Separex™ membrane systems (130 units installed worldwide), capable of removing CO_2 , H_2S and water vapor from a hydrocarbon stream or the Cynara® Membrane Units (40 units installed worldwide) are used to capture bulk quantities of CO_2 from hydrocarbon gas stream and is even capable of handling condensing liquid hydrocarbons. Hydrogen upgrading facilities using the UOP Polysep™ Membrane by Air Liquide (125 installations worldwide) are capable of producing a 90 to 99% hydrogen product stream, these are all processes reaching the initial stages of maturity [32], [76]. The general advantages of membrane processes include its low capital and operating costs, the possibility of modular upscaling and simple process flow sheets. However the technology is often not economical for the production of very large amount of product.

For gas separation, a trade-off is often encountered between the permeability and selectivity of a material and will characterise the performance of the final product. A high permeability will increase the flow through the membrane or reduce the pressure drop over the system, downside is that selectivity decreases as molecules can diffuse more easily through the membrane. And vice versa for a low permeability a higher selectivity is often seen. This is graphically displayed in Figure 2.3. Here the O_2/N_2 selectivity is displayed on the y-axis and permeability on the x-axis, it is suggested that an upper boundary exist for many polymeric membranes and to overcome this limit is subject to intensive research.

Within membrane gas separation various membrane materials exist, those include polymeric mem-

branes, inorganic membranes, Metal-organic framework membranes, Mixed Matrix Membranes and some other materials [78].

2.6.1. Polymeric Membranes

Polymeric membranes are extensively used in industry for their low costs and their wide range applications and some examples include silicone rubber, polycarbonate, polyimides or larger copolymers [75]. Typically they are divided into glassy or rubbery polymers, depending on the glass transition temperature of the material. Rubbery membranes consist of long chain which can be stretched and when the stress is released the membrane will return to its original state. Glassy membranes on the other hand consist of rigid chains, that will break when tension is increased. Generally glassy polymers have good separation characteristics, e.g. high selectivity, combined with low permeability, this effect is explained by the presence of less free volume within the chains. For rubbery polymers the opposite is observed. This effect is also displayed in Figure 2.3, where the rubbery polymers are represented more significantly in the bottom right corner and glassy polymers in top left corner [78].

2.6.2. Inorganic membranes

Inorganic membranes contain typically oxides, metals or elementary carbon and compared to polymeric membranes, they are more durable, show less plastification and have better control over pore size and distribution. They are typically characterised based on their internal pore size range between dense (<0.5nm) and macroporous (>50 nm). The microporous range (pore size ranging between 0.5 and 2 nm) is interesting for CO₂ and hydrocarbon separations. Examples include silicates, zeolites and carbon molecular sieves (CMS) [78], [79]. For example Salinas et al. describe the use of high performance CMS that was pyrolysed between temperatures of 500 and 800 °C. The membranes were capable of ethylene capture in a binary, equimolar ethylene/ethane mixture with a selectivity up to 14 at 4 bar and which claimed to be the highest to date. Molecular sieves are identified for their stability and high permeability, but have not been produced at industrial sized scale [78], [80].

2.6.3. Facilitated transport membranes

Facilitated membranes have a special agents incorporated into their polymer matrix that can selectively and reversely bind with the target molecule, providing an additional route next to normal diffusion. This way, for a decent permeability, very high selectivities of 165 have been reported for the ethylene/ethane mixture [81] and of 60 for propylene/propane [82]. This is achieved for example by implementation of silver ions into a polymeric membrane, which are capable to form a metal complex with the π -bond of olefins (see Figure 2.2). In a recent patent it was shown that for increased silver ion concentration in the membrane a higher permeability and selectivity was observed, while still being able to produce a 99.5 m% permeate stream, [83]. In practise however, these membranes were found to be too unstable during longer continuous operation [78].

2.6.4. Pilot scale OCM processes

PolyActive membrane, a commercial blockcopolymer, is produced on a commercial scale and installed into membrane modules by Brinkmann et al.[84]. In their pilot scale investigations they assessed the capability of this membrane to capture CO₂ from gaseous hydrocarbons (CH₄, C₂H₄). It was concluded that the membrane was stable for longer periods under continuous operation and was able to capture carbon dioxide from hydrocarbons with good selectivity towards methane and moderate selectivity towards ethylene. However the CO₂ recovery of 44% at 10 bar feed pressure and 70% at 20 bar feed pressure, indicate that a hybrid separation system (the authors suggested amine-based absorption) is needed to minimise losses. Besides ethylene losses through the permeate were in the range of 25%, so another membrane stage would be required to reduce losses [84]. Additionally Schuldts et al. reported a "strong swelling influence of CO₂" which has a negative effect on the CO₂/C₂H₄-selectivity as CO₂ partial pressures increase, meaning that process pressure ranges are limited [85].

Comparable results were seen in pilot scale tests by Stunkel et al. They investigated four membranes to study CO₂ capture in OCM reactor effluent and the effect of ethylene losses. Cellulose acetate (CA), polyethylene oxide (PEO), polydimethylsiloxane (PDMS) and matrimide (PI) were investigated and

the highest CO₂/C₂H₄-selectivity of 16.5 was found for PI. However in their initial screening with PI it was found that for 90% CO₂-capture, ethylene losses would be in the range of 40%. To improve the pilot experiments they aimed to capture half of the CO₂ of a feed consisting of 25% CO₂, and subsequently implement an amine-based absorption step. This way unacceptable ethylene losses could be prevented [86]. Both cases show that for commercial membranes loss of product is considerable.

2.6.5. Olefin/paraffin separations

Olefin/paraffin separations are notoriously difficult to achieve, due to large similarity between molecules and are conventionally performed using distillation. On the other hand over 2000 publications and patents have been published on hydrocarbon membrane separation over the last 30 years, indicating the interest in enhancing existing membranes and commercialise them [76].

Hou et al. published a comprehensive review where the latest developments concerning olefin/paraffin separations and over 50 different types of membranes are reported. From a separation point of view they discovered that the selectivity/permeability barrier was the main limitation for industrial applications. Separation occurs either through chemical interactions, based on the preferential diffusion through dense polymers and alternatively through sieving molecules using judicious materials with appropriate pore sizes and shapes. From a material point of view two general types of materials are seen, e.g. dense and porous membranes. Dense membranes, consisting of linear branches of polymer, are diffusion based and are therefore limited by the selectivity/permeability upper bound. As solution porous materials with micropores (e.g. MOFs, zeolites, carbon molecular sieves) are being designed [19]. For both points of view, MOFs are obtaining significant attention, as these polycrystalline membranes can be varied in organic linker molecules, creating the possibility to tune size, shape, internal cavities and chemical affinity [78]. To find the ideal ethylene selective membrane Xu et al. used non-equilibrium molecular dynamic and DFT simulations. In their results the designed AHT zeolite was found to be superior relative to the other reported membranes, having a permeability of 958 Barrer and a C₂H₄/C₂H₆-selectivity of 102, see the red star in Figure 2.3a [77].

2.6.6. Metal-organic framework membranes

Introduction of metal-organic frameworks (MOFs) into membranes is a relatively new phenomena and is obtaining an increasing amount of attention due to properties as large pore size, high surface area and good selectivity towards small or chiral molecules. Bachman et al. report the use composite membranes consisting of MOFs dispersed into a polyimide polymer phase, with ethylene/ethane selectivity's of around 5. The membranes consisting of Ni₂(dobdc) or Co₂(dobdc) nanocrystals were also found to have greater ethylene selectivity or consisting of Mg₂(dobdc) or Mn₂(dobdc) with greater permeability and increased durability, all operating above the upper bound, seen in Figure 2.3b). Besides this increased separation performance, the authors reported suppression of the plastification effect caused by mobile polymer chains that are being dissolved by the penetrating gas as pressure increases, decreasing selectivity. The polymer membranes were able to handle high pressures, without loss in selectivity, making them applicable for separations previously inaccessible for membrane separations [28]. The same group also reported a solid sorbents (e.g. Mn₂(*m*-dobdc) and Fe₂(*m*-dobdc)) capable of highly selective ethylene capture from a mixture containing CO₂, CO, H₂. These nanocrystals could also be incorporated into membranes to boost ethylene capture [26].

2.6.7. Conclusion on membranes

Membrane based separation is a maturing technique that is increasingly common in industry, typical applications are for example bulk CO₂-capture in flue gas, biogas and natural gas upgrading or hydrogen capture. Advantages of membrane technology include low capital costs, limited operating costs, no moving parts, modular up-scaling and the lack of phase changes. Weaknesses of this technique are its sensitivity to fouling, plastification or compaction, that is generally deterioration of pores caused by pressure or temperature effects and a selectivity/permeability trade-off.

To find an ethylene selective membranes three types of membrane were examined, e.g. polymeric, inorganic and facilitated transport membranes. To 'examine/scout/look into/investigate' different options, the OCM-process and olefin/paraffin separation procedures were examined(, because of their similar outflow compositions)

Polymeric membranes are the simplest type of membrane examined and known for their wide applicability and low costs, however ethylene selective processes are scarce. Pilot scale experiments of OCM reactor effluent using membranes matrimide was the most suitable with the highest ethylene/carbon dioxide selectivity of 16.5, but was used only to reduce CO₂ concentrations and subsequently another separation step was proposed. Alternatively PolyActive membrane, proved to have decent recovery of CO₂ from a hydrocarbon stream (methane, ethylene), but ethylene losses were significant in the range of 20%, also indicating multiple stages or additional separation techniques are needed to make the process economical. Polymeric membranes also have the tendency to be bound by the selectivity/permeability line, making industrial applications limited. To overcome this limitation inorganic and facilitated transport membranes, which include carbon molecular sieves, zeolites and metal-organic frameworks, are used. Pyrolysed carbon molecular sieves are able to have high fluxes with good stability, but currently are limitedly available on commercial scale.

From both a material as a separation point of view the tune ability of MOFs and zeolite is an effective way to overcome the selectivity/permeability bound by tuning size, shape, internal cavities and chemical affinity and can therefore specifically be designed to be ethylene selective. Similar to adsorbents, Co₂(*m*-dobdc) and Mg₂(*m*-dobdc) dispersed into a polymer phase proved to yield ethylene from ethane with respectively high selectivity or high permeability. An alternative strategy is to use metal complexes which can form a bond with the π -orbital of olefins, metal ions as Ag⁺ or Cu⁺ can be incorporated into a polymer matrix, and be used as facilitated membranes to improve performance. Additionally it may be worthwhile to use simulations to find the ideal material to push the limits of selectivity/permeability boundary.

2.7. Other technologies

2.7.1. Reactive separation

By using a reactant the properties of ethylene can be changed in such a way separation is significantly easier. Oligomerization would be the first option that comes to mind, by creating repeating units, the boiling point of the carbon chain would increase, to the point where distillation is more feasible or even liquefies at room temperature. High grade ethylene (>99.9%) is polymerized on catalysts (for example titanium(III) oxide or chromium(VI) oxide) to produce polyethylene [14]. However in this case other gases in the mixture would foul the catalyst, making this step inaccessible. Alternatively the Shell higher olefin process (SHOP) is used to produce linear branched olefins of lengths up to approximately 20 repeating units [87].

Graf et al. describe a combined process for the oxidative coupling of methane and reactive alkylation of benzene to the intermediate ethylbenzene using ZSM-5. Conversion ranged between 90 and 98% for reactor temperatures between 320 and 400 °C. No effect with other species in the mixture, e.g. CO, CO₂, CH₄, C₂H₆ and H₂O, was observed and water even had a positive effect on the stability of ZSM-5 [88]. The liquid ethylbenzene can easily be recovered from the gas mixture, for example using a flash or distillation. The ethylbenzene can be used as intermediate in the production of methylbenzenes and sold as such. Otherwise a dealkylation procedure in this case or cracking process in case of oligomerization would be required, which typically occurs under high temperature and pressure conditions or using catalysts [14]. This additional process step would significantly increase capital and operational costs.

2.7.2. High temperature looping

High temperature solid looping is a technique commonly used to capture CO₂ from flue gases and is based on the reaction of calcium oxide with CO₂ to form CaCO₃. In a fluidized bed reactor operating around 650 °C the lean absorbent chemically binds to the CO₂ and is transported to a stripping column. This column operates at around 900 °C to recover and produce a pure stream of CO₂. Advantages of this technique are that CO₂ is inherently separated from other components in the flue gas, it can easily be retrofitted into existing infrastructure and the absorbent material, essentially limestone, is abundant. Downsides include the high operating temperatures, meaning efficient heat integration needs to be implemented to keep energy requirements to a minimum. Also the technique has limitedly proven itself in industry, with a few pilot plants being the largest scale to date [60]. Although this technique captures

CO₂ with high purity, it does not provide an ethylene selective handle, meaning additional separation steps would be required. Also no information is available on the effect of C₂H₄, CO and H₂ in the process.

2.7.3. Hybrid technologies

Combining different types of separation techniques is an efficient way to overcome the weaknesses of a single technique. Also using specific techniques the different unique handles of specific molecules can be targeted more efficiently.

Several options were already suggested before, for example Stunkel et al. proposed a separation set-up for ethylene capture of a OCM gas mixture consisting of a membrane module, amine based absorption and distillation. The resulting hybrid system yielded a 40% reduction in energy requirements compared to the original base case [45], [86]. Moreira et al. implemented a cryogenic adsorption process as an alternative for a distillation column for the upgrading of natural gas. This way an energy reduction was achieved combined with a higher methane recovery [89]. As discussed in section 2.5, adsorption with tailormade adsorbents can be an alternative option to produce high grade ethylene. Especially as impurities commonly removed via distillation, a relative large amount of energy is required for the removal of trace impurities. A hybrid set-up where bulk quantities are removed with distillation/absorption/membrane technologies and further purified with adsorption could be an interesting approach [18].

Hybrid technologies will vastly increase the number of process configurations, in practice most processes consist of multiple technologies, however in this case focus will be on a single method and can later be expanded to a hybrid scheme.

2.8. Selection process

2.8.1. Selection criteria

In the beginning of this section, four selection criteria were given. The goal of this review is to screen existing separation technologies and find the one most suitable for our given reactor effluent. The criteria are shortly repeated below.

- A considerable amount of information is available in literature concerning the material and/or process.
- The technology should be ethylene selective for the given reactor effluent
- Experimental testing can be performed on a small scale and can be upscaled to be applied to the effluent of a 100kW electrolyzer cell.
- The process should operate at low driving forces, in other words energy requirements should be low.

By means of an overview (given in Table 2.4), Technology Readiness Levels and the given criteria, one technique is chosen and developed further into a suitable downstream separation process for within the e-Refinery framework.

2.8.2. TRL explanation

First introduced by NASA in the 1970s, Technology Readiness Levels (TRL) can be used to estimate the maturity of a technology and provide a uniform, quantitative method to compare them to each other [60], [90]. For application in chemical separation processes an alternative scale is required and is given in Table 2.3. This scale is based on continuousness of processes, power output and the industrial scale it is currently applied.

Even with these straightforward guidelines, assessing every technique is not always obvious, factors as discrepant reporting methods or industrial confidentiality, all influence the TRL reported here. Other limitations of TRL, such as actual industrial relevance or the fact that readiness is not necessarily scales with appropriateness, are important to keep in the back of your mind. Nevertheless, when interpreted

Table 2.3: Technology Readiness Levels (TRL) applied to chemical separation processes, based on [60].

TRL#	Power usage	Comment
TRL 1		basic principles observed
TRL 2		basic process design
TRL 3		experimental proof of concept
TRL 4	<50 kW	continuous lab-scale experiments
TRL 5	0.05–1MW	pilot scale experiments at industrial conditions
TRL 6	1–10MW	prototype demonstration, steady state operating in industry conditions
TRL 7	>10MW	system demonstration in operational environment
TRL 8		complete system and operational at industrial scale
TRL 9		fully proven system, competitively used in the field

correctly, this scale can aid in selection of a separation process. And in a few years from now, can be used to see which technologies have developed significantly over the years.

2.8.3. TRL Table

In this table the investigated technologies are summarised, included are the reported application and the corresponding TRL number based on Table 2.3, and the most important comments regarding implementation in the e-refinery and towards ethylene capture.

Table 2.4: Overview of the screened technologies. Included are the reported application, estimated TRL and most relevant comments regarding implementation. O/P-separation = olefin/paraffin separation (includes C₂H₄/C₂H₆ and C₃H₆/C₃H₈ split); OCM-separation = Oxidative coupling of methane separation

Separation process	Reported application	TRL	Comments
Absorption			
Physical	CO ₂ -capture	9	<ul style="list-style-type: none"> • high energy requirement • CO₂-selective
Chemical	CO ₂ -capture	9	<ul style="list-style-type: none"> • Regeneration requires significant energy • Extensively used for CO₂-capture
Ionic liquid	CO ₂ -capture	5	<ul style="list-style-type: none"> • Limitedly proven in industry
	O/P-separation	1	<ul style="list-style-type: none"> • Many configurations possible • Ethylene selective IL are very novel
Cryogenic methods			
Distillation	O/P-separation	9	<ul style="list-style-type: none"> • Mature technology, high purity products
	OCM-separation	6	<ul style="list-style-type: none"> • High energy requirements • Selectivity of unity for CO₂/C₂H₄ mixture for low CO₂ fractions
Stirling coolers	CO ₂ -separation	4	<ul style="list-style-type: none"> • Not stand-alone method • No pilot scale experiments reported
Cryogenic packed bed	H ₂ O and CO ₂ -capture	4	<ul style="list-style-type: none"> • Removes CO₂ and H₂O simultaneously, no ethylene capture • Uneconomical without cheap cold source
Controlled freeze zone	CO ₂ and sour gas capture	7	<ul style="list-style-type: none"> • Upgrade of distillation column to handle solids • C₂+ hydrocarbons end up in CO₂ stream
Adsorption			
PSA/TSA in general	CO ₂ -capture	9	<ul style="list-style-type: none"> • Ethylene selective (for particular adsorbents)
	H ₂ -upgrading	9	<ul style="list-style-type: none"> • Low energy requirement
	NG-upgrading	9	
Metal organic frameworks, Zeolites	O/P-separation	4	<ul style="list-style-type: none"> • Highly tuneable to specific needs
	OCM-separation	2	<ul style="list-style-type: none"> • Complicated synthesis procedures for non-commercial materials
Active carbon	OCM-separation	2	<ul style="list-style-type: none"> • Ethylene selective • Cheap and commercially available

Membrane Technology			
Polymeric membranes (in general)	CO ₂ -separation	9	<ul style="list-style-type: none"> • Widely available • Considerable ethylene losses • Strong selectivity/permeability trade-off
Advanced Polymeric membranes	O/P-separation OCM-separation	3	<ul style="list-style-type: none"> • Implementation of MOFs create more diverse properties, e.g. being ethylene selective • Synthesis more complicated • Fouling and degradation issues
Facilitated transport membranes	O/P-separation	3	<ul style="list-style-type: none"> • Highly olefin selective, e.g. using Ag⁺-ions • Increase selectivity without losing permeability • limited stability and durability
Inorganic membranes	O/P-separation	4	<ul style="list-style-type: none"> • More durable, less plastification • Industrial use is limited, because of complicated preparation procedures
Other			
Reactive separation	Oligomerisation Alkylation with benzene	1 1	<ul style="list-style-type: none"> • Untested reversibility to ethylene
High temperature looping	CO ₂ -capture	6	<ul style="list-style-type: none"> • Inherent CO₂-capture from other components, no ethylene capture • High temperatures and advanced heat integration required

2.9. Result

Based on the available information the choice was made to further investigate an adsorption based separation process as it meets the most criteria. Those criteria include the affinity for ethylene for particular adsorbents, the ability to test at lab scale without the need for expensive or complicated experimental set-ups. Additionally adsorption based processes can be considered to be relatively low energy consuming and has been proven on various scales in industry. Depending on the type of adsorbent used, the TRL of these processes ranges between the discovery phase, for new custom MOFs or zeolites to demonstration and deployment phase, for industrial hydrogen production or CO₂-capture facilities.

This technique will be investigated further in the next chapters. An extensive screening for ethylene selective adsorbents will be done, an experimental set-up will be made to test one adsorbent and a corresponding model will be created to improve and help with developing a suitable downstream separation process process.

3

Adsorption Theory, Screening and Selection

This chapter is dedicated to finding a suitable adsorbent capable of selective capture of ethylene. Also the fundamentals of adsorption equilibria and other important parameters and its application in separation technologies are described. Many of these properties are essential in *all* adsorber design stages and therefore also useful for later work.

3.1. Fundamentals of adsorber design

Kneabel describes three types of considerations, which are used in adsorption based separation [91]; those include:

1. Adsorbent properties

The fundamental concepts of adsorbents are comprised of, but not limited to, isotherms and parameter estimation, IAST and selectivity calculations, mass transfer effects, particle characteristics, kinetics and pressure drop. [91].

2. Application review

For the application of the system considerations should be made for the basic operations conditions, the type of regeneration technique, corresponding energy requirements. As well as sensitiveness of the adsorbent material for fouling, aging and swelling.

3. Process design

Finally the equipment and integration of the system are to be considered. This includes bed design (fixed, fluidized bed), geometry of the bed, column types and insides as well as other miscellaneous factors as safety, system framework, maintenance or start-up/shut-down.

These concepts and their effects will be discussed in the following sections. Although all of these considerations are important, this thesis will focus predominantly on the first part; adsorbent properties. Attempted will be to discuss as many of the design factors to find a suitable framework which is able to selectively capture and produce high purity ethylene.

3.2. Adsorbent Screening

In this section various adsorbents are investigated and their separation potential is assessed, where the main focus lies on their ethylene capture abilities. In this extensive screening analysis, factors as (theoretical) selectivity, synthesis difficulty, stability and industrial relevance will be used to find a suitable candidate. The adsorbent of choice will be examined further and the details will be used to set up numerical and experimental analysis.

Common adsorbents that are seen in industrial gas separation are zeolites, metal organic frameworks (MOFs), activated carbon, silicates and alumina or ion exchange resins [29]. Experimentally testing all of these would require considerable experimental effort, besides most of these adsorbents have substantial literature data available on them for various gas mixtures. In Table 3.1 an extensive overview for these adsorbents is provided and are briefly explained in the following sections.

3.2.1. General Adsorbents

Activated carbon and silicate adsorbents are common in industrial gas separations. In section 2.5 activated carbon was described as good potential candidate for ethylene capture. The screening analysis in Table 3.1 is extended further as separation potential of other combinations of species in the mixture are examined and include an additional C₂H₄/CO₂ mixture as well as CO₂/CO and C₂H₄/H₂ mixtures. The additional C₂H₄/CO₂ source resulted in comparable IAST selectivity as previously found, indicating that different AC types can have similar performance. Ideally an C₂H₄/CO sample would be examined but at the time of writing this data was unavailable, alternatively a CO₂/CO mixture was investigated and yielded a selectivity between 18–24, depending on the mole fraction. Now based on the similar physical properties between C₂H₄ and CO₂, cautiously, a decent separation potential between C₂H₄ and CO could be expected, however only experiments can verify this statement. Finally H₂ capture by AC is marginal and this is verified by a C₂H₄/H₂ selectivity of over 200.

Silica gels are hydrophilic in nature and therefore suitable capturing of water from cracking gas or natural gas or H₂S removal from organic solvents [29]. This makes silica gel generally unsuitable for alkene capture and is not mentioned in existing literature and therefore this adsorbent type is not investigated further.

3.2.2. Zeolites

Zeolites are aluminosilicate crystalline structures originally found in nature, but nowadays mass produced to be used as commercial adsorbents. They generally consist of structured cages consisting of six windows, which can imbibe a large number of guest molecules. The structure of the cage is determined by negatively charged aluminium atoms that are balanced with cations (e.g. Na⁺, K⁺, Ag⁺ and more) and the size of the window apertures is dependent on type and number of cations and can range from 3 Å to 10 Å [92]. These cations are loosely bound to the structure and can be exchanged with its environment by contacting the zeolite to a solution. For example Sue-aok et al. who modified the NaY-zeolite by exposing it to dilute solutions containing various group I metals and making them tuneable to meet specific needs, such as ethylene capture [93].

The primary structure of zeolites consists of tetrahedral SiO₄ and AlO₄ units, which are assembled into various geometrical shapes, such as cubes or octahedra. The units are connected via the oxygen atoms and size of the windows depends, besides cations, on the amount of oxygen atoms in the ring. A lot of zeolite structures exist, but only the ones common for gas separation will be discussed, classified as type A, X and Y [92]. All types are build from the same sodalite cages, main difference however between these types is their spacial orientation and the location of the cations in the structure. The four-member ring structure in Figure 3.1 is characteristic for type A zeolites and the six-member rings for type X and Y. Second main characterisation is the location of the cationic molecules, which can be spread over positions I, II and III, in decreasing order of likeliness. Type Y is differentiated from type X by having a higher Si/Al ratio in the framework (typically 1–1.5) [94].

As mentioned, by incorporation of different types of cations, different aperture sizes can be achieved, for example by exchanging K⁺ with Na⁺ resulting in type [K]A zeolite with an smaller effective aperture of 3 Å due to the large size of K⁺ ions and therefore dubbed 3A zeolite. Alternatively, the double charge of Ca²⁺-ions means 2 Na⁺ are replaced by one cation, yielding a bigger aperture size of 5 Å, yielding [Ca]A or 5A zeolite [92]. Similarly, aperture sizes are controlled for [Ag]A, [Ca]X, [Na]X, [Na]Y or ZSM-5 zeolites. For ethylene and carbon dioxide separation this size is of major importance as too small apertures will kinetically block both molecules, prohibiting adsorption of ethylene (3A or 4A zeolite), while for too large aperture can lead to co-adsorption of other species. Alternatively, ions with sites that bind specifically to ethylene can help increase selectivity, for example [Ag]A zeolite was able to bond its silver metal with ethylene by complexation of the π -bond, yielding a promising selectivity

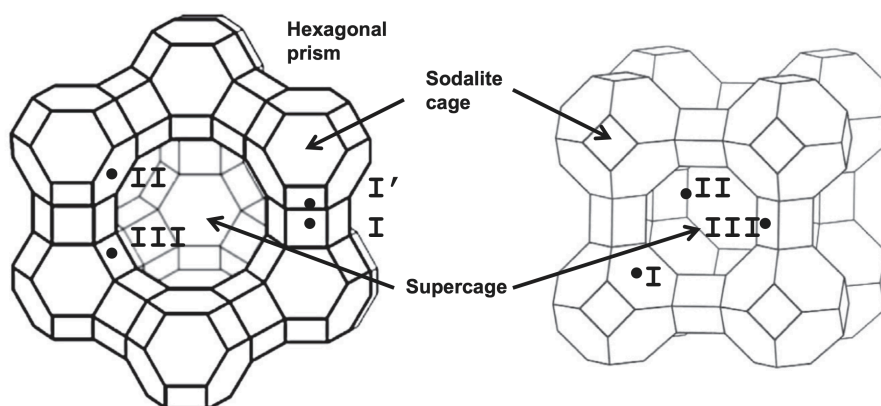


Figure 3.1: Structure and positions of cations in zeolite four member prisms (type A) (right) and six member prisms (type X and Y) (left). Roman numerals indicate cations sites. [96]

of 10.3. Major drawback of this zeolite is the decreasing selectivity and capacity seen after multiple cycles, Zandvoort et al. mentioned this might be due to reduction to metallic silver or agglomeration of silver ions, blocking the pore entrances [95].

Alternative to these common zeolites, they can be modified with other metal ions. Sue-aok et al. reported that NaY zeolites exposed to solutions of group I metals will incorporate these into their structure, without losing its crystalline structure [93]. This way M-NaY is able to adsorb ethylene, whereas pure NaY is not. Identically C_2H_4 adsorption performance was considerably improved by implementation of silver ions in NaY and HY zeolites [74].

From the screening analyses in Table 3.1 it was concluded that non of the investigated standard zeolites was able to selectively capture ethylene and therefore those were not investigated further. The modified zeolites were only tested for their ethylene adsorption capacities and not for their separation performance in reaction mixtures, therefore these modified zeolites are no longer considered.

3.2.3. Metal Organic Frameworks

The third major group of adsorbents for gas separation are metal organic frameworks (MOFs) already covered extensively in section 2.5. MOFs tested for gas mixtures similar to the the mock-up reactor effluent are scarce. Most promising was Mn(*m*-dobdc) as reported by the group led by Prof. Long at Berkeley. Interesting to mention is the Qc-5-Cu MOF reported by He et al., although not ethylene selective it is able to effectively remove low volume fractions of CO_2 from ethylene bearing streams, which in turn might be key to obtain polymer grade ethylene.

3.2.4. Overview of screened sorbent materials

Table 3.1: Screening of adsorbents for selective ethylene capture

Adsorbent type	Mixture	S_{12}^i	Notes	Ref.
General Adsorbents				
Active carbon ⁱⁱ				
AC1 (Pittsburgh)	$C_2H_4(1)/CO_2(2)$	3-4 ⁱⁱⁱ		[97]
AC2 (KF15000)	$C_2H_4(1)/CO_2(2)$	3-4 ⁱⁱⁱ	• Similar separation potential compared to AC1	[98]
AC3 (Norit B4)	$CO_2(1)/CO(2)$	21 ⁱⁱⁱ		[68]
AC4 (Calgon Co.)	$C_2H_4(1)/H_2(2)$	210 ⁱⁱⁱ	• Marginal H_2 uptake by AC	[99]

Table 3.1: Continued on next page

Table 3.1: continued from previous page

Adsorbent type	Mixture	S_{12}^i	Notes	Ref.
Silicates	Hydrocarbon/H ₂ O- Hydrocarbon/H ₂ S		• Used as desiccant	[29]
Zeolite Adsorbents				
[K]A (3A) zeolite	C ₂ H ₄ /N ₂	-	• Pores are too small for ethylene capture	[95]
[Na]A (4A) zeolite	C ₂ H ₄ (1)/CO ₂ (2)	0.7	• CO ₂ selective	[67]
[Na]A (4A) zeolite	C ₂ H ₄ /C ₂ H ₆ / CH ₄ /N ₂	-	• Kinetic limitations towards Ethylene	[95]
[Ca]A (5A) zeolite	C ₂ H ₄ /CO ₂ /N ₂ CH ₄ /CO	-	• Slow desorption of ethylene • Fully recoverable • Co-adsorbs C ₂ H ₆ and CO ₂	[95]
[Ca]A (5A) zeolite	C ₂ H ₄ (1)/CO ₂ (2)	0.8-1.2	• Selectivity dependent on mole fraction	[67]
[Ag]A zeolite	C ₂ H ₄ (1)/CO ₂ (2) /CH ₄ /C ₂ H ₆ /N ₂ / CO	10.3 ^{iv}	• Unstable after multiple cycles • Strong π -interaction between olefins and transition metals	[95]
[Ca]X (10X) zeolite	C ₂ H ₄ (1)/CO ₂ (2)	1	• Non-selective towards neither specie	[26], [95]
[Na]A (13X) zeolite	C ₂ H ₄ (1)/CO ₂ (2)	0.7 ⁱⁱⁱ	• CO ₂ selective • Behaves non-ideally	[67], [100]
[Na]Y zeolite	C ₂ H ₄ (1)/CO ₂ (2)	0.9	• Non selective	[67]
ZSM-5	C ₂ H ₄ (1)/CO ₂ (2)	0.8-1.3 ⁱⁱⁱ	• Si/Al ratio of 15, 30 and 60 analysed • Selectivity dependent on Si/Al ratio	[101]
Modified Zeolite Adsorbents				
AgNO ₃ /NaY	C ₂ H ₄ (1)/CO ₂ (2)	-	• Ag ⁺ -sites form strong chemical bond with ethylene	[74]
AgNO ₃ /HY	C ₂ H ₄ (1)/CO ₂ (2)	-	• Ag ⁺ ions on HY show better stability compared to AgNO ₃ /NaY • Both Ag-NaY/HY zeolites are capable of deep removal of C ₂ H ₄ of CO ₂ -bearing stream	[74]
NaY modified with group I metals		V_{max}^v		
NaY zeolite	C ₂ H ₄	0	• Standard zeolite not susceptible to ethylene	
K-NaY zeolite	C ₂ H ₄	103.5	• Best adsorption due to cation- π and CH \cdots O interactions	[93]
Rb-NaY zeolite	C ₂ H ₄	98.5	• Poorer adsorption due to large size of Rb ⁺ -ions	
Cs-NaY zeolite	C ₂ H ₄	90.2	• Large Cs ⁺ -ions cause blockages of CH \cdots O adsorption sites	
Metal Organic Framework Adsorbents				
M ₂ (m-dobdc)		S_{12}, S_{13}^{vi}		
M ₂ = Mg	C ₂ H ₄ (1)/C ₂ H ₆ / CH ₄ /H ₂ /CO ₂ (2)/ CO(3)	1,-	• Co-captures CO ₂	
M ₂ = Mn		8,100	• Suitable for selective ethylene capture	[26]
M ₂ = Fe		12,120	• Unstable in air	
M ₂ = Co		7,1.2	• Effective for no/low CO feeds	
M ₂ = Ni		4,0.8	• Effective for no/low CO feeds	

Table 3.1: Continued on next page

Table 3.1: continued from previous page

Adsorbent type	Mixture	S_{12}^i	Notes	Ref.
Qc-5-Cu	C ₂ H ₄ (1)/CO ₂ (2)	0.025	• Tested for deep removal of CO ₂ /C ₂ H ₄ (1:99, V/V%)	[18]

ⁱ Selectivity of compound (1) and (2) given in the *Mixture*-column at 298K. For $S_{12} < 1$, the adsorbent is selective to compound (2)

ⁱⁱ Note that all active carbon types are different and cannot simply be compared with one another.

ⁱⁱⁱ Based on IAST predictions.

^{vi} Selectivities for binary, equimolar mixtures. Based on IAST predictions.

^v Maximum volume of C₂H₄-adsorption in cm³/g. The modified NaY zeolites were synthesised for various ion exchange concentrations, only the highest adsorption volumes are reported here.

^{iv} Selectivity calculated from experimental breakthrough data using the method described in section 4.6.

3.2.5. Uninvestigated Options

In the previous sections more proven options are discussed, which means that the sorbents contained C₂H₄ and at least and one other component of the reaction mixture. Especially in the field of MOFs but also for zeolites options lie in unexplored options. A starting direction could be towards the fields of splitting light hydrocarbon gases or olefin/paraffin separations.

Numerous examples exist, for example, Plonka et al. report SBMOF-1 and SBMOF-2, which are able to split C₁ and C₂ hydrocarbons, and additionally the same group also states that SBMOF-1 can selectively capture CO₂ in a CO₂/N₂ mixture [102], however they did not report how this specific MOF would perform for a C₂H₄/CO₂ mixture. Also Chen et al. who propose a packed bed with three different sorbent beds in series, which capture acetylene, ethane and CO₂ impurities to yield ethylene as product from the respective quaternary mixture [103]. Or Hao et al. who report the robust framework TJT-100, capable of selectively capturing ethane and acetylene through C-H...O interactions, from a C₂H₂/C₂H₄/C₂H₆ mixture and thus producing highly pure ethylene [104]. Other examples are MIL-101-Cr-SO₃Ag [105], MOF-74-Fe [106] or PAF-1-SO₃Ag [107] for ethylene/ethane separations.

These examples may look promising in regard of producing high purity ethylene, however physical differences between alkanes/alkynes and CO₂ (e.g. alkanes are hydrophobic, no carbonyl groups, have small/no quadrupole moment) are significant. This means that materials that are proven, highly ethylene selective for olefin/paraffin mixtures, may not be able to split C₂H₄/CO₂ mixtures. A way to screen these materials is to use isotherm data and calculate the IAST selectivities, however for custom MOFs this data is very often not available, alternatively the materials would have to be synthesised locally and breakthrough experiments have to be performed.

3.3. Adsorbent Selection

Important characteristics that were looked for in the screened adsorbents: 1. the ability to selectively capture ethylene; 2. industrially relevant and easily accessible; 3. long term stability and regenerability. Also keeping in mind the selection criteria of section 2.2, activated carbon (AC) is chosen as candidate to be examined further. Some of the general advantages of AC over other adsorbents are the good regenerability, it is easily available and producible, cheap in large quantities, low toxicity. The most significant downside of AC is the relatively low C₂H₄/CO₂ selectivity, especially compared to custom produced MOFs.

3.4. Adsorption Equilibria

3.4.1. Classification of Isotherms

The IUPAC uses a general classification of adsorption isotherms and is given in Figure 3.2. Their characterisation is based on pore sizes and gas adsorption behaviour, where type I is typical for microporous materials, type II for polymolecular adsorption in non- or macroporous materials and type III is seen when sorbate-surface interactions are weaker than sorbate-sorbate interactions. Types IV

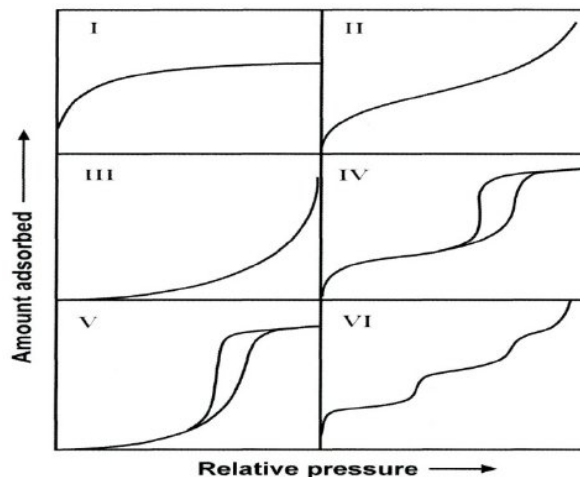


Figure 3.2: IUPAC classification of adsorption isotherms. For type IV and V hysteresis is observed [109].

and V are similar to types II and III, but for macroporous or mesoporous materials respectively. Type VI is more rare and represents stepwise multi-layer adsorption on homogeneous surfaces. Another classification that is seen in favourable isotherms (Types I, II, IV), recognised as the concave is down and unfavourable isotherms (Types III and V), as the concave is up [58], [108], [109]. The behaviour of the concave is fundamental for the design, as it describes the preferred direction of mass transfer, for a favourable isotherm the direction is from gas to solid phase and for unfavourable vice versa. Noteworthy is that for desorption the boundary conditions are reversed, meaning that favorable isotherms become unfavourable [58]. For types IV and V a hysteresis loop is observed, meaning adsorption and desorption take different pathways. The exact nature of this effect is not entirely known, but its linked with inkbottle pore geometry and the nucleation mechanism for capillary condensation [110].

In the development of adsorption based separation generally isotherms of the first and second type are used and are therefore this thesis is limited to these types. An noticeable exception however is the adsorption of water on carbon surfaces, which is categorised as a type V isotherm [58], [92].

3.4.2. Isotherm Models

To describe the adsorption of gases onto an adsorbent, isotherm models are commonly used. These models mathematically describe the amount of adsorbate that is captured by the adsorbent as a function of pressure for a given temperature. Ayawei et al. describe in their overview a total of 27 unique isotherm models ranging from one to five parameters, with each their own advantages and suitable application ranges [111]. For the design purpose of this thesis only a selection of these models and their extensions will be explained in following sections. The most used models include the linear, Langmuir, Freundlich, TOH and Langmuir-Freundlich (SIPS) models, see Table 3.2.

Linear isotherm

The linear adsorption model is the only *one* parameter model and resembles Henry's law as it is proportional to the partial pressure of the adsorbate gas. This model can be used for some adsorbent-adsorbate mixtures for low partial pressures and when particles are secluded of neighbouring particles. [111]. Advantage of this model is that linearity allows for analytical solutions modelling the behaviour of adsorber column, however in reality this model becomes inaccurate for moderately high concentrations, as it keeps increasing indefinitely, not taking into account saturation of the adsorbent. Besides increased computer power makes solving non-linear systems very accessible and more accurate isotherms model can easily be used.

Langmuir isotherm

The langmuir model is based on monolayer surface coverage and it assumes adsorption and desorption as reversible processes. It is based on the assumptions of an isothermal system with an ideally flat adsorbent surface, where a clear distinction between free and occupied sites can be made. The

Table 3.2: Selection of the most common used adsorption isotherms.

Isotherm model	Expression	Parameters	Ref.
Linear	$q = K_H P$	K_H [kg mol ⁻¹ bar ⁻¹]	[111]
Langmuir single site	$q = q_{sat} \frac{K_L p}{1 + K_L p}$	q_{sat} [kg mol ⁻¹] K_L [bar ⁻¹]	[111]
Langmuir Freundlich	$q = q_{sat} \frac{K_L P^{1/\nu}}{1 + K_L P^{1/\nu}}$	q_{sat} [kg mol ⁻¹] ν [-]	[112]
TOTH	$q = q_{sat} \frac{K_T P}{(1 + (K_T P)^\nu)^{1/\nu}}$	q_{sat} [kg mol ⁻¹] K_T [bar ⁻¹] ν [-]	[108]
Dual site Langmuir model	$q = q_{sat,A} \frac{K_{LT,A} P}{1 + K_{LT,A} P} + q_{sat,B} \frac{K_{LT,B} P}{1 + K_{LT,B} P}$ $K_{LT,A} = K_{LT,A0} \exp\left\{\frac{E_A}{RT}\right\}$ $K_{LT,B} = K_{LT,B0} \exp\left\{\frac{E_B}{RT}\right\}$	$q_{sat,A/B}$ [kg mol ⁻¹] $K_{LT,A/B,0}$ [bar ⁻¹] $E_{A,B}$ [J mol ⁻¹]	[67]
Langmuir Freundlich model (SIPS)	$q = q_{sat,A} \frac{K_{S,A} P^\nu}{1 + K_{S,A} P^\nu} + q_{sat,B} \frac{K_{S,B} P^\nu}{1 + K_{S,B} P^\nu}$ $K_{S,A} = K_{S,A0} \exp\left\{\frac{E_A}{RT}\right\}$ $K_{S,B} = K_{S,B0} \exp\left\{\frac{E_B}{RT}\right\}$	$q_{sat,A/B}$ [kg mol ⁻¹] $K_{LF,A/B,0}$ [bar ⁻¹] $E_{A,B}$ [J mol ⁻¹] ν [-]	[26], [67]

systems that accurately adhere to this model are limited, however it is a good approximate conformity. This model is often used to describe microporous (Type I) adsorbents [58], [111]. Similar to the linear model, the adsorbed amount keeps increasing for increasing pressure and to overcome this effect, the Langmuir Freundlich isotherm was introduced.

Langmuir Freundlich isotherm

The Langmuir Freundlich or SIPS model is based on the idea that adsorption sites are distributed according to an exponential form based on the heat of adsorption and is generally applicable for heterogeneous surfaces. The additional parameter ($1/\nu$) creates a finite limit when the pressure is sufficiently high [112]. For low pressures the isotherm reduces to the standard Freundlich form and has equal poor performance in this region. This model is commonly used to describe heterogeneous surfaces [113], [114]. To overcome the weakness in the low pressure region the TOTH isotherm was introduced.

Toth isotherm

The Toth isotherm is empirically derived from the monolayer-based Langmuir isotherm to reduce errors between experimental adsorption spectra and its anticipated isotherm. The heterogeneity of the system is described by the ν parameter. For $\nu = 1$ this equation reduces to the Langmuir isotherm and the more it deviates from unity the system can be characterised as heterogeneous. This isotherm is able to describe adsorption behaviour for low and high pressures [111], [114].

Number of parameters and multi-site coverage

The parameters in the isotherm models described above are determined by fitting experimental data. Since all models are non-linear, linear isotherm being the obvious exception, a non-linear regression method is applied, which can have a large number of independent parameters. By increasing the amount of parameters in the fitting equation, the error with data points can be reduced. Simply put, a two parameter model will generally will have a larger error compared to a three parameter model,

depending on the type of function and type of data. On the other side, as the number of parameters increases in a function the parameters will lose their physical significance [100]. In reality, isotherm data will be prone to measurement error and increasing the amount of parameters will lead to lower standard deviation, however could also induce overfitting and make the model unreliable when estimating intermediate data points. In other words the noise in the data is incorporated into the model [111]. This effect is for example seen in the fitting of the CO₂ isotherm using the SIPS isotherm in Figure A.2d. Here the parameters that were found in the fitting procedure, produce a nonphysical curvature for the low pressure region, caused by overfitting of the original isotherm data.

Another method to increase the number of parameters, without losing physical significance, is to consider the existence of multiple adsorption sites on the adsorbent. To better account for heterogeneity an extension can be introduced to account for these multiple adsorption sites. A summation over identical terms can be implemented to the isotherm equation, where each term accounts for a different type of adsorbent-adsorbate bonding site. In this model gas molecules adsorb first on the easily accessible sites and then the less favourable sites. The real number of different adsorption site may in reality be very large, but in practice two types of sites will accurately describe an isotherm [115]. This dual site model is implemented for the Langmuir and Langmuir-Freundlich isotherms in Table 3.2.

Temperature dependence of isotherm model

Experimental adsorption equilibria that are ranged over a temperature domain can be fitted with parameters that are made temperature dependent by implementation of an Arrhenius type exponential, i.e. $K = K_0 \exp\{E/RT\}$. This term also contains the activation energy, which quantifies the minimal interaction energy required for the adsorbate to start binding to the adsorbent. This term is substituted for the equilibrium constant K , seen in Table 3.2 [89], [116].

3.4.3. Error analysis

To determine the quality of a given fit often an error analysis is done. One method is to transform a non-linear isotherm into linear equations, which allows for simple linear regression analysis to find a dependent and independent variable of the form: $y = ax + b$. Also this method is used to find an appropriate fitting relation, as well to verify consistency of isotherm models [111]. An example for such a transformation is the linearization of the Langmuir isotherm into $P/q = 1/q_{sat}K_L + P/q_{sat}$, where $a = 1/q_{sat}$ and $b = 1/q_{sat}K_L$. This simple regression has however the disadvantage that the error structure is susceptible to change due to this transformation [117]. Also the fact that more elaborate isotherm models have forms that cannot be linearized, causing that non-linear regression methods are more suitable. These non-linear regression methods are based on minimizing the residual error between data and predicted isotherm values. Several methods to calculate this error exist, Ayawei et al. mention seven different methods, for example Sum of Square Errors or Marquardt's Percent Standard Deviation methods [111].

The fit quality of a specific isotherm and its corresponding data set is based on the normalised standard deviation (iso-nSTD), given in Equation 3.1 [116]. Here $q_{i,exp}$ and $q_{i,model}$ are respectively the measured experimental value and the calculated value by the respective isotherm. Here a distinction is made between isotherm models that are dependent on temperature and those that are not. Only when isotherm data is available over a temperature range, the data is fitted using a temperature dependent model.

$$\text{iso-nSTD} = 100 \sqrt{\frac{1}{N-1} \sum_{i=1}^n \left(\frac{q_{i,exp} - q_{i,model}}{q_{i,exp}} \right)^2} \quad (3.1)$$

3.4.4. Model selecting criteria

To ultimately pick the the most suitable model, three different aspects are considered. First the result of the error analysis described in the previous section. Secondly the isotherm should be thermodynamically consistent, this means: 1. when the pressure goes to zero, the isotherm should become linear. Meaning the isotherm adheres to Henry's law; 2. there should be a saturation of adsorbent for

increasing pressure. In other words the solid phase has a finite amount of pores and surface area and therefore only a finite amount of gas can be adsorbed. An example where this is not the case is for a Freundlich isotherm of the form $q = KP^{1/\nu}$; 3. for increasing pressure, the derivative of the slope should always be positive. This is to ensure that the amount adsorbed always increases with increasing pressure [108]. Thirdly, the applicability of the given model should be considered, this includes: 1. the given range is suitable for the given application; 2. the isotherm expression should be able to be implemented without increasing the computational effort substantially; 3. the parameter fitting using standardised algorithms should be able to produce physical consistent results. Additionally, factors as initial conditions should have no influence on the resulting parameters, as well as local minima or insensitive parameters should be avoided.

3.5. Isotherm data and parameter estimation

3.5.1. Activated carbon isotherm data

In contrast to other adsorbents, each specific active carbon type has a different precursor, different production process and is sieved to obtain a specific particle size, yielding different surface structures and mass transfer properties, this makes comparing isotherms of various sources unreliable. In total seven species of activated carbon are examined, containing at least two components from the mock-up reaction mixture; an overview is given in Table 3.3. Included in this overview is the particle size and specific surface area. The particle size ranges from small (0.15 mm/85 mesh) to pellet size (3mm in length/6 mesh) and the BET surface area is between typical values of AC; 500 and 1500 m²/g. Finally the equilibrium data range of the unary isotherm experiments is provided and similar conditions are seen, the temperature at ambient and slightly above ambient temperatures (data from Reich et al. being the exception) and pressure ranging from 0 to at least 700 kPa (excluding the Hwang data). Noteworthy is that a non of the available sources contained the full reaction mixture, consequently only the separation potential of parts of the reaction mixture could be examined.

3.5.2. Results of data fitting and parameter estimation

All data sets were fitted using the previously described dual site, temperature dependent Langmuir and SIPS isotherms. The parameters are found using the Levenberg-Marquardt least squares algorithm in MATLAB, e.g. using the build-in function `nlinfit.m`. All the parameters and plots, including the normalised standard deviation, are given in Appendix A. Based on the arguments in section 3.4.4, the dual-site Langmuir model proved to be the most suitable. The main arguments to discard the dual-site Langmuir Freundlich model was that some parameters in the model proved insensitive for least squares algorithm and in some cases overfitting was observed, i.e. Figure A.2b and A.2d.

Some general notes regarding the data fitting.

- Since no tabulated data was available, the isotherm data from Hwang, Grande and Lopes was extracted from graphical data using Data Thief software [65]. The accuracy of this method is inherently prone to error and this is reflected in a higher standard deviation. This is for example clearly seen in Figure A.5e or A.6d.
- In case of H₂ isotherm data, the single site model yielded better results for both models.

3.6. Selectivity analysis

To gain insight in the separation performance of each type of active carbon, a selectivity analysis for various binary mixtures of the reactor effluent is made. This analysis is based on the Ideal Adsorbed Solution Theory (IAST), which requires as input the fitted parameters of section 3.5. The details of the IAST methodology are given in the next section.

3.6.1. Ideal Adsorbed Solution Theory (IAST)

First described by Myers and Prausnitz in 1965, the Ideal Adsorbed Solution Theory (IAST) is based on the elemental equation analogous to Raoult's law of vapour liquids equilibrium [97].

$$P_i = P_i^o x_i \quad (3.2)$$

Table 3.3: Overview of different sources of isotherm data for active carbon. A hard requirement was that it contained a minimal of two compounds of the mock-up reactor mixture.

Authors [Ref.]	Supplier/name	Particle size	BET [m ² /g]	Pressure range [kPa]	Temperature Range [K]	Components
Reich et al. [69]	Pittsburgh Chemical Co.	20×85 mesh	990	0 - 3800	213, 260, 301	C ₂ H ₄ , CO ₂
Osterkamp et al. [98]	KF-1500	-	1400	0 - 1000	273, 298, 323	C ₂ H ₄ , CO ₂
Hwang [68]	NORIT B4	14×18 mesh	1100-1200	0 - 100	298	CO ₂ , CO
Choi et al. [99]	Calgon Co.	6×16 mesh	1150-1250	0 - 2000	293, 303, 313	C ₂ H ₄ , H ₂
Grande et al. [71]	<i>Commercial</i>	-	-	0 - 2200	303, 323, 343	CO ₂ , CO, H ₂
Lopes et al. [118]	<i>Commercial</i>	6×10 mesh	480	0 - 700	303, 323, 343	CO ₂ , CO, H ₂ , H ₂ O
Park et al. [112]	Kuraray Chemical Co.	8×12 mesh	1300	0 - 1000	293, 308, 323	CO ₂ , CO, H ₂

where P_i is the partial feed pressure for component i , x_i is the mole fraction of component i in the adsorbed phase given by:

$$x_i = \frac{q_i}{\sum_{i=1}^n q_i} \quad \text{where } \sum x_i = 1 \quad (3.3)$$

P_i^0 is the sorption pressure of component i , q_i is the molar loading in kg per mole adsorbent in the adsorbed phase, n is the number of components in the mixture.

Using the Gibbs adsorption isotherm the adsorption potential Ψ , units mol kg⁻¹, given by $\pi A/RT$, where π is the "spreading pressure which should be equal for each of the pure components as for the mixture", yielding:

$$\Psi = \frac{\pi A}{RT} = \int_0^{P_i^0} \frac{q_i^0(P)}{P} dP \quad (3.4)$$

Where q_i^0 is the pure component isotherm which are described by various adsorption models, for example the dual site SIPS or dual-site Langmuir isotherms. For the dual-site Langmuir isotherm the integration can be solved analytically and is given in Equation 3.5. All other integrals were calculated numerically.

$$\int_0^{P_i^0} \frac{q_i^0(P)}{P} dP = \int_0^{P_i^0} \left(\frac{q_{A,sat} b_A P}{1 + b_A P} + \frac{q_{B,sat} b_B P}{1 + b_B P} \right) \frac{1}{P} dP = q_{A,sat} \ln(1 + b_A P_i^0) + q_{B,sat} \ln(1 + b_B P_i^0) \quad (3.5)$$

Finally the single components and the mixture are related, for the same temperature and spreading pressure over the adsorbed phase, in the following equation:

$$\frac{1}{\sum_i^n q_i} = \sum_i^n \frac{x_i}{q_i^0(P_i^0)} \quad (3.6)$$

The system given in Equations 3.2 to 3.6 has to be solved numerically to obtain the loading q for each component i . Using the loading in the adsorbed phase and the mole fraction y in the gas phase the selectivity S_{12} of species 1 and 2 is determined via Equation 3.7.

$$S_{12} = \frac{y_1/y_2}{q_1/q_2} \quad (3.7)$$

Assumptions

To apply the IAST methodology the following assumptions, given by Walton & Sholl, are made [119]:

- adsorbate molecules in the mixture have equal access to the entire surface area of the adsorbent
- The adsorbent is homogeneous
- The adsorbed phase is an ideal solution in which interactions between molecules are equivalent in strength

3.6.2. Binary selectivities

Binary selectivities for ethylene and other components in the gas mixture were calculated via IAST methodology with dual-site Langmuir isotherms. For more comprehensive overview, all binary pairs in the gas mixture of all literature sources are included and allows for quantitative comparison between different activated carbon types. The analysis results for 298K and 1 bar are given in Figure 3.3 and are plotted as function of the gas mole fraction of the most adsorbed specie of both, so selectivities are always greater than 1. Missing in this overview is the binary mixture of ethylene and carbon mono-oxide due to lack of experimental data.

Additionally to the selectivities already presented in section 3.2.4 a more extensive analysis is provided in the coming section for five binary gas mixtures. For the first binary mixture C_2H_4/CO_2 (Figure 3.3a) two different datasets are used, the dataset of Reich is the same used by Zandvoort et al. and their calculations generated identical results, verifying that the used calculation methodology is correct [67]. The dataset of Osterkamp provided slightly lower IAST selectivities, however is in the same range, strengthening the case that the general selectivity is in this region. For the CO_2/CO mixture (Figure 3.3c) the difference between different AC types is clearly visible; for identical conditions the IAST model predicts a selectivity range between 8 and 13. Differences in surface area, pore and micropore volumes, BET and external surface areas contribute to these varying selectivities [66]. Based on the relative selectivity of the C_2H_4/CO_2 and CO_2/CO mixtures, it is reasonable to assume that C_2H_4/CO selectivity will be of a similar magnitude. Low affinity of AC for hydrogen is observed in Figure 3.3b and d, for ethylene/ H_2 only a single dataset is used and yielded a selectivity of 200 to 225. For CO_2/H_2 the selectivity varied quite significantly ranging between 120 for the Park dataset and 250 for the Grand data set. This effect can partially be explained by different AC particle characteristics, but additionally the fitted parameters for the hydrogen isotherm for the Lopes and especially the Grand dataset are less reliable because of the method of data collection, see section 3.5. Similarly, the difference in selectivity for CO/H_2 mixtures (Figure 3.3e) can be explained.

Concluding from this IAST analysis is that 1. selectivity between C_2H_4 and CO_2 is limiting and therefore essential in final adsorber design; 2. Difference between AC types are significant and have major influence on the ultimate selectivity.

3.6.3. Limitations and extensions to IAST

The IAST methodology is a simplification of the real phenomena and therefore loses accuracy in case of non-ideal situations. For example IAST calculations are inaccurate when there is a non-homogeneous distribution of species throughout the framework; when there is strong hydrogen bonding between adsorbate molecules, e.g. water/hydroxyl or hydroxyl/aromatic mixtures; when segregation effects are present in the column, e.g. preferential sitting of adsorbates at the side of the column or in voids [15]. For example the IAST selectivity of ethylene and CO_2 on 5A zeolites predicts that recovery of ethylene from this mixture is not possible, while in breakthrough experiments it was observed that for feed ratios below unity recovery of ethylene was possible. The non-idealities describing this phenomena can be quantified using the Real Adsorbed Solution Theory (RAST) [120]

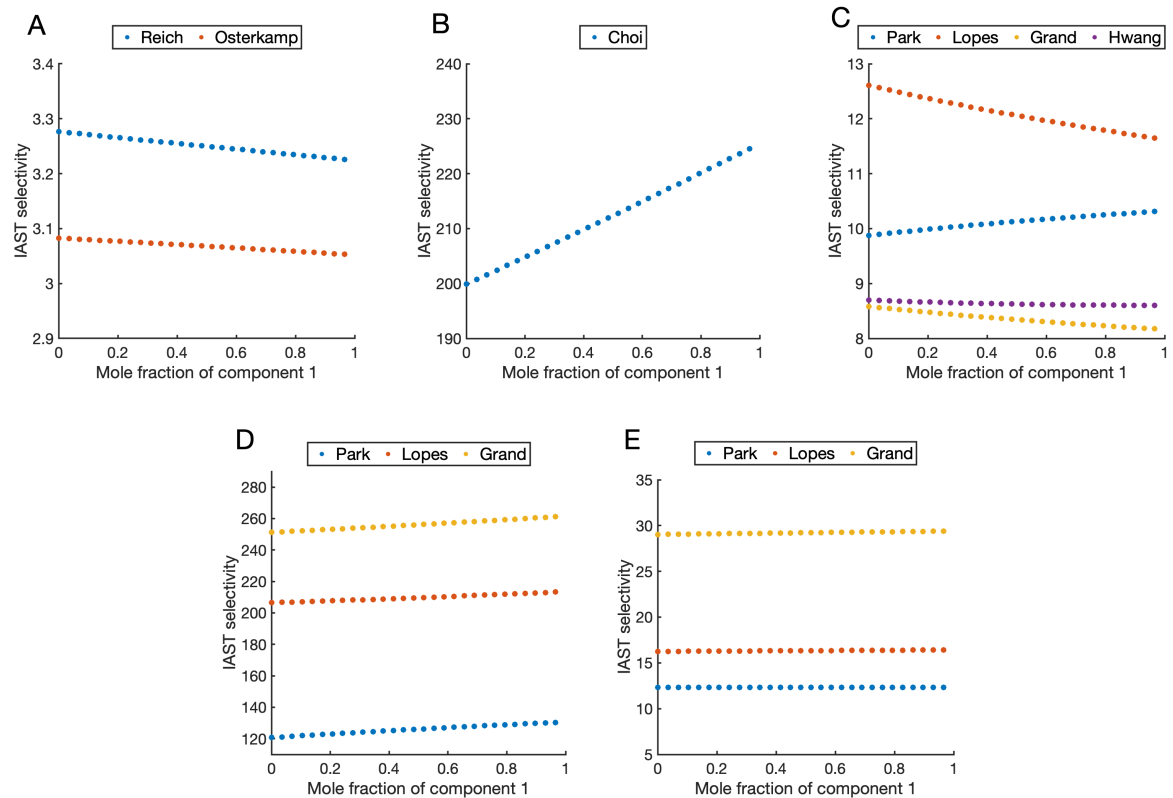


Figure 3.3: IAST selectivities for five binary mixtures at 298K and a total pressure of 1 bar. A: C_2H_4/CO_2 B: C_2H_4/H_2 C: CO_2/CO D: CO_2/H_2 E: CO/H_2 . For information on the references, see [Table 3.3](#)

In the analysis given above only binary mixtures were examined, but the IAST methodology can be extended to multiple components, however as a mixture gets more complex, it will start deviating from ideal conditions. The departing from ideality is mainly contributed from heterogeneity of the adsorbent and the increasing variation between adsorbate molecules. If the contribution of the adsorbate-adsorbate interaction is significant relative to the adsorbate-adsorbent interactions, the system will be governed by adsorbate interactions and consequently lead to non ideal behaviour [121]. Bachman et al. report IAST methodology for a five specie mixture and used it to predict equilibrium conditions for various separation stages and in their calculation obtained 99.9% pure ethylene. However the authors mention no accuracy of the calculation nor do they provide an experimental data to verify their results [26].

3.6.4. Effect of water vapour on AC

It is known that water adsorption onto active carbon is classified as type V isotherm, meaning that for increasing pressure initial uptake is slow, followed by a steep increase, before slowly reaching saturation (Figure 3.2). Lopes et al. investigated the adsorption of water on AC in a gas mixture containing H_2O , CO_2 , CH_4 , CO , N_2 and H_2 ; it was found that water adsorbed most of all components in this mixture [118]. A similar conclusion was obtained by Cen et al., who investigated the effect of 3% water vapor in flue gas for CO_2 capture. The adsorption of CO_2 on AC is negatively affected when water vapour is present and further decreases over multiple adsorption-desorption cycles. This effect could be contributed to water vapour exhibiting unfavourable competition with CO_2 . Moreover, after an increasing amount of cycles, blockage of the pore entrances would lead to additional diffusional resistance towards the active sites of AC [122].

Because of this strong adsorption of water, it is often removed in industrial PSA processes. Multiple approaches exist to remove this water; for example adsorption based methods include: a separate separation unit containing active silica or alumina as adsorbent, or use the initial layer of the active carbon bed as water remover [118].

3.7. Kinetics

Kinetics or more specifically mass transfer kinetics is an all-inclusive term that is used to describe intraparticle mass movement. Knowledge concerning the kinetics of an adsorber bed is essential as it controls the rate of adsorption and desorption phases in a cycle [91]. Slow kinetics will lead to dispersed breakthrough behaviour and fast kinetics in turn lead to very sharp breakthrough fronts. Generally physical rate of adsorption is controlled by four steps [29];

1. External mass transfer. This is a thin film surrounding the adsorbent particle where the outside border is at solute bulk concentration and the inside is at the solid outside border of the adsorbent particle.
2. Internal mass transfer. This term describes the diffusion from the outside of the adsorbent particle towards the inner pore structure.
3. Surface diffusion of the solute inside the pore surface
4. Adsorption onto the porous surface.

3.7.1. Governing kinetics of gases in activated carbon

In reality for gas-phase systems the effect of the thin film layer is marginal compared to the diffusional limitations. This implies that kinetic behaviour is governed in the macro- and/or micropore region [58].

Diffusion in macro- and mesopores

Macropores (> 50 nm) and mesopores (ranging 2 to 50 nm) are categorised together as in both the same four diffusion types are distinguishable. In these pore size regions, when pore size is large relative to the free mean paths a gas particle travels, bulk diffusion is dominant. For decreasing pore size or lower pressure, particles will have a large change to collide into walls and Knudsen diffusion will become dominant. Additionally at high pressure or large pore size, influence of forced convection or Poiseuille flow will play a role. Finally the fourth type, surface diffusion can occur when the gas phase molecules are sufficiently mobile and pressure is high. Last two types of diffusion are in parallel with bulk and Knudsen diffusion and are therefore additive [58].

Diffusion in micropores

In the case of micropores (< 2 nm) diffusion, pores are of equal size order as the diameter of the gas molecules and the molecules are continuously attracted to the solid phase. In these pores it does not make sense to distinguish between adsorbed or gas phase molecules and it is common to assume all molecules are in the adsorbed phase. The driving force of this diffusive process is the difference in chemical potential, which in an ideal case will yield Ficks first law of diffusion. Secondly, contrary to bulk or Knudsen diffusion, micropore diffusion is strongly dependent on temperature and is generally described using an Arrhenius exponential [58].

3.7.2. Modelling of kinetics

To mathematically describe all mass transfer and diffusion types described in the previous section into one system is an enormous task. This model would require knowledge of inaccessible parameters (i.e. diffusion coefficients for all species), while also being a highly non-linear system. Simplification of the system would lead to less bulky systems, while retaining accurate solutions. In reality micropore diffusion is the rate limiting step for most adsorbent systems and this can be described by a setting up a mass balance over the adsorbent particles. This would however still require solving bulky differential equations with additional boundary conditions. To overcome this issue, the differential equation can be substituted by a simple linear rate expression, e.g. the linear driving force (LDF) model [29]. This model assumes all diffusion and mass transfer rates are packed into one first order rate constant k . This model is commonly used to describe adsorbent beds and provides a reasonable prediction for a wide range of operating conditions [58].

3.8. Pressure Drop/Fixed bed dynamics

Additionally to kinetics, large scale (flow and mass transfer) behaviour of the adsorber bed is essential for designing the separation system. Dimensionless relations are often used to generalise flow and mass transfer behaviour inside fixed bed columns, some expressions that are very common are the Reynolds, Peclet and Nusselt numbers.

As mentioned in the previous section, mass transfer coefficient k is used to describe all transport from the gas to the solid phase. It is dependent on properties of the flowing medium (density, viscosity and diffusion coefficient), flowrate of the medium and adsorbent particle diameter. For low Reynolds numbers¹ ($Re < 50$) an adaptation of the Colburn-Chilton j-Factor given by Yoshida et al. [91], see Equation 3.8. Where ψ is the particle shape factor and the modified Reynolds number is given by $Re' = \rho v_s / \mu \psi a_i$ and $a_i = \text{interfacial area/volume} = 6(1 - \varepsilon) / d_p$. Generally it is desired to have a large mass transfer coefficient and from Equation 3.8 two useful relations are extracted that can easily be adapted to control mass transfer rate. First that $k \propto v_s^{0.49}$, meaning for two times higher velocity the mass transfer increases only by factor 1.4. Controlling flowrate is straightforward, however the major disadvantage of increasing velocity is that it is inversely proportional with time and therefore adsorbate has less time to form an equilibrium with the adsorbent phase.

$$J_d = \frac{k}{v_s} Sc^{2/3} = 0.91 \Psi Re'^{-0.51} \quad Re < 50 \quad (3.8)$$

Secondly, $k \propto d_p^{-0.51}$, meaning to increase mass transfer by a factor 2, particle size has to decrease by a factor 0.7. Smaller particle size inherently will increase flow resistance in the adsorbent bed in the form of pressure drop. The pressure drop in a fixed bed is commonly described using the Ergun equation (Equation 3.9) and consists of a laminar region (left hand side) and turbulent region (right hand side). The pressure difference is quadratically inversely proportional to the particle size for the laminar region and inversely proportional for the turbulent region. Also related to pressure drop is the ratio between length and diameter of the column. For small L/D, a lower pressure drop is seen, but flow distribution is more difficult to control and the system is susceptible to dead volumes and vice versa for high L/D.

$$\frac{\partial P}{\partial z} = \frac{150\mu}{d_p^2} \frac{(1 - \varepsilon_b)^2}{\varepsilon_b^3} u + \frac{1.75L\rho}{d_p} \frac{(1 - \varepsilon_b)}{\varepsilon_b^3} u|u| \quad (3.9)$$

3.9. Application review and Process design

The main focus in this stage is on adsorbent properties, but as mentioned in the introduction of this chapter, more considerations are essential for developing a separation system. Regarding the application of a fixed bed with AC as adsorbent, it is advantageous to know how the bed responds to different temperatures, both in the adsorption and in the desorption phase, other considerations as fouling or energy requirements should be kept at the back of your mind. Full process development is too early in this stage; however thinking about factors that could reduce maintenance or safety risks, will be beneficial in later process design stages.

¹The Reynolds number in the experiments in chapter 4 is below 50, therefore not the original Chilton and Colburn analogy is given, but the Yoshida adaptation

4

Experimental Procedure

4.1. Introduction

After the process of screening potential adsorbents in the previous chapter, transient breakthrough experiments are performed. Various test set-ups or commercial equipment are being used for these type of experiments. For example Zandvoort et al. report the use of a Flowrence platform, which is a specialised tool that is capable of simultaneous and flexible testing of 16 adsorbent materials [67], [95], [120]. When such highly specialised equipment is unavailable, a custom made solution is a good alternative, for example Bachman et al. report a sample holder immersed in a water bath, fed by a feed controlled with mass flow controllers and then measuring the outflow composition using a mass spectrometer or gas chromatograph [26]. In this chapter the development of a simple, custom-build experimental set-up is described which can be used to analyse adsorbents and examine their ethylene capture abilities. The results of these experiments can subsequently be used for verification of numerical simulations, which are essential when developing a separation process.

4.2. Adsorber bed design

4.2.1. Geometrics of the column

The function of the adsorbent bed is to hold the adsorbent material in place and to ensure that the desired adsorbate is captured. The main design parameters of the adsorbent bed are its length and diameter. Previously mentioned in section 3.8, high L/D will lead to less dead volume in the column, better flow distribution, but higher pressure drop compared to a low L/D ratio. For the experimental work it is considered more important to have sharp breakthrough behaviour and improved flow distribution then reduced pressure drop. Additionally high L/D ratio allows for quick heat transfer.

To find a suitable L/D ratio is dependent on the system conditions, industrial systems commonly have ratios ranging between 2.5 and 4 [123] but ratios between 10 up to 75 are more common for lab scale experiments. To allow for not-to-long breakthrough times of around 5 minutesⁱ and flowrates that are not high, to reduce chemical gas use and waste, a L/D ratio of approximately 20 is used. Since standardised Swagelok tubing is used, the column is bound to a limited amount of diameters; for an outer diameter of 12 mm and corresponding internal diameter of 9 mm, a bed length of approximately 180 mm is found. Further it is suggested to have a column diameter/particle diameter ratio of approximately 50 to avoid channelling effects [124], with an average particle size of 0.15 mm (see section 4.2.2) and a diameter of 9 mm, this ratio is 60. Including the inert place holders, the total length of the bed will be 250 mm.

4.2.2. Adsorbent properties

The two main adjustable adsorbent properties influencing the behaviour of the column are the particle diameter d_p and the bed porosity ε_b . No unambiguous method exists for determining the ideal particle diameter and Gabelman states that the preferred particle size is the smallest one that still has a tolerable pressure drop [125]. For example for gas separation process in industrial applications larger mesh

ⁱBecause sample taking is done manually, faster breakthrough times will result in less sample taking

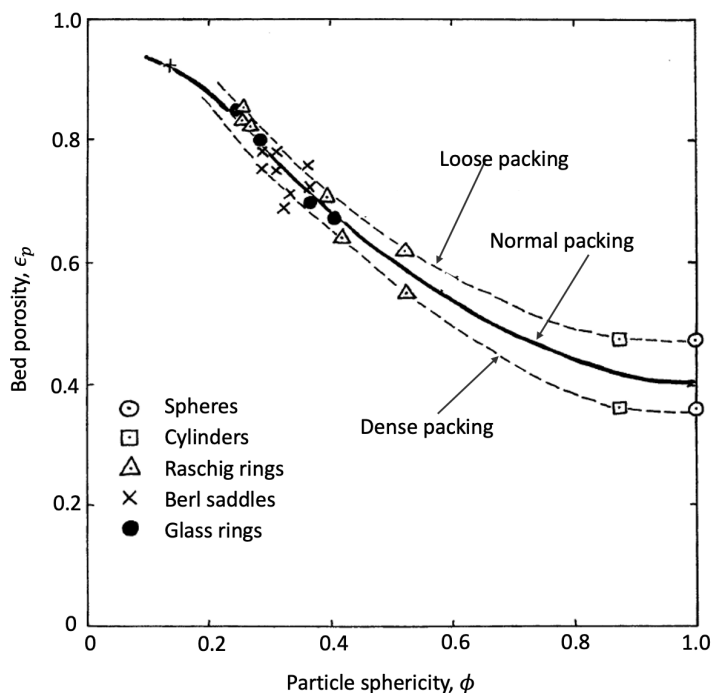


Figure 4.1: Dependence of particle sphericity and packing density on bed voidage. Modified from Levenspiel [126]

sizes (6×10 or 6×16 mesh size) are commonly chosen (see Table 3.3).

At the time the experiments were performed, two types of activated carbon were available in the lab, e.g. granular 4×8 mesh and 100 mesh. Based on the heuristic Gabelman mentioned, the smaller particles were chosen for the experiments. Besides the 4×8 mesh are quite sizeable compared to the column diameter and would without crushing them into smaller particles, lead to voids and excessive wall effects. Note that active area of the adsorbent varies marginally with different particle size, as most active area is inside the pores and an insignificant amount on the exterior surface [125].

The bed porosity is determined by the amount of adsorbent in the column with respect to the empty space, note that this is not the same as the particle porosity which is the void inside the particle. The bed porosity can for example be controlled during the loading of the adsorbent into the column, when applying force on the adsorbent a more dense loading can be achieved. The advantage of a more densely packed bed is that more mass of adsorbent occupies the same volume in the bed, disadvantage is that this decreases bed porosity and therefore increases the pressure drop. The dependence of sphericity and packing density for various particle geometries is displayed in Figure 4.1.

4.2.3. Other factors

The safety risk for this type of set-up is low and no additional measures were taken. Because of the low flowrates, the gases leaving the column were directed away from the user and purged into the air.

4.3. Chemicals

CO₂, N₂ and Ar were accessible in the lab though build-in gas lines. Ethylene or C₂H₄ (99.5%) was purchased from Sigma-Aldrich in a 14L pressurised cylinder and used without any further purification. Activated Charcoal DARCO G-60, 100-mesh particle size was used from Sigma-Aldrich and was used without modification.

4.4. Experimental set-up

4.4.1. Framework

Breakthrough experiments were conducted using a custom-build set-up consisting mainly of Swagelok fittings and 6 mm teflon tubing. The flowchart of the set-up is given in [Figure 4.2](#) and additionally a picture of the set-up is provided in [Appendix C](#). The adsorber column consists of 12 mm Swagelok tubing and can be circumvented using a bypass, from which the composition of the gas mixture can be measured directly. A cylinder containing ethylene gas is connected to the system using a Dräger pressure reducing valve. The remaining gases are fed to the system by installed gas lines in the lab. Pressures of all gases could be regulated between 0 and 7 bar. The composition of the gas inflow was regulated using Omega FL-2501-VL rotameters and were subsequently mixed in-line to produce the gas mixture. Due to the low viscosity of gases, further mixing (for example using mechanic agitation or a static mixer) is rarely needed and in most cases a long pipe with turbulent flow does suffice [127]. The adsorber column is connected to the system using two 6x12 mm tube fittings which in turn also keep the inert material in place. The adsorber bed is held in place by 3 cm of glass wool on top and bottom sides to prevent possible migration of solid material through the inlet or outlet.

4.4.2. Column

The column and its supporting valves are held in place by a dual adjustable clamps. Temperature of the column is controlled by RKC Instruments SB1 digital temperature controller fitted into a IP65 distribution box. The controller was connected to Horst HB Heating tape with Textile Glass Insulation and was chosen for its ability to fit small radii. The thermocouple was installed underneath the heating tape and measures the temperature at the end of the tip at approximately halfway of the column. The tape was densely packed over the full length over the column to allow for quick and efficient heating. The heating tape was fixed in place and isolated using fiberglass tape bound together with aluminium tape.

4.4.3. Loading of the column

The unmodified AC was loaded into the column straight from its packaging container. Important is the way the adsorbent is loaded, the AC can be pressed to create a dense bed or can be loaded gently to create a more loosely packed bed. The way this is loaded affects the bed porosity, the interstitial velocity and ultimately the breakthrough time. As the particle diameter is small compared to what is commonly used in industrial applications, adsorbent was packed as loosely as possible into the column.

4.4.4. Fraction collection

To determine the outflow composition, fractions were collected at predefined timesteps using disposable 3 mL syringes and were closed air tight using syringe valves. The syringes valve could be connected to the 6 mm tubing and this connection was considered air tight. After each experiment the labelled syringes could all separately be analysed using the micro GC. By preliminary analysis, breakthrough times could be estimated and the frequency interval of sample taking could be increased to have additional datapoints at times outflow composition is changing rapidly. After each experiment all syringes were flushed two times with nitrogen and stored full of gas for the next run.

4.4.5. Micro Gas Chromatograph

The composition of the out flowing gas was analysed using a Varian CP-4900 micro gas chromatograph (micro GC). First introduced in 2003, this micro GC is a small, compact and portable gas analyser intended for on-field analyses of natural gas, refining, specialty gases or fuel cell samples. It consists of two columns fitted with a micro-machined Thermal Conductivity Detector (TCD), which is a common detector used in gas chromatography. At the time of manufacturing the supplier stated that the operating range is between 1 ppm and 100% [128]. Calibration was done before the start of the experiments by TU Delft technicians after discussing the requirements of the set-up. After calibration of all components the settings were kept constant for all experiments.

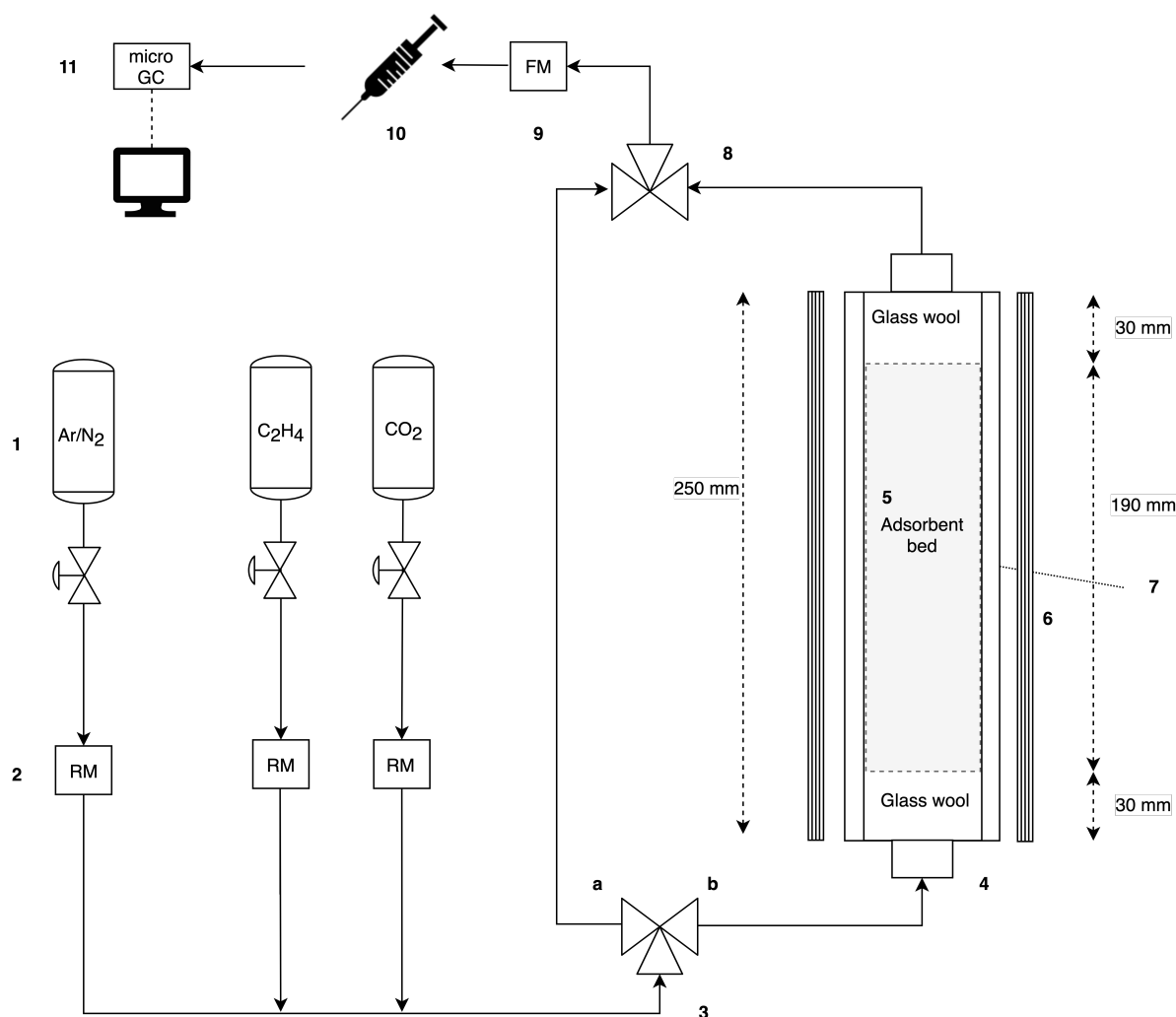


Figure 4.2: Flow chart of the experimental set up. 1 Feed of chemicals; 2. Rotameters; 3a. Bypass 3b, Feed to column; 4. Column fittings; 5. Adsorbent bed; 6. Heating tape; 7. Temperature sensor; 8. 3-way valve; 9. Flowmeter; 10. Sample collector 11. Micro GC

4.4.6. Limitations of set up

Comparing this set up to the flowrence platform used by Zandvoort et al. or the set up used by Bachman et al. controlled by digital mass flow controllers and flowmeters, described in section 4.1, this simpler, cheaper set up is bound to lose accuracy in flow and composition control. Nonetheless this set-up should be able to study the qualitative behaviour of gas adsorption.

A few examples of limitations that were encountered were:

- Rate of sample taking; because of the manual operation sampling rate is limited to one sample every 10 seconds. However at this maximum rate human errors are more likely to occur.
- Analysing time per sample; since the micro GC required 9 minutes per sample, continuous sampling was not possible as the interval would simply be too large. The micro GC did not allow for simultaneous measurements.
- Because of the manual sample taking, long analysing time and flushing of the syringes air contamination was inevitable.
- The rotameters were used on the lower limit of their operating range; the means accurately controlling the flowrate was difficult. Additionally small changes in pressure in feed lines, also influenced the flowrate.

- Age limit of the micro GC; all equipment deteriorates over time therefore it is not unusual the accuracy has decayed.
- Sensidyne Gilian Gilibrator 2 was used for flow measurements and was not able to take automated, continuous measurements.

4.5. Column heating

For the desorption experiments it is essential to know how much time is required to heat the column to a uniform temperature. The most accurate approach would be to solve a time dependent heat balance over the radius of the column, alternatively the Fourier instationary heat transfer relation is used. To use this relation the following assumptions are made: 1. The wall of the column is at constant temperature T_w ; 2. the column is considered homogeneous in temperature when $\bar{T} = 0.99T_w$; 3. Since the column consists of two composite layers, e.g. the metal tubing and the adsorbent bed, the lowest thermal diffusivity of both layers is used; 4. the heat transfer from the heating equipment to the wall and from the metal layer to the adsorbent bed is neglected; 5. The column is considered infinitely long.

First the temperature ratio \bar{M} is determined via Equation 4.1, where T_w is the wall temperature, \bar{T} is the average temperature at time t and T_0 is the initial bed temperature. Subsequently the Fourier number is determined using the Heisler chart provided by Janssen and Warmoeskerken in their Transport Phenomena Data Companion [129]. Using the relation for the Fourier number $Fo = \frac{at}{D^2}$, the time required to reach a homogeneous temperature can be determined. Here a is the thermal diffusivity and D is the characteristic diameter, in this case the diameter of the column. For active carbon $a_{AC} = 2.03e-6 \text{ m}^2 \text{ s}^{-1}$ [130] and for type 310ⁱⁱ steel $a_s = 3.40e-6 \text{ m}^2 \text{ s}^{-1}$ [132]. The results for $T_w = 308, 318, 328$ and 353K are given in Table 4.1.

In reality the first assumption is not realistic, as the column is heated the wall temperature rises accordingly. However when comparing the time required to reach 99% homogeneity with constant wall temperature (t_{99}) with the time required for the heating tape to reach the setpoint temperature (t_{SP}), it is seen that the duration of heating is a factor 4–5 longer than the homogenisation time, meaning the heating rate of the system is limiting. In reality this implies that the time the setpoint temperature is reached, it can be assumed that the temperature in the column is at approximately homogeneous temperature.

$$\bar{M} = \frac{T_w - \bar{T}}{T_w - T_0} \quad (4.1)$$

4.6. Numerical analysis of breakthrough times

4.6.1. Mass balance

To obtain quantitative information about the separation performance, breakthrough data is analysed numerically. The required data consists of the volumetric fraction of each specie of the outflowing gas (y_i) with respect to time. The separation performance is compared in terms of breakthrough time (t_b), uptake capability of specie i (q_i), mole fraction in the solid phase (x_i) and selectivity ($S_{i,j}$). The calculation of these parameters is done using the following methodology. First the breakthrough time is

ⁱⁱSwagelok fittings and pipes are made of type 316 steel, type 310 steel however has very similar thermal properties [131]

Table 4.1: Overview of applicable heating times in the adsorber bed. t_{99} was determined using Heisler charts and t_{SP} was measured experimentally.

T_w [K]	\bar{M}	Fo	t_{99} [s]	t_{SP} [s]
308	0.035	0.16	11.3	40
318	0.023	0.18	12.8	55
328	0.018	0.20	14.2	70
353	0.006	0.28	19.9	90

defined as the time were the concentration in the outlet stream has reached >5% of the inlet concentration. Next the uptake capacity of each specie is determine via a material balance to determine the amount of gas transferred from the gas phase to the solid phase. The mass adsorbed is simply the difference between the inlet and the outlet concentration over a given time range, with an additional term accounting for the dead volume fraction in the column.

$$m_{i,ad} = m_{i,in} - m_{i,out} - c_t y_{i,exit} (V_{col} - V_{ads}) \quad (4.2)$$

where V_{col} is the column volume given by $A \cdot L$ and V_{ads} is the apparent or bulk volume. However to determine V_{ads} experimentally is not straightforward and the ultimate effect of the dead volume on the selectivity calculation is small, therefore it is neglected. The amount of mass fed to the column for a constant inlet concentration of specie i is multiplied by the total flowrate and a given time period, given in Equation 4.3. The amount of material leaving the column is calculated similarly, except that the outflow fraction is dependent on time and is calculated by integrating the area under the breakthrough curve, depicted in Equation 4.4. The loading can subsequently be determined by plugging in these equations into Equation 4.2 and using that $m_{i,ad} = q_i \cdot m_{ads}$, where m_{ads} is weight of the adsorbent in the column. The result is given in Equation 4.5.

$$m_{i,in} = c_t y_{i,in} Q (t_2 - t_1) \quad (4.3)$$

$$m_{i,out} = c_t Q \int_{t_1}^{t_2} y_{i,out} dt \quad (4.4)$$

$$q_i = \frac{c_t Q}{m_{ads}} \int_{t_1}^{t_2} (y_{i,in} - y_{i,out}) dt \quad (4.5)$$

Subsequently the mole fraction of specie i in the solid phase is given by Equation 4.6. The selectivity for a binary mixture is given by Equation 4.7.

$$x_i = \frac{q_i}{\sum_{j=1}^n q_j} \quad (4.6)$$

$$S_{12} = \frac{q_1/q_2}{y_1/y_2} \quad (4.7)$$

To evaluate the integral of Equation 4.5 the outlet composition data of need to be transformed into some continuous function. Three commonly used techniques to numerically estimate the area under the curve are the midpoint rule, trapezoidal rule, and Simpson's rule. The midpoint rule approximates the area using rectangular Riemann sums with equal width. This method is accurate when the amount of intervals becomes really large, however in the case of limited data points this method is inaccurate. Alternatively, the curve in between data points is approximated linearly, in this case the area is approximated using trapezoids instead of rectangles, e.g. trapezoidal rule. It is important to note that when the concave is up, the trapezoidal approximation tends to underestimate the area under the curve and vice versa.

For type I adsorption isotherms (section 3.4.1) the expected function has a sigmoid or "S"-shaped curve and to better account for this shape the curve in between data points can better be approximated using a parabolic formula. This is known as Simpson's rule or parabolic rule. Compared to the trapezoidal rule, Simpson's rule uses multiple weighted data points to estimate the shape of the parabola. Generally is it considered that the Simpson's rule yields the most accurate results [133]. To test if this statements holds when the amount of datapoints is limited, an numerical analysis done.

4.6.2. Accuracy of numerical analysis

To examine the performance of trapezoid and Simpson rule on a sigmoid shaped function they are compared with a function with similar shape. This function (Equation 4.8) is chosen to behave similarly as the mass transfer zone seen inside an adsorber column. Advantage of this function is that α can be altered to change the slope of the curve, this way the approximations can be verified for various types of MTZs. Another advantage is that for any value of α the integral between 0 and 1 will have the same solution, e.g. 0.5, making comparison to trapezoid and Simpson approximations straightforward. The trapezoid calculations are performed using the MATLAB build-in function `trapz.m` and the parabolic calculations are performed using an adaptation of the `trapz.m` function, `simps.m`. This code was retrieved from MATLAB file exchange, an open source community driven platform, and used without modification [134]. Noteworthy is that both functions work for any length array, are able to handle arbitrary spaced data points and are vectorised for short run times.

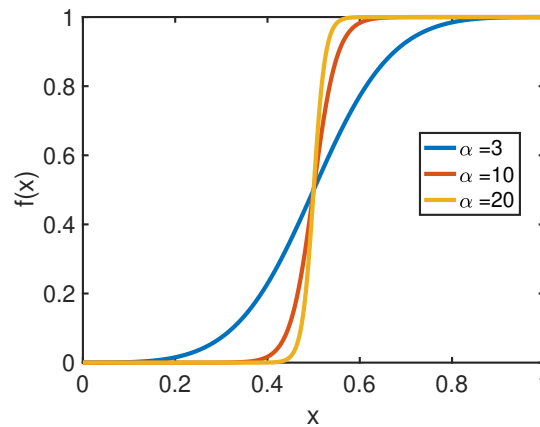


Figure 4.3a: Plot of an analytical sigmoid function for increasing α

To simulate the unevenly distributed time steps encountered in experiments, the space vector was divided into n -distributed points, each having a $U(0,0.1)$ deviation, only the initial, halfway and final coordinates ($x = 0, 0.5, 1$) were fixed in all simulations. The numerical analyses was performed for eight semi-arbitrary values of α , ($\alpha = 3, 5, 10, 15, 20, 30, 40, 50$), to account for wide and sharp MTZs. In Figure 4.3a it is observed that for increasing α , the slope becomes steeper. The amount of data points in the experimental section is limited; it is expected that for a low number of data points the integration can have a significant error. The significance of this effect is tested in the analytical function by using an increased amount of data points, for $n = 10, 15, 20, 30, 100$. To eliminate any integration outliers due to the random distribution of the spacial coordinates, this analysis is repeated 10 000 times, essentially making this a Monte Carlo simulation. From the results, the relative error (Equation 4.9) is calculated for each combination of gridsize and α and used to calculate the percentual error with respect to the exact solution. The result is depicted in Figure 4.3b, where the results for each n are subdivided in rectangles. Qualitatively analysing the error for increasing n it is observed that error decreases, for example the error for $n = 100$ remains under 0.5% for all values of α . Secondly, for both types of approximation and all values of n it can be seen that for increasing α (cf. increasing slope) the approximation be-

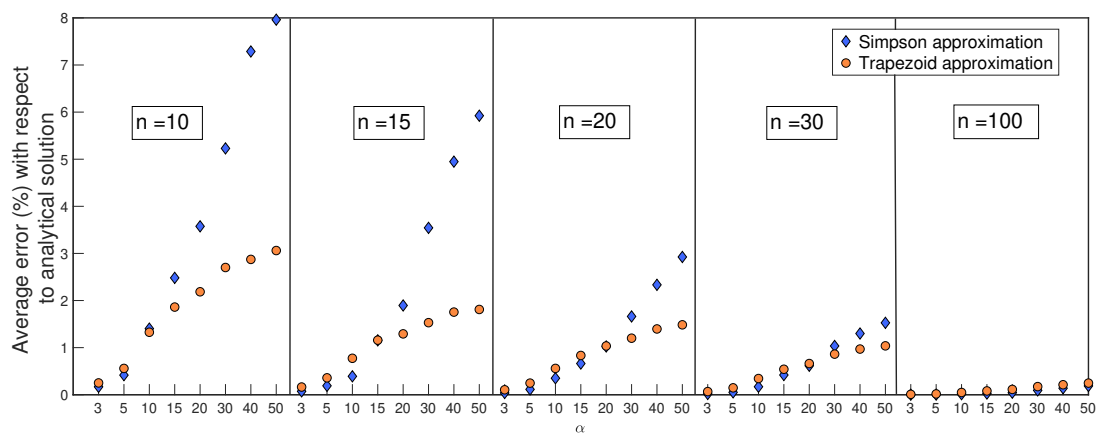


Figure 4.3b: Monte Carlo analysis of the Simpson and Trapezoid approximation for a sigmoid function

comes increasingly more inaccurate. For the first limit $\alpha \rightarrow 1$, Equation 4.8 becomes linear, no large changes of $f(x)$ are seen and can therefore easily be approximated. The increasing error effect can be explained by the change of nature of the function for increasing α ; when $\alpha \rightarrow \infty$, Equation 4.8 becomes a step function. In this limit, the change in $f(x)$ is too large and both approximations tend to break down. Finally, a significant error is seen for the Simpson approximation as α increases, especially for small values of n . It is hypothesised that the combination of polynomial fitting, which requires three points to determine the parabola, and the large change of $f(x)$ causes this large deviation.

Because the amount of samples taken in the experiments is small and the columns high L/D ratio is designed to have sharp mass transfer zones (cf. high values of α), which can lead to significant errors based on the type of approximation used. Based on this analysis, the trapezoid approximation is used for the numerical analysis of the breakthrough times.

$$f(x) = \frac{1}{1 + \left(\frac{x}{1-x}\right)^{-\alpha}} \quad (4.8)$$

$$\text{Error}_{\alpha,n} = \frac{1}{k} \sum_{i=1}^k \frac{|A_{i,\text{model}} - A_{\text{analytical}}|}{A_{\text{analytical}}} \cdot 100\% \quad (4.9)$$

5

Experimental Results

After the considerations for the experimental set-up in the previous chapter the transient breakthrough experiments were performed. The goal of these experiments was to test the newly build set-up, the separation potential of activated carbon and compare the results with the theoretical IAST calculations. Further will the results be used to verify the mathematical model given in [chapter 6](#).

First the results of the unary breakthrough experiments for C_2H_4 and CO_2 mixtures are given, the error in the system is analysed and then adsorption and desorption of C_2H_4/CO_2 binary mixture is investigated for different temperatures. Experiments are limited to C_2H_4 and CO_2 mixture, because of the safety risks that are associated with working with CO. As the experiments were performed on a limited time scale, upgrading to a CO-safe working environment would take considerable effort, besides the amount of fume hoods at the time of experiments was limited. Additionally, adsorption of H_2 on active carbon is very poor, studying breakthrough behaviour of C_2H_4/H_2 mixtures is less significant for the final separation process. Therefore this thesis focuses only on the C_2H_4/CO_2 binary mixture.

5.1. Unary breakthrough analysis

These experiments were conducted to test the performance of the set-up and to assess the behaviour of components in the column. The experiments were performed twice for each specie, because of varying flowrates and composition, only one run per specie is displayed. The unary breakthrough analyses were performed with an approximately equivolume feed with the remainder of the flow being an inert carrier, e.g. argon gas. Argon gas was chosen as it was possible to differentiate between air contamination (extensively explained in section 5.2) and the carrier gas. The results for C_2H_4/Ar and CO_2/Ar are given in [Figure 5.1](#). Flowrates of adsorbate gas streams were equal for both experiments, e.g. 60 mL min^{-1} , however the flowrates of the carrier were 65 and 82 mL min^{-1} for the C_2H_4 and CO_2 mixture respectively. The final composition measurements were taken at 600 seconds and were considered the steady state flowrates. Before analysing the experimental breakthroughs, it should be noted that the micro GC was unable to measure argon gas; therefore the percentage was determined by summing the volume fraction to 100%. Secondly the nitrogen seen in the diagram is the contamination that entered the system due to leakage or processing the samples. The amount of nitrogen in the system was between 0 and 2%.

As seen in the IAST predictions, adsorption of both C_2H_4 and CO_2 on active carbon is observed. The qualitative behaviour is as expected in an adsorber column; for ethylene, a sharp, sigmoid-shaped mass transfer zone which reaches the steady state feed concentration after saturation, the sharp breakthrough can be traced back to the large L/D ratio of the column. The mass transfer zone for CO_2 is broader compared to ethylene and takes longer to reach the state steady concentration. In particular, after the breakthrough of CO_2 , the outflow concentration increases rapidly before slowly reaching steady state. In the breakthrough experiments of Al-Janabi et al., similar behaviour is seen for a equivolume CO_2/N_2 mixture on AC [135]. When quantitatively comparing [Figure 5.1a](#) and [b](#) the first thing to notice is that the breakthrough times for C_2H_4 and CO_2 are almost identical, being 135 and 130

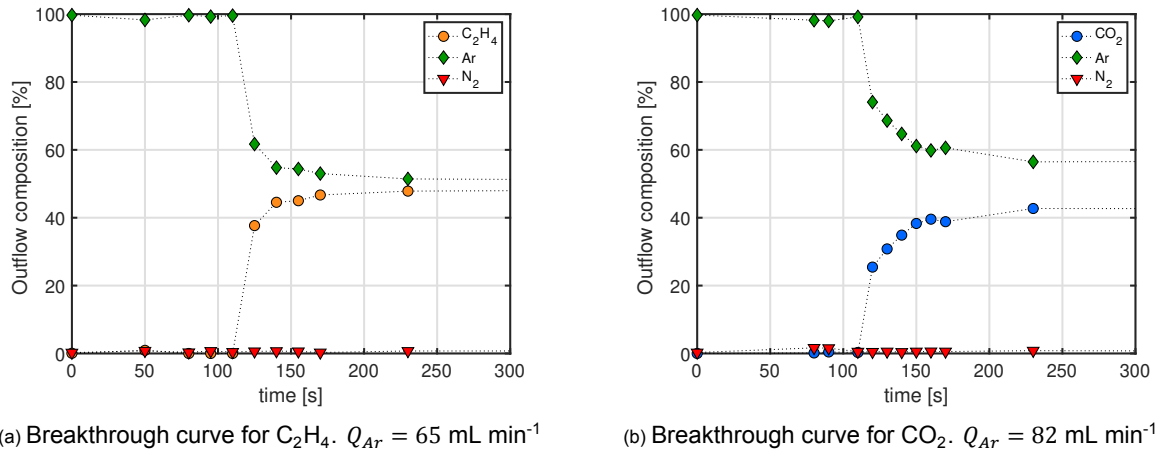
(a) Breakthrough curve for C₂H₄. $Q_{Ar} = 65 \text{ mL min}^{-1}$ (b) Breakthrough curve for CO₂. $Q_{Ar} = 82 \text{ mL min}^{-1}$

Figure 5.1: Unary breakthrough diagrams. Flow consisted of an approximately equivolume feed containing the adsorbent and the inert carrier; argon gas. $P_{feed} = 2 \text{ bar}$, $T = 298\text{K}$, $m_{ads} = 2.01\text{g}$, $Q_{adsorbate} = 60 \text{ mL min}^{-1}$

seconds. An important remark is that the feed concentration of CO₂ is lower than C₂H₄, e.g. 0.42 and 0.48 respectively. The uptake capabilities q_i (for calculation procedure, see section 4.6) for both components are 2.68 and 2.17 mol kg⁻¹ respectively. Two preliminary observations could be made until this stage; 1. ethylene uptake is larger than carbon dioxide uptake, however not substantially. This is an important observation, because this means CO₂ uptake in unary experiments is significant and could subsequently lead to lower ethylene selectivity in the binary experiments; 2. Based on the mass transfer zone, uptake of CO₂ is slower. An explanation for this effect could be that the mass transfer rate of CO₂ into the pores is slower compared to ethylene adsorption rates, indicating that ethylene diffuses into the pores quicker.

5.2. Error analysis of the system

5.2.1. Types of errors

As the set-up was custom build and untested, possible errors in the system should be carefully examined. Parts or steps that were susceptible to error are given below. From this list, the types of errors that were considered significant are discussed further and their effects are incorporated quantitatively in the results.

1. Air contamination due to sampling procedure
2. Calibration error
3. Random system error
4. Gas leakage
5. Syringe contamination
6. Measurement time error
7. Mixing error
8. Human error

1. Air contamination error

The manual fraction collection means that the system is prone to air contamination, as there is a brief moment the sample opening is in contact with air, meaning inevitably a small amount of air is present in the sample. This contamination is typically between 1 and 2 V%, however outliers up to 5V% are seen. As the contamination occurs before the sample is taken, it has no effect on the composition ratio and lead to a dilution of the outflowing gas. This diluting effect can become problematic when comparing composition at different timesteps, as this will cause a variable underestimation of the actual composition. To make uptake samples at different timesteps quantitatively comparable, it is assumed that the sample can be normalised. This means it is assumed when there were no contamination, the remaining composition scales linearly to fill the contamination void. This calculated is via Equation 5.1.

$$c_{i,norm} = c_{i,measured} + \frac{c_{i,measured}}{\sum_{k=1}^n c_{k,measured}} \cdot c_{contamination} \quad (5.1)$$

The main issue with this method is that initially there is air (measured as nitrogen) present in the set-up and this is not to be confused with the air contamination. Therefore it is assumed when the first sample amount of nitrogen is under 2V%, this is due to air contamination and the correction equation mentioned above is applied. Before this moment, in the initial phase of the experiment, there is no way of differentiating between contamination and air that was in the column before the experiment. Therefore it is assumed that the air contamination error initially is equal to the average of the last five measurements.

2. Random error

This error is associated with the repeatability of measurements, as identical measurements of the same sample should have identical results. The supplier of the GC, Varian Inc, reported in their original brochure a precision of 0.13% relative standard deviation for the measurements. [128]

Ideally, to eliminate or decrease the significance of this error, every experiment could be repeated multiple times and every measurement performed in duplicate or triplicate. In the current experimental procedure this would however be very time consuming and therefore an alternative method was used to estimate the size the system error. This method is based on analysing a pre-mixed sample of an approximately equivolume CO₂/N₂ mixture twelve times and determining the normalised standard deviation (nSTD). Details and procedure are given in [Appendix B](#). This resulted in standard deviations of $nSTD_{N_2} = 1.42\%$ and $nSTD_{CO_2} = 1.37\%$. It is assumed that the presence of one component in the mGC is not influencing the result of another component, and therefore that both variables can be considered independent. Subsequently both standard deviations are summed in quadrature to yield the normalised random error, $nSTD = 1.97\%$. Although this normalised error is based on a CO₂/N₂ containing mixture, it is assumed valid for all components for all volume fractions. The 95% confidence interval is consequently given by $1.96 \cdot nSTD$.

3. Calibration error

The mGC was calibrated with pure component gases before starting the experiments, but nevertheless physical inconsistencies were observed. In other words, the total volume fraction of the outflowing gas should always be 100%, but this was not always the case. In reality it was seen that for mixtures of gases the total volume percentage was on average a few percent short of 100%, indicating some sort of system error. Reasons for this bias could be due to bad calibration, attraction of molecules to each other in mixtures, non-linear behaviour of components on the column.

A normalisation step was done for two reasons. Firstly it makes measurements physically consistent, but more importantly it makes quantitative comparison possible, when assuming that all components can be scaled linearly with the same normalisation factor, independent of the fraction of that component. A side effect of this normalisation step is that the error determined in the previous sections is also affected, this error therefore scales with same factor.

Note the difference between the random error and the calibration error. As this random of error assess the ability of the GC to repeat measurements, independent of calibration or experiment.

4. Leakage

Gas systems are inherently sensitive to leakage. The system consists of Swagelok fittings and when installed correctly are considered air tight, especially for the low pressure system in these experiments. More susceptible to leakage are the disposable syringes. To test the air tightness over time the composition was measured once and then again after a 24 hour interval. From this simple test it was concluded that no nitrogen was measured in the syringe and it can be considered air tight. The syringe valve must of course be securely tightened and the syringe was unmoved over the time interval. Finally the syringe connection to the set-up and to mGC remain, the first connection is straightforward as the valves are made to fit directly into the 6mm tubing. More problematic is the syringe connection to the mGC which required a unique adaptor, this was custom made as no pre-fabricated adaptor was available. Although improvised, the adaptor showed no signs of leakage, as tests with pure ethylene or CO₂ showed no air contamination in the mGC.

5. Syringe contamination

To minimise the effect of contamination of the previous sample, each sample is flushed three times with nitrogen. Before each sample the nitrogen is purged and connected to the system, leaving trace amounts of nitrogen in the syringe. The effect of these trace amount are insignificant compared to the air contamination and therefore not included in this analysis.

6. Time measurement error

Samples are manually obtained from the system on predetermined time stamps and has two possible sources of error. First, the process of taking a sample takes roughly four seconds, meaning a sample is always the average composition over these seconds and secondly the manual factor implies that sample taking is never exactly on the predefined time stamp. Without an automatic sampling system it is impossible to prevent these errors and besides it is impossible to quantify or mathematically estimate the size of this error. Therefore the time error was chosen to be the same as the sampling time, e.g. four seconds.

7. Mixing error

Since the mGC requires samples in the order of microliters, inhomogeneous gas mixtures will lead to skewed measurements. As there is no straight forward way of verifying this is the case in reality, let alone determine the error associated with mixing, it is not included in this analyses and all samples are considered homogeneously mixed, including the sample to determine the random error.

8. Human error

As in any experimental procedure human error affecting measurements is never inevitable and is only excluded when experiments are repeated for multiple times.

5.2.2. Propagation of error and calculation

From the analysis of the previous section three error types are used to determine to 95% confidence interval of the volume fraction. The effect of the air contamination error and calibration error are based on the normalisation factor used to standardise the measurement, while the random system error is fixed for each measurement and scaled to relative amount of each component, resulting in general Equation 5.2, where $y_{i,n}$ is the volume fraction of specie i of measurement n , $\alpha_{ace,n}$ and $\alpha_{ce,n}$ respectively the normalisation factors of air contamination error (ace) and calibration error (ce) for measurement n and nSTD the normalised system error. The coefficient 1.96 is used to find the 95% confidence interval [136]. All terms in the equation are dimensionless.

Time scale related error was used as described in the previous section and the 95% confidence interval is estimated to be equal to the sampling time, e.g. four seconds.

$$y_{i,n} = y_{i,n} \pm 1.96\alpha_{ace,n}\alpha_{ce,n}nSTD \quad (5.2)$$

5.3. Binary breakthrough experiments

From the unary breakthrough experiments and the adsorbent screening, it was observed that activated carbon has greater affinity towards ethylene than to carbon dioxide. Using binary transient breakthrough experiments the actual separation potential of DARCO G-60 activated carbon could be evaluated.

5.3.1. Experimental results

The results are displayed in Figure 5.2 including the 95% confidence intervals described in the previous section. Reviewing these binary transient breakthrough experiments it is immediately clear that two fronts have formed. For example in Figure 5.2a for $T = 298K$, first the CO_2 front breaking through after 160 seconds and secondly the C_2H_4 front after 220 seconds, verifying that the bed is ethylene selective. Noticeable is the sharpness of the CO_2 stoichiometric front compared to the ethylene front. It is hypothesised that the sharpness can be explained by a 'pushing' effect, where the nitrogen in the column is pushed out of the column by the entering feed. The phenomena will be discussed more extensively in section 6.7.4.

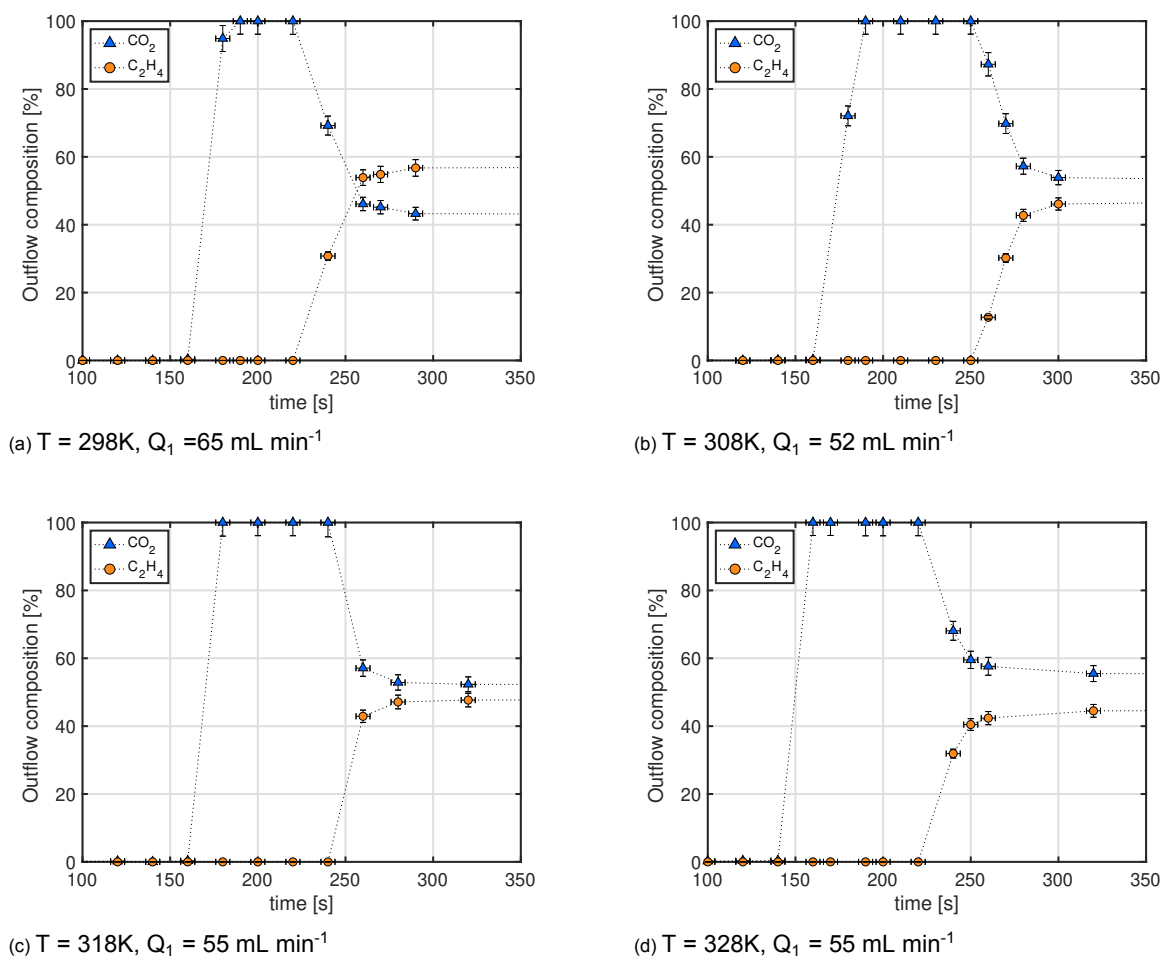


Figure 5.2: Transient breakthrough experiments for $\text{C}_2\text{H}_4/\text{CO}_2$ gas mixtures for various temperatures (298K–328K) with inlet pressure of 2.5 bar. The remainder of the composition is nitrogen left in the column after purging.

Similarly to the unary breakthrough analysis, the adsorption uptake q_i is calculated and is displayed in [Table 5.1](#). For a complete overview the volume feed fraction y_i and selectivity S are included. Inspecting the selectivity values it is immediately clear that those are significantly lower than what the IAST calculations predicted, e.g. between 1.5 and 2 for the experiments versus 3 and 4 for the predictions. This means that the separation potential of the adsorbent bed is lower than the IAST predictions would suggest. The question that arises is, why is the selectivity in these experiments so low compared to the predictions.

5.3.2. Comparison to IAST methodology

To answer this question, first the IAST calculations are investigated in more detail. In [Figure 5.3](#) a quantitative comparison between the IAST calculations using isotherm data of Reich and Osterkamp (given in [A.2](#) and [A.3](#)) and the numerical analysis of the breakthrough time is shown. To reduce the effect of ambiguous behaviour of identical species on various AC types, two isotherms sources were used in the IAST prediction. The ethylene fraction y is displayed as a function of molar fraction in the adsorbed phase x , where for a binary mixture $x_1 = q_1/(q_1 + q_2)$. In [Figure 5.3a](#) the breakthrough mixture $\text{C}_2\text{H}_4/\text{CO}_2$ with a summed partial pressure of 0.4 bar given by Zandvoort et al. is compared with IAST calculations and adsorption experiments of Bering and Serpinsky. They studied the adsorption equilibria of ethylene and propylene on activated carbon between 0.07 and 0.36 bar [[137](#)] and the data for 0.36 bar is depicted in the figure. Upon inspection it can be seen that the experimental equilibria correlate well with the IAST predictions. It should be noted that three different types of active carbon were examined, however this verifies that AC is ethylene selective independent of the type used. The

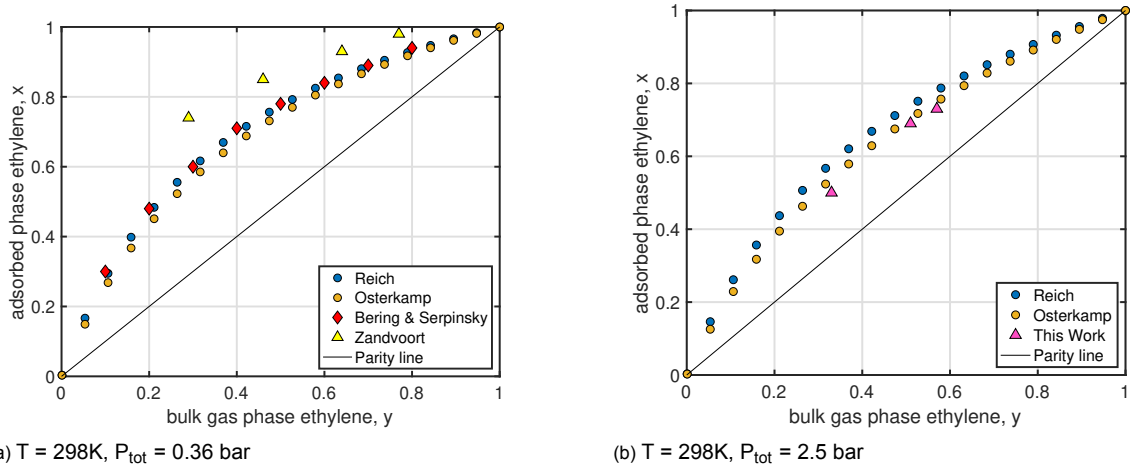


Figure 5.3: Comparison of theoretical IAST calculations with experiments for binary C_2H_4/CO_2 mixture. The ethylene fraction y in the gas phase is plotted as function of molar fraction in the adsorbed phase x . Theoretical IAST data is represented as \bullet, \circ . Numerical analysis of breakthrough time $\triangle, \blacktriangle$; Experimental data \blacklozenge . The parity line is given by $x = y$ and represents a selectivity of unity.

Zandvoort experiments were performed at 313K and the data breakthrough data was calculated using a similar methodology as described in section 4.6 and was extracted from their paper without modification [67]. Based on the IAST calculations, the amount adsorbed in the solid phase decreased on average 1.5% when increasing the temperature from 298K to 313K, because of this small difference it is assumed that the experimental data of Bering and Serpinsky is comparable to the Zandvoort experiments. Using this assumption it is clear that loading of ethylene in the Zandvoort experiments is significantly higher than predicted by the IAST calculations *and* the equilibrium experiments. Zandvoort et al. only provide a qualitative comparison between IAST prediction and breakthrough experiments and do not mention the loading difference [67].

In Figure 5.3b the IAST prediction for 298K at 2.5 bar is given together with the numerical analysis of the breakthrough times conducted in this work. Three breakthrough experiments were performed with varying ethylene feed concentrations, e.g. $y = 0.33, 0.50$ and 0.57 with the remainder of the feed consisting of carbon dioxide. Comparing the experimental results with the IAST prediction, it is seen that the prediction slightly overestimates the ethylene loading found from the experiments. The most obvious reason for this discrepancy would be the different loading capabilities of various AC types. Other possible explanations include; competitive adsorption between C_2H_4 and CO_2 , meaning that in reality, interactions between both species negatively influence the selectivity towards ethylene. This non-ideal behaviour is not incorporated in the IAST methodology (and in the theoretical model described in chapter 6). Also the effect of pressure drop along the z-direction in the column is neglected in the IAST methodology, where constant pressure is assumed. Finally mistakes in the error analyses or under- or overestimating of specific errors could lead to a distorted calculation.

The results in Figure 5.3a and b lead to an interesting observation that for increased pressure the

Table 5.1: Loading q , volume feed fraction y and selectivity S for transient breakthrough experiments. Subscripts 1, 2 indicate C_2H_4 and CO_2 respectively.

	T=298K	T=308K	T =318K	T=328K
q_1 [mol/kg]	3.1	3.0	2.6	2.4
q_2 [mol/kg]	1.6	1.9	1.8	1.7
y_1	0.5	0.45	0.42	0.40
y_2	0.42	0.49	0.47	0.50
S_{12}	1.5	1.7	1.6	1.7

selectivity towards ethylene decreases. An explanation for this loss of selectivity can be that for higher pressure, CO₂ is more easily adsorbed onto the adsorbent. Similar behaviour is also seen in the pure component isotherm data (see Appendix A), where for pressures from 0 to 3 bar ethylene adsorption is higher compared to carbon dioxide adsorption. While for pressure over 5 bar carbon dioxide adsorption is more prevalent.

5.3.3. Effect of temperature variation

In the previous sections it was made clear that the selectivity is dependent on the pressure of the system and higher pressure has a negative effect on ethylene/carbon dioxide separation. This section investigates the effect of an increased temperature on the selectivity of the system. For adsorption systems it generally is known that increased temperature results in higher kinetic energy of the particles and the absolute adsorption capacity decreases [58]. This results in faster saturation of the bed and therefore shorter breakthrough times. In Figure 5.2a-d the transient breakthrough diagrams for the temperature range 298K–328K are given and the general trend is that as temperature increases, breakthrough times shorten. It should be noted that breakthrough times are highly dependent on the flowrate as well as the feed concentrations and with the used set-up controlling these parameters was not straightforward. The small deviations in experimental conditions this caused, makes quantitative comparison of breakthrough times unreliable.

The selectivity was determined using the mass balance in Equation 4.5 and 4.7. As flowrate and gas feed fraction are incorporated into the mass balance, the effect of the small deviations in experimental conditions could be rectified. The result of the selectivity analysis is given in Table 5.1. In this table it is observed that selectivity is marginally dependent on the temperature in the adsorbent bed. Additionally with a lower absolute adsorption capacity, increased temperature does not lead to benefits in terms of separation potential. Since temperature had a small effect of heat on selectivity, this supports the assumption of neglected heat of adsorption.

$$q_i = \frac{c_t Q}{m_{ads}} \int_{t_1}^{t_2} (y_{i,in} - y_{i,out}) dt \quad (4.5)$$

$$S_{12} = \frac{q_1/q_2}{y_1/y_2} \quad (4.7)$$

5.3.4. Conclusion on binary breakthrough experiments

The following conclusions were drawn from the breakthrough experiments

- For a feed consisting of approximately equivolume feeds of C₂H₄/CO₂, AC is ethylene selective
- Selectivity towards ethylene is lower than predicted by the IAST methodology
- Reduced pressure has a positive effect on the selectivity towards ethylene
- In the temperature range 298K–323K no significant effect on selectivity is observed

5.4. Desorption experiments

An essential step in an adsorption based separation process is the removal of the adsorbed species. To study the desorption behaviour of AC, the bed was saturated with a predefined flow with a C₂H₄/CO₂-ratio of 40/60 V%. The equilibrated bed was subsequently flushed with a constant flow of pure nitrogen, e.g. 70 mL min⁻¹ ⁱ. Regarding the desorption of ethylene and carbon dioxide on AC, Zandvoort et al. state that in the later stages of the desorption phase it is possible to obtain a nearly pure stream of ethylene. In their transient desorption experiments for various ethylene/carbon dioxide feed ratio's, CO₂ desorption was significantly quicker, resulting in a ethylene rich phase after all CO₂ has desorped.

The transient desorption results are displayed in Figure 5.4. In the current experimental methodology, the column was saturated and subsequently heated to its respective desorption temperature and after

ⁱThe flowrate was measured at 298K

thermal equilibrium was reached, the desorption process started. This means there is a some time between stopping the feed and reaching thermal equilibrium in which the adsorbent bed can change in composition, this thermal transition zone is depicted in the results as the grey shaded box ranging from $t = t_s$ to $t = 0$. The first observation is that due to the introduction of the N_2 gas the composition at the start of the desorption experiment (at $t = 0$) has lowered with respect to the time of saturation ($t = t_s$). More interesting however is that in the same transition period the volume fraction of CO_2 decreases while the C_2H_4 fraction remains equal or increases for all desorption temperatures, in other words CO_2 desorbs more significantly out of the bed relative to C_2H_4 due to the increased temperature. This effect becomes stronger as the desorption temperature is increased.

After the desorption stage started it is clear that for all temperatures, desorption of CO_2 is faster than ethylene, this is in agreement with the desorption experiments of Zandvoort et al. [67]. When inspecting the desorption of both species in a more quantitative way it is interesting to compare the times that $y_{C_2H_4}$ surpasses y_{CO_2} . Again it is seen that for increasing temperature this time reduces from ~ 130 seconds for 298K to ~ 60 seconds for 328K and for 353K this moment is even immediately after thermal equilibrium was formed in the adsorbent bed. Verifying again that the effect that an increased temperature has on positive effect on CO_2 desorption behaviour of the gas mixture.

The statement at the beginning of this section that a nearly pure stream of ethylene could be recovered in the final stage of the desorption process is not entirely true for these experiments. For example for $t > 200$ seconds for $T = 328K$ or $353K$ a flow with C_2H_4/CO_2 -ratio of > 5 could be obtained, but it would be after losing a considerable amount of ethylene in the initial phase of the desorption process.

5.5. Summarising the experimental results

Summarising, three types of experiments were performed; transient unary and binary adsorption and binary desorption experiments. In the unary breakthrough experiments, behaviour of one single adsorbate specie was examined. The first goal was to test the new set-up and examine behaviour of the main components of the reaction mixture on the adsorbent bed. The results showed that both ethylene and carbon dioxide adsorbed on the bed, as was expected from literature. Additionally an extensive error analysis was performed to find and describe weaknesses in the system, where main flaws of the system were the amount of air contamination and the reliability of the micro GC. Mapping those weaknesses is essential for the reliability of further experiments using the set-up.

After validation of the system, breakthrough experiments with a binary C_2H_4/CO_2 feed were examined. Based on IAST predictions a selectivity of 3.0 to 3.5 in favour of ethylene was expected. Numerical analysis of the experiments however showed that actual selectivity was substantially lower, ranging between 1.5 to 1.7. This difference might be caused by competitive adsorption between ethylene and carbon dioxide, this non-ideal behaviour is not included in the IAST methodology and therefore could lead to higher selectivity values. The competitive behaviour could be more significant for increased pressure, as selectivity towards ethylene decreases for increasing pressure. Additionally it should be noted that differences in AC types will have effect on adsorption behaviour and ultimately the selectivity. Additionally an increase in temperature had limited effect on selectivity.

During the desorption phase two main observation were made. Firstly, the CO_2 fraction decreased faster than the ethylene fraction, meaning at later stages of the process a more concentrated ethylene fraction could be obtained, however not at significant ethylene loss during the initial phase of the desorption stage. Secondly desorption of CO_2 was more sensitive to changes in temperature, as for increased temperature the desorption rate increased, while for the same temperatures no significant change in C_2H_4 desorption rate was observed.

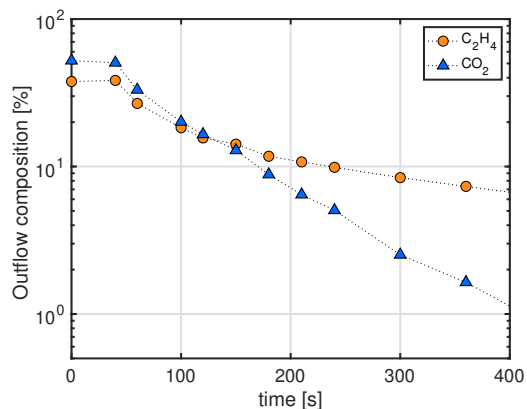
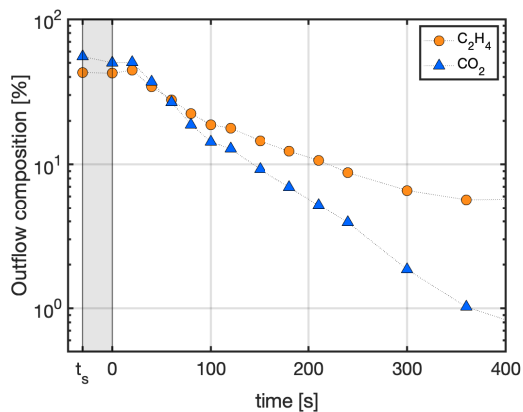
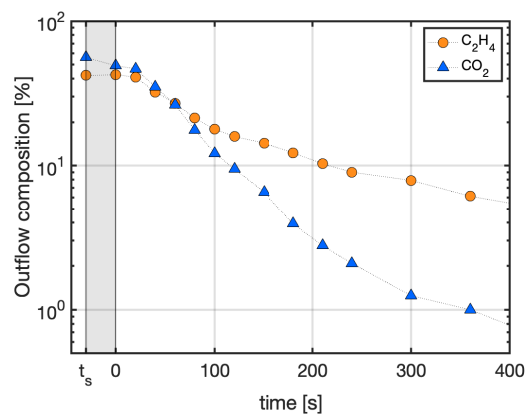
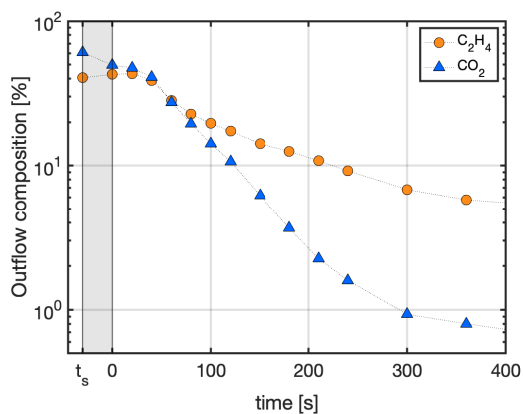
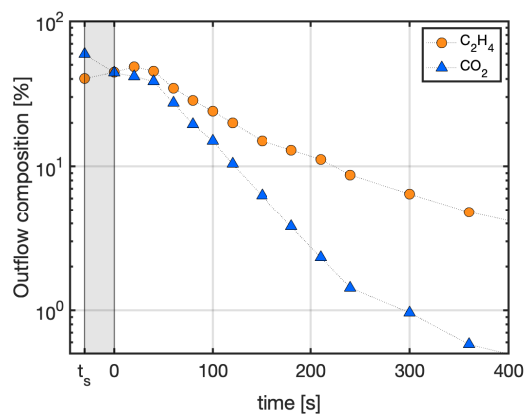
(a) $T = 298\text{K}$ (b) $T = 308\text{K}$ (c) $T = 318$ (d) $T = 328\text{K}$ (e) $T = 353\text{K}$

Figure 5.4: Transient desorption experiments for $\text{C}_2\text{H}_4/\text{CO}_2$ gas mixtures for various temperatures (298K–353K) with constant flow of N_2 gas. The grey shaded rectangles indicate the thermal transition zone were the saturated bed is allowed to heat up from 298K to the desired desorption temperature.

Modelling and Simulation Results

6.1. Introduction

The increase in computation power has made process simulation an essential part of a process engineers life. Modern processors are capable of calculating numerous complex equations in a reasonable time and this way the process parameters (i.e. pressure, composition, temperature etc.) can be varied to accurately estimate their effects. This can and has proven itself to lead to increases in efficiency and productivity without performing extensive experimental work. Contrary to distillation or absorption processes, modelling of adsorption process is inherently transient, therefore analytical methods used for the firstly mentioned technologies do not suffice.

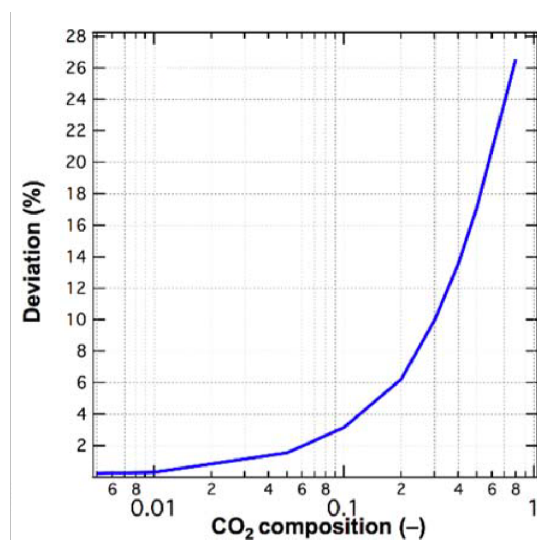


Figure 6.1: Velocity deviation of CO₂ adsorption on AC, calculated using two different models with various velocity assumptions. The first model assumed no velocity change (validated with the analytical solution), the second model assumed variable velocity change (validated with experimental results). The breakthrough deviation is calculated by taking the time at $c/c_0 = 0.5$ concentrations [135].

variation in packed beds and reported that for light adsorbing gases (for example methane or ethane on AC) have a deviation of 2% in breakthrough time for feed concentration of 20%. For strong adsorbing gases this effect is more significant; for the same feed concentration a deviation of 6% was observed

In an adsorbent bed, generally modelled as a packed bed, the adsorbent is initially free of adsorbate and compositions at fixed positions in the column change as the adsorbent particles saturate at the end of the adsorption cycle. The moment of saturation of the bed for a specific specie is observed experimentally by breakthrough times and these times give a good indication of the separation efficiency of the adsorbent for a given mixture, as both adsorption capacity and selectivity are weighted in in the calculations [138]. The bed is governed by simultaneous mass, momentum and heat transfer balances of gaseous components, the transport to the solid phase and physical properties of the bed accompanied with a set of initial and boundary conditions.

During the experiments it was observed that the temperature increase was marginal, 1-2K for each experiment, therefore the heat effects are neglected in this thesis and system is considered isothermal. The momentum balance on the other hand cannot be neglected; as the gas phase get adsorbed the volumetric flowrate decreases. El-Janabi et al. investigated the effect of velocity

[135]. The general trend is that for a increase in feed concentration the deviation rises significantly, this is depicted in Figure 6.1. Note that extensive PSA or TSA modelling is beyond the scope of this thesis and will only focus on describing breakthrough behaviour.

6.2. Assumptions

To formulate a model describing the fixed bed adsorber, several assumptions are made to simplify the model and decrease complexity and computing power [139].

1. Components in the gas phase are modelled using ideal gas law
2. Adsorption equilibria are described by best fitted corresponding isotherm, e.g. Dual site Langmuir isotherms.
3. all adsorbent particles are assumed to be homogeneous in shape, size and density
4. Mass transfer between adsorbent particles and the bulk phase is described by a linear relationship with mass transfer coefficient k , known as linear driving force model.
5. Pressure and concentration gradients in radial direction are neglected
6. The pressure drop in the z -direction is modelled using the empirical Ergun equation,
7. Any temperature effects due to adsorption are neglected
8. In the column backpressure is not possible, in other words $P_{z=i} \geq P_{z=i+1}$
9. the concentration gradient in the adsorbent particle is neglected: $q_i(r, t) = \bar{q}_i(t)$, where r is the radius of the adsorbent particle.

6.3. Model equations

6.3.1. Axial dispersion model

The fixed bed column is governed by the following material and kinetic balance equations and include the overall mass balance, component mass balance, Ergun equation and rate of adsorption or driving force equation. The component mass balance for specie i is given in Equation 6.1 and the overall mass balance over the full column is given by Equation 6.2. Here the specific concentration in the mixture is given by c_i in mol m^{-3} , u is the superficial gas velocity in m s^{-1} , \bar{q}_i the radially averaged loading in the adsorbent particles in mol kg^{-1} , P the pressure in bar, ε_b is the bed porosity without units, \mathfrak{D}_{ax} is the axial dispersion coefficient in $\text{m}^2 \text{s}^{-1}$, ρ_s the bed density in kg m^{-3} , t is the time in seconds, z the length of the column in meter and n the amount of components in the mixture.

$$\frac{\partial c_i}{\partial t} + \frac{\partial u c_i}{\partial z} - \mathfrak{D}_{ax} \frac{\partial^2 c_i}{\partial z^2} + \rho_s \left(\frac{1 - \varepsilon_b}{\varepsilon_b} \right) \frac{\partial \bar{q}_i}{\partial t} = 0 \quad (6.1)$$

$$\frac{\partial c_{tot}}{\partial t} + \frac{1 - \varepsilon_b}{\varepsilon_b} \rho_s \sum_{i=1}^n \frac{\partial q_i}{\partial t} + \frac{\partial u c_{tot}}{\partial z} = 0 \quad (6.2)$$

Substituting the ideal gas law, $c = P/RT$, and knowing that $c_{tot} = \sum_{i=1}^n c_i$, rewriting yields Equation 6.3. The equation is used in this form to relate the individual component concentrations to the total system pressure.

$$\frac{\partial P}{\partial t} = -RT \frac{1 - \varepsilon_b}{\varepsilon_b} \rho_s \sum_{i=1}^n \frac{\partial q_i}{\partial t} - \frac{\partial u P}{\partial z} = RT \frac{1 - \varepsilon_b}{\varepsilon_b} \rho_s \sum_{i=1}^n \frac{\partial q_i}{\partial t} - RT \frac{\partial}{\partial z} \left[u \sum_{i=1}^n c_i \right] \quad (6.3)$$

The amount being adsorbed in the solid phase is giving by the linear driving force model, which assumes a linear gradient between the solid and gas phase, where the gradient is given by k_{LDF} , the mass transfer coefficient. q_i^* is a adsorption isotherm and in this case described by the dualsite Langmuir model. The LDF model is often used for its simplicity, while still providing an reasonable prediction over

a wide range of conditions and is most accurate when the isotherm approaches linearity and tends to breakdown as the MTZ becomes sharper [58]. Alternative to the LDF model is to set up a intra-particle mass balance describing the diffusion of adsorbate into the adsorbent particle, however is not applied in this thesis [67], [139].

$$\frac{\partial \bar{q}_i}{\partial t} = k_{LDF}(q_i^* - \bar{q}_i) \quad (6.4)$$

$$q_i^* = q_{sat,A,i} \frac{K_{A,i} P_i y_i}{1 + \sum_{i=1}^n K_{A,i} P_i y_i} + q_{sat,B,i} \frac{K_{B,i} P_i y_i}{1 + \sum_{i=1}^n K_{B,i} P_i y_i} \quad (6.5a)$$

Where K is given by Equation 6.5b and 6.5c.

$$K_{A,i} = K_{A0,i} \exp\left\{\frac{E_{A,i}}{RT}\right\} \quad (6.5b)$$

$$K_{B,i} = K_{B0,i} \exp\left\{\frac{E_{B,i}}{RT}\right\} \quad (6.5c)$$

The kinetic balance is given by the laminar part of the empirical Ergun equation which accounts for the pressure drop over the column.

$$\frac{\partial P}{\partial z} = \frac{150\mu(1 - \varepsilon_b)^2}{d_p^2} \frac{1 - \varepsilon_b}{\varepsilon_b^3} u \quad (6.6)$$

6.3.2. Mass transfer coefficient

k_{LDF} (s^{-1}) is calculated by the relation given by Equation 6.7 as described by Seader [140], where k_{ext} is the external mass transfer resistance in $m s^{-1}$, a for a spherical particle is given by V_{sphere}/A_{sphere} or $d_p/6$ and D_{eff} is the effective diffusivity inside a particle. Since the Reynolds number is low in some of the experiments, the effect of external mass transfer layer becomes more significant, therefore this relation is used.

$$\frac{1}{k_{LDF}} = \frac{a}{k_{ext}} + \frac{d_p^2}{60D_{eff}} \quad (6.7)$$

The external mass transfer coefficient is determined using the relation provided by Dwivedi and Upadhyay in Equation 6.8 and was chosen for its suitability in the low Reynolds number region [141]. Note that the Reynolds number in this case is defined as: $Re' = d_p \rho_g u / \mu \varepsilon_b$, the Schidt number is defined as: $Sc = \mu / \rho_g \mathfrak{D}_m$.

$$k_{ext} = 2.40uRe'^{-0.66} Sc^{-0.58} \quad 0.08 < Re < 125, \quad 160 < Sc < 1.3 \cdot 10^4 \quad (6.8)$$

The effective diffusivity is determined via the Bosanquet correlation and is given in Equation 6.9 [142]. The tortuosity τ_p describes the convoluting pathways of particles inside a porous medium and can in this case considered to be equal to 3 [142]. The effective diffusivity is dependent on the molecular diffusivity \mathfrak{D}_m and the knudsen diffusivity \mathfrak{D}_k .

$$\mathfrak{D}_{eff} = \frac{\varepsilon_b}{\tau_p} \left(\frac{1}{\mathfrak{D}_m} + \frac{1}{\mathfrak{D}_k} \right)^{-1} \quad (6.9)$$

The Knudson diffusion coefficient is derived from the kinetic theory of gases and given in Equation 6.10. Since in this regime the particle is more likely to collide with the pore wall instead of other particles the mean free path is replaced with the pore diameter of the adsorbent particle d_{pore} . M_i is the molecular weight of specie i is given in $kg mol^{-1}$, hence the additional factor 10^3 in the equation.

$$\mathfrak{D}_{k,i} = \frac{d_{pore}}{3} \sqrt{\frac{8RT}{\pi M_i \cdot 10^3}} \quad (6.10)$$

The molecular diffusion coefficient between specie i and j ($\mathfrak{D}_{m,ij}$ in $m^2 s^{-1}$) is given by the Fuller-Schettler-Gridding (FSG) correlation in Equation 6.11 [142], [143]. The diffusion volume ζ_i ($cm^3 mol^{-1}$)

is given in Table 6.3. In this table the diffusion volumes of various common species are given and additionally the diffusion volume of organic compounds could be calculated by summing the atomic and structural diffusion volume increments.

$$\mathfrak{D}_{m,ij} = \frac{10^{-7} T^{1.75} \left(\frac{1}{M_i} + \frac{1}{M_j} \right)^{0.5}}{P \left(\zeta_i^{1/3} + \zeta_j^{1/3} \right)} \quad (6.11)$$

6.3.3. Boundary Conditions

The solutions of this system requires suitable initial and boundary conditions. For an open-open type column in the adsorption stage it is assumed that the column is filled with inert, non adsorbing gas (i.e nitrogen or argon) and that the adsorbent bed is free of any adsorbed material. At time $t = 0$, the entrance of the fixed bed is exposed to a stream of constant inlet pressure, inlet velocity and composition for the remainder of the experiment and are given as Dirichlet boundary conditions. The inlet superficial velocity is related to the flow rate and is determined via $u = Q/A$. Additionally at the column exit Neumann boundary conditions apply. All conditions are summarised in Table 6.1.

Table 6.1: Initial and boundary conditions for an open-open fixed bed column.

Initial conditions	Boundary conditions	
$c_{inert}(z, t = 0) = \frac{P}{RT}$	$c_{inert}(z = 0, t) = 0$	$\frac{\partial c_{inert}}{\partial z}(z = L, t) = 0$
$c_i(z, t = 0) = 0$	$c_i(z = 0, t) = \frac{y_i P}{RT}$	$\frac{\partial c_i}{\partial z}(z = L, t) = 0$
$q_i(z, t = 0) = 0$	$P(z = 0, t) = P_{inlet}$	
	$u(z = 0, t) = u_{inlet}$	

6.4. Solving method

The system of equations given in section 6.3 cannot be solved analytically and therefore require a form that is computationally solvable. The system parameters vary over on the length of the column and are transient. Various methods exist for the computation of partial differential equations and in this thesis the method of lines (MoL) is applied. In this method the spacial derivatives are discretized using finite difference methodology, creating a system of ODEs to be solved in the temporal domain. As the ODE solvers used are initial value based, a requirement of using MoL is that the PDE is well-defined in the time dimension. Since the initial conditions are known for the column, this condition is met.

6.5. Discretisation

The backwards difference and central difference approximation are used for respectively the first and second order spacial derivatives, given in Equation 6.12 and 6.13. Note that the subscripts in these and the following equations in this section do not refer to specie i , however denote the spacial mesh point i and the temporal mesh point j . The discretised equations of the overall mass conservation equation (Equation 6.14), component mass balance equation (Equation 6.15) and adsorption rate equation (Equation 6.16) are given next.

$$\frac{\partial c_{i,j}}{\partial z} \simeq \frac{c_{i,j} - c_{i-1,j}}{\Delta z} \quad (6.12)$$

$$\frac{\partial^2 c_{i,j}}{\partial z^2} \simeq \frac{c_{i-1,j} - 2c_{i,j} + c_{i+1,j}}{(\Delta z)^2} \quad (6.13)$$

$$\frac{\partial P_{i,j}}{\partial t} = -RT \frac{1-\varepsilon}{\varepsilon} \rho_s \sum^n \frac{\partial q_{i,j}}{\partial t} - \frac{RT}{\Delta z} \left(u_{i,j} \sum^n c_{i,j} - u_{i-1,j} \sum^n c_{i-1,j} \right) \quad (6.14)$$

$$\frac{\partial c_{i,j}}{\partial t} = \frac{1-\varepsilon_b}{\varepsilon_b} \rho_s \frac{\partial q_{i,j}}{\partial t} + \frac{\mathfrak{D}_{ax}}{\Delta z} \left(\frac{c_{i+1,j} - c_{i,j}}{\Delta z} - \frac{c_{i,j} - c_{i-1,j}}{\Delta z} \right) - \frac{1}{\Delta z} (u_{i,j} c_{i,j} - u_{i-1,j} c_{i-1,j}) \quad (6.15)$$

$$\frac{\partial q_{i,j}}{\partial t} = k_{i,j} (q_{i,j}^* - q_{i,j}) \quad (6.16)$$

The velocity in the adsorber bed is determined using the pressure difference calculated via the laminar region of the Ergun equation (Equation 6.17). This implies that the pressure derivative is calculated not at the centre of the grid cell but at the grid cell border and consequently the velocity too. To correct for the half-way velocity, simply the average of $u_{i-1/2}$ and $u_{i+1/2}$ is determined via Equation 6.18.

$$\frac{P_{i,j} - P_{i-1,j}}{\Delta z} = 150 \frac{(1-\varepsilon)^2}{\varepsilon} \frac{\mu}{d_p^2} u_{i+1/2} \quad (6.17)$$

$$u_i = \frac{u_{i-1/2} + u_{i+1/2}}{2} \quad (6.18)$$

Because of the dependence of k_{ext} on velocity, via the Reynolds number in Equation 6.8 and the dependence of $\mathfrak{D}_{m,i,j}$ on the pressure (Equation 6.11), k_{LDF} is recalculated for each space step.

6.6. Model validation

In order to validate the described model it was tested using experimental data of a equivolume, binary mixture of CO₂ and N₂ adsorbing on active carbon. Experimental breakthrough data at various flowrates was collected from Al-Janabi et al. [135] and plotted as diamonds in Figure 6.2. The corresponding isotherm parameters for the dualsite Langmuir model were obtained from the single component isotherms found in the supplementary information accompanying the experimental data. The parameters are given in appendix A.8. All further operation conditions were identical to the reported parameters and can be found at the original publication [135].

The results of the model for the CO₂ outflow composition for flow rates 10, 20 and 100 mL min⁻¹ are displayed as the coloured continuous lines in Figure 6.2. The bed was discretized into 50 equally sized nodes in the z-direction and 200 time steps. It is observed that the model slightly underestimates the composition relative to the experimental data, indicating that the mass transfer rate k_{LDF} is undervalued. Some of this difference might be associated by the estimated physical parameters not provided by Al-Janabi, e.g. d_{pore} , τ_p , ρ_s , ρ_b . Also the isotherm fitting process, identical to the procedure described in section 3.5, was prone to small errors, which propagate into the isotherm parameters. Finally N₂ was considered as an inert component and adsorption of this specie was neglected. Taking these factors into account the model does provide an accurate estimation of the breakthrough times, confirming the validity of the model.

6.7. Transient breakthrough simulations

6.7.1. System parameters

All system parameters are given in Table 6.2. The gas density is of air at 25 °C at 2.5 bar, the gas viscosity is of air at 25 °C. The bed porosity is determined using the correlation chart given by Walas which correlates bed void fraction to the ratio between particle diameter to the column diameter and the particle morphology resulting in a bed porosity of 0.28 [144]. The pore diameter is measured using a Micrometrics TriStar 2 and ranged between 1.8 and 2.4 nm, in the simulations an average of 2.1 nm was used. Additionally the feed fraction is specified per experiment, the diffusion volumes are provided in Table 6.3 and the isotherm parameters are given in Appendix A.

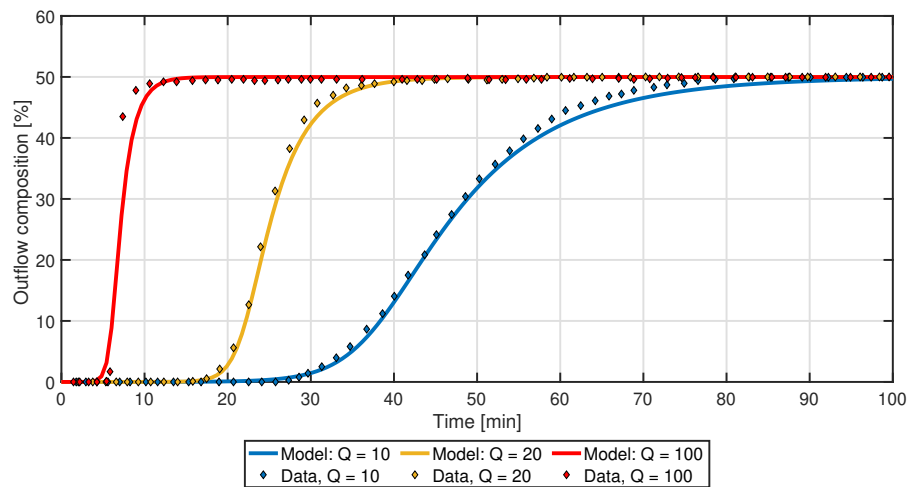


Figure 6.2: Validation of the model with experimental transient breakthrough data for $Q = 10, 20, 100 \text{ mL min}^{-1}$. The solid diamonds represent the CO_2 volume fraction in the outflowing gas and the continuous lines the numerical model. The remainder of the composition consists of N_2 .

Table 6.2: Column properties and input parameters

Parameter	Value	Parameter	Value
Bed length (L)	0.19 m	Pore diameter (d_{pore})	$2.1 \text{e-}9 \text{ m}$
Bed diameter (D)	$9 \text{e-}3 \text{ m}$	Gas viscosity (μ)	$1.85 \text{e-}5 \text{ kg m}^{-1} \text{ s}^{-1}$
Flowrate (Q)	$50\text{--}65 \text{ mL min}^{-1}$	Temperature (T)	$298\text{--}353 \text{ K}$
Particle diameter (d_p)	$1.5 \text{e-}4 \text{ m}$	Bed porosity (ε_b)	0.28
Gas density (ρ_g)	2.94 kg m^{-3}	Spacial increment (Δz)	$1.9 \text{e-}3 \text{ m}$
Apparent density AC (ρ_s)	2000 kg m^{-3}	Time increment (Δt)	2.0 s

Table 6.3: Diffusion volumes ζ for various simple molecules in $\text{cm}^3 \text{ mol}^{-1}$. These parameters are used for the determination of the molecular diffusion coefficient. Diffusion volumes of organic molecules can be determined by summing the respective volume increments, e.g. $\sum_{i=1} \zeta_i$. Data obtained from Kinaci et al. [143].

Atomic and structural diffusion volume increments		Diffusion volume of simple molecules	
C	16.5	CO_2	26.9
H	1.98	CO	18.9
O	5.48	N_2	17.9
		H_2O	12.7
		H_2	7.07

6.7.2. Simulation Results

The results of the numerical simulations are compared with the transient breakthrough experiments in Figure 6.3, where the experimental data is represented using the error bars as described in section 5.3.1. The bed is initially filled with non-adsorbing nitrogen, which is "pushed" out of the column by the entering gases, this effect is shown qualitatively by the sharp breakthrough front appearing after 100 – 150 seconds. In reality, beside diffusion effects, mixing caused by flow through a porous medium will lead to the development of a broader mass transfer zone. Additionally the numerical breakthrough behaviour of ethylene, represented by the yellow line, shows comparable qualitative features as the experiments, in other words the behaviour of the mass transfer zone is predicted correctly. In agreement to the experiments the increase in temperature will lead to lower adsorption capacity and faster breakthrough times.

Comparing the numerical breakthrough times quantitatively with the experiments the match is poor. For all simulations the CO₂ breakthrough is predicted earlier than the experiments and the C₂H₄ breakthrough is predicted later. This indicates that the model underestimates CO₂ and overestimates C₂H₄ adsorption.

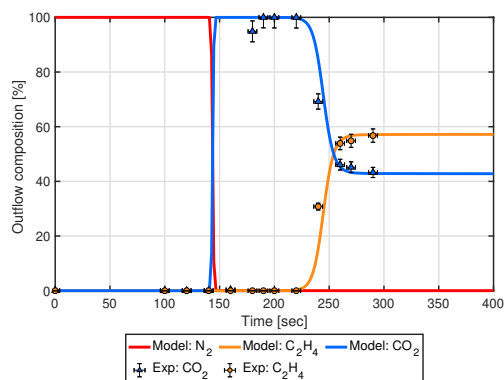
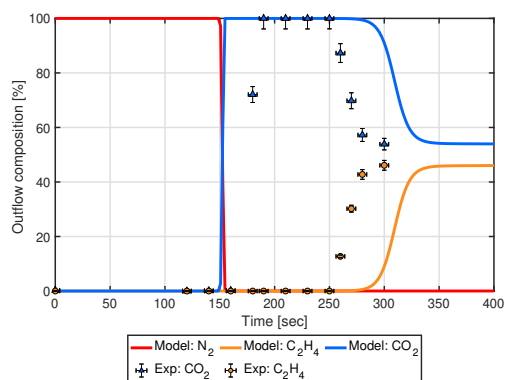
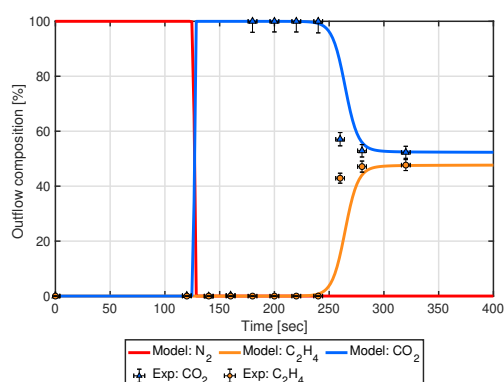
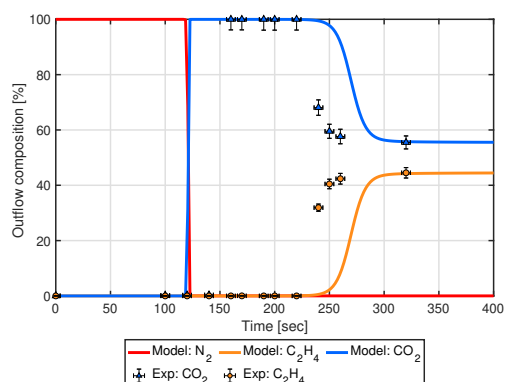
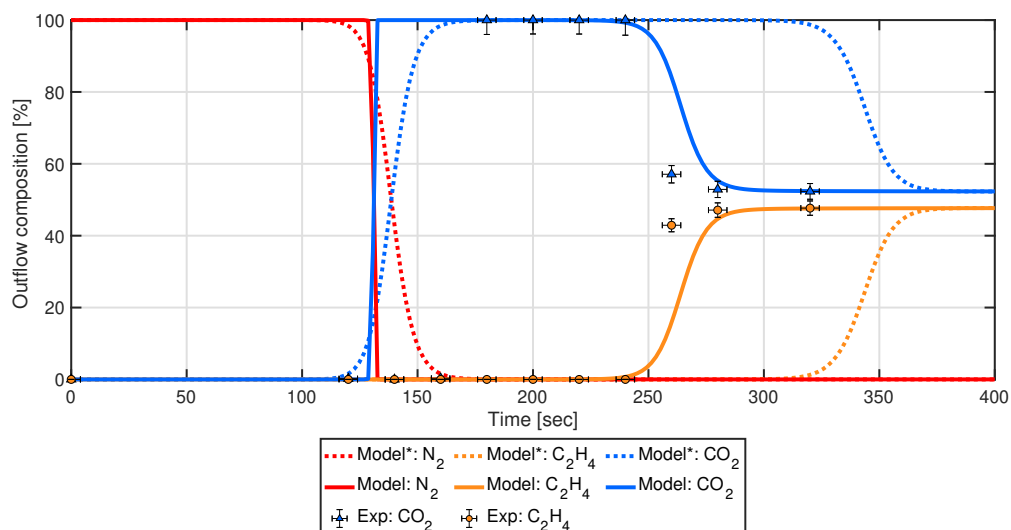
Fundamentally two justifications could be given for the mismatch between the experimental and numerical results. First there could be some unknown factor during the experiments which led to more CO₂ and/or less C₂H₄ adsorption. Such factors could be non-ideal interaction between ethylene and carbon dioxide molecules, CO₂ molecules saturating the easily accessible sites or something else. Secondly something could be off in the methodology of the numerical model, the used parameters or the isotherm data. In sections 6.7.3-6.7.5 the last three arguments will be discussed.

6.7.3. Effect of variable velocity on breakthrough behaviour

To investigate the methodology of the numerical model, the velocity behaviour, and indirectly the pressure behaviour, is first considered. In Figure 6.4 a comparison between variable and constant velocity model shows that a significant shift in breakthrough time is observed, where the constant velocity breakthrough is approximately 150 seconds later. The shifting of breakthrough time for both velocity models was also reported by Al-Janabi et al. [135] and by Babu et al. [139], both mention that the constant velocity model overestimated the breakthrough time. In the introduction of this chapter in Figure 6.1 the deviation in breakthrough time was plotted as function of adsorbate feed concentration, in the case of a fully adsorbing feed the deviation will be most significant and based on Figure 6.1, is around 30%. Inspecting the ethylene breakthrough times, it is indeed observed that for both compounds $c/c_0 = 0.5$ appears approximately 30% earlier.

Interesting is the difference in breakthrough behaviour for the carbon dioxide front, which is substantially more dispersed for the constant velocity model. It is hypothesised that this effect is caused by how velocity and pressure behave in both models; in the constant velocity model at arbitrary grid cell i , the adsorbate gases are partially adsorbed and the remainder will flow to the next grid cell, since this is dictated by the constant velocity assumption. At grid cell $i + 1$ the material is again partially adsorbed and the remainder flows to grid cell $i + 2$, this is repeated until all material is adsorbed and equilibrium at the time step is reached. This effect is repeated for all timesteps and will eventually lead to a broader mass transfer zone at the column end. For the variable velocity model this is not the case; for grid cell i the adsorbate gases are adsorbed, causing a decrease in pressure and consequently a decrease in velocity. Depending on the adsorption rate, in this case k_{LDF} , grid cell i will adsorb all gas passing the node until saturation before the flow reaches grid cell $i + 1$. This way the adsorbing gases propagate through the column, creating a sharp CO₂ front at the column exit. This effect also discussed in section 6.7.4. Note that axial dispersion effects will lead to some broadening of the mass transfer zone in the column, however this effect is small for columns with a large L/D ratio.

Additionally a large pressure drop over the column will contribute to the break through difference between both models. For a large pressure drop, the pressure near the exit of the column is considerably lower compared to the entrance region, meaning at the end of the column the adsorbent is saturated faster, decreasing the breakthrough time.

(a) $T = 298\text{K}$, $Q_{\text{tot}} = 65 \text{ mL min}^{-1}$, $y^{\text{et}} = 0.57$ (b) $T = 308\text{K}$, $Q_{\text{tot}} = 52 \text{ mL min}^{-1}$, $y^{\text{et}} = 0.46$ (c) $T = 318\text{K}$, $Q_{\text{tot}} = 55 \text{ mL min}^{-1}$, $y^{\text{et}} = 0.48$ (d) $T = 328\text{K}$, $Q_{\text{tot}} = 55 \text{ mL min}^{-1}$, $y^{\text{et}} = 0.45$ Figure 6.3: Comparison of numerical simulations (continuous solid lines) versus the breakthrough experiments for the $\text{C}_2\text{H}_4/\text{CO}_2$ mixture for various temperatures.Figure 6.4: Effect of model having variable velocity (continuous lines) and constant velocity (dotted lines and *) in the column, the solid symbols represent the experimental results. $T = 308\text{K}$, total inlet flow was 52 mL min^{-1}

6.7.4. Velocity behaviour inside the fixed bed

The velocity behaviour of an adsorber bed is displayed as contour plots in Figure 6.5, however to experimentally validate the velocity profiles in a fixed bed is complicated. In a first attempt to qualitatively validate the velocity behaviour, breakthrough behaviour of experiments and the model is compared and the results are described physically.

In Figure 6.5a and 6.5b the velocity contours of the first 40 seconds after the start of the experiment are displayed on a fine grid size, since the change in velocity is initially very large. The fine grid size was a factor ten denser in the temporal domain and a factor three denser in the spatial domain compared to all other simulations in this report. This yields the following increments for the fine grid; $\Delta t = 0.2\text{s}$ and $\Delta z = 6.3\text{e-}4\text{m}$ compared to $\Delta t = 2\text{s}$ and $\Delta z = 1.9\text{e-}3\text{m}$ for the normal grid, seen in Figure 6.5c and 6.5d.

In Figure 6.5a the gas in the column is stagnant at $t = 0$ until the fresh feed enters the column. As the bed is initially free of adsorbent, uptake is largest in the first moments when the feed enters the column. This causes the pressure to drop locally due to adsorption of the gases, giving rise to a large pressure difference and will lead to a large local superficial velocity, as predicted by the Ergun equation. The effect of the large pressure difference decreases as the column becomes more saturated in the z -direction, because the unsaturated front is moving away from the entrance of the tube. In Figure 6.5a-6.5c, the adsorption effect is clearly seen, as the velocity decreases to 0 immediately as the front reaches unsaturated parts of the bed, this will ultimately give rise to the sharp breakthrough front seen in Figure 6.4. In Figure 6.5e the intersection of the superficial velocity for three different moments is plotted as function of the column length. The blue line shows the velocity profile after ten seconds and the sharp decrease in velocity is clearly seen.

The same effect is seen for the the adsorption of ethylene creating a second, local velocity drop. Since only a part of the flow is adsorbed, the resulting pressure drop is smaller and so is the effect on the velocity. The effect is clearly visible in the red line in Figure 6.5e, where a small drop in velocity is seen after 0.08 m. The broadness of the ethylene mass transfer zone could be explained using similar arguments as the CO_2 breakthrough in the constant velocity model. As the ethylene front is moving slower through the bed compared to the CO_2 front, the higher velocity of the CO_2 particles will 'carry' the ethylene forward, causing more dispersed breakthrough.

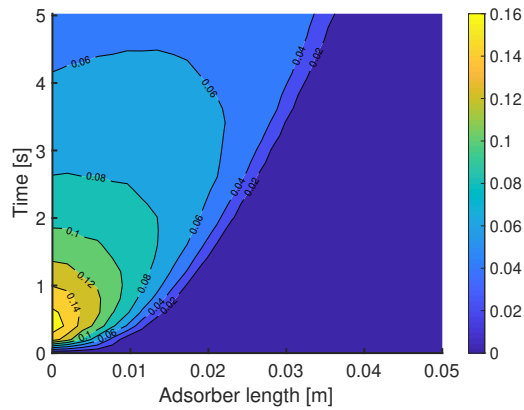
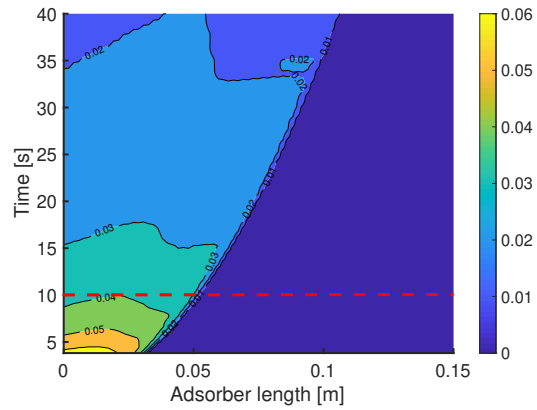
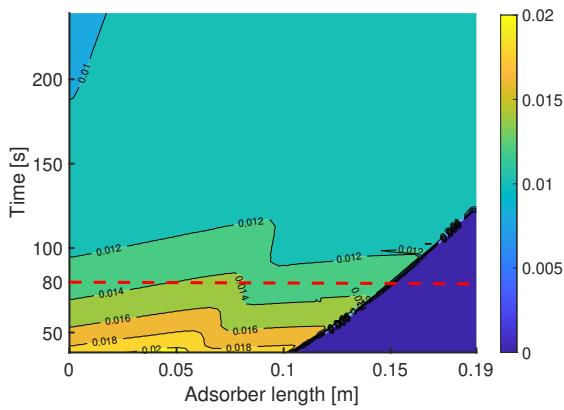
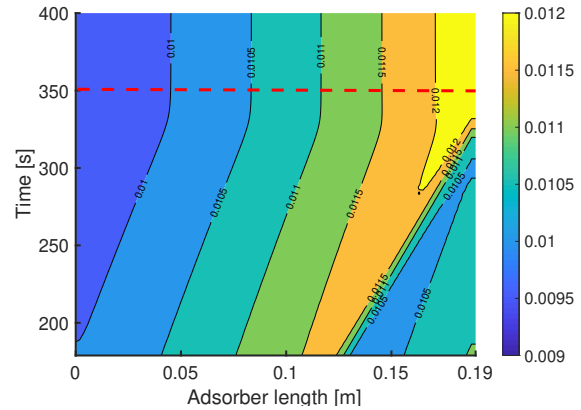
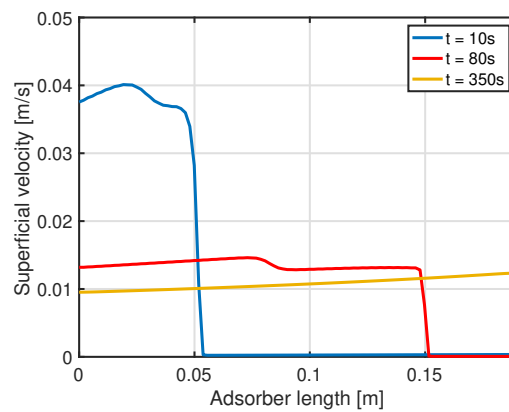
After all components have broken through after ~ 330 seconds the bed is saturated and a steady state situation prevails. In this case the velocity difference is only dependent on the pressure drop caused by the fixed bed. In Figure 6.5e this is displayed by the yellow line, increasing gradually towards the end of the column.

6.7.5. Model and isotherms parameters

Most parameters of the system could easily be determined and are used with very small uncertainties and therefore not discussed in this section. The flow input is one crucial exception; as the flow was measured using a bubble meter, the measurements were not continuous and susceptible to inaccurate readings. Moreover, flowrate has a critical effect on the breakthrough time, meaning that small deviations in flowrate potentially have large effect on the accuracy of the model.

A second factor that has substantial effect of the breakthrough behaviour are the isotherm parameters for the dualsite Langmuir model used in the adsorption uptake equation. As mentioned, every type of AC behaves differently due to differences in pore and surface structure, meaning the isotherm data used *will* produce different results than the experiments, this effect is also reported by Zandvoort et al. [67]. The best solution to overcome this issue is to obtain isotherm data locally of the same type of AC.

In Figure 6.6 the model results are given for two different sets of isotherm parameters, where the continuous lines represent the parameters obtained from experimental data from Osterkamp et al. and the dotted lines the experimental data from Reich et al.. For both parameter sets the estimated CO_2 breakthrough time was almost identical, however a more considerable variation is seen for the C_2H_4 breakthrough time. As all other parameters in the model are identical, the difference in breakthrough behaviour could be fully accounted to the parameter sets.

(a) Fine grid: $\Delta t = 0.2\text{s}$ and $\Delta z = 6.3\text{e-}4\text{m}$ (b) Fine grid: $\Delta t = 0.2\text{s}$ and $\Delta z = 6.3\text{e-}4\text{m}$ (c) Normal grid: $\Delta t = 2\text{s}$ and $\Delta z = 1.9\text{e-}3\text{m}$ (d) Normal grid: $\Delta t = 2\text{s}$ and $\Delta z = 1.9\text{e-}3\text{m}$ 

(e) Intersection of the velocity profile for different time steps

Figure 6.5: a–d: Contour plots of the superficial velocity profile in the fixed bed column. e: Comparison of the velocity profile at different times in the fixed bed, also represented by the red, dashed lines in Fig. b, c and d. The colour bars on the right-hand side of the contour plots represent the superficial velocity in m s^{-1} . $T = 308\text{K}$, total inlet flow was 52 mL min^{-1}

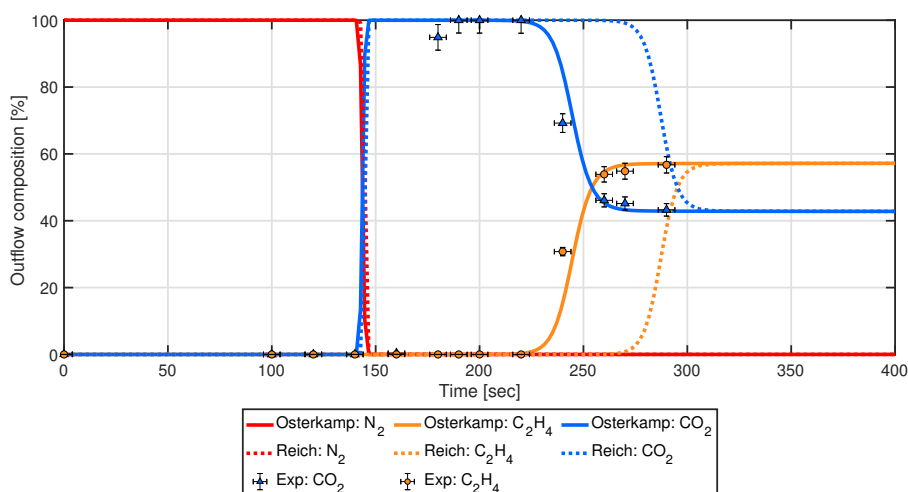


Figure 6.6: Comparison of two different sets of isotherm parameters on breakthrough behaviour. The continuous lines represent the isotherm parameters obtained from Osterkamp et al., the dotted lines data isotherm data from Reich et al.. All other parameters in the model are identical. $T = 298\text{K}$, $Q_{tot} = 65 \text{ mL min}^{-1}$

Table 6.4: Comparison of selectivities found using experiments in this work and selectivities found using IAST methodology and the numerical model using parameters sets based on isotherm data from Osterkamp et al. [98] and Reich et al.[69].

Column temperature	Experimental	Osterkamp		Reich	
		IAST	Numerical	IAST	Numerical
298K	1.5	2.3	2.0	2.8	2.9
308K	1.7	2.4	2.1	2.9	2.7
318K	1.6	2.4	2.2	2.9	2.8
328K	1.7	2.4	2.3	3.0	2.9

In Table 6.4 a quantitative comparison is given of the effect of the isotherm parameters, again underlining the importance of the isotherm parameters. Here the $\text{C}_2\text{H}_4/\text{CO}_2$ -selectivity found in the experiments, the IAST methodology and in the numerical model for both parameter sets is given. To better compare the results, numerical selectivities are calculated via the same approach as the experimental selectivities, see section 4.6. For the same isotherm parameters, it is seen that the IAST methodology and numerical model produce almost analogous results, indicating that both methods perform similarly under the same conditions. Both however are not able to accurately predict the experimental selectivities.

6.7.6. Conclusion on the theoretical model

In this chapter a theoretical model was developed to estimate the breakthrough behaviour of fixed bed columns. In the experiments, both components are captured and the effect on pressure and subsequently velocity is significant. Considering the mock-up mixture (among other things, consists of 20% ethylene, 55% carbon dioxide and 15% carbon monoxide) velocity effects are considerable and should be included.

The model was validated using experimental breakthrough data of a binary mixture consisting of CO_2 and N_2 and the model provided an accurate estimation of the breakthrough time and behaviour. After validation, the model was used to estimate the adsorption behaviour in the custom build set-up and the quantitative match between the numerical and experimental results was poor. To explain the poor match, first the velocity profile was investigated and it was seen that the qualitative velocity behaviour could explain the experimental breakthrough well. Additionally the velocity behaviour made sense from

a physical point of view, confirming the validity of the model.

Secondly, the input variables were reconsidered and it was hypothesised that the effect of inaccurate flow measurements *and* isotherm data obtained from a different AC type was of major influence on the simulation results and could explain the poor match between numerical and experimental results. To verify this statement, the isotherm data for the specific type of AC used in these experiments should be obtained and used with this model.

Conclusively, this model will contribute to understanding velocity behaviour in an fixed bed column *and* is good step in the direction of qualitative *and* quantitatively describing adsorption behaviour of ethylene and carbon dioxide on active carbon.

Conclusions and Recommendations

7.1. Conclusions

The aim of this thesis was to find and develop a new downstream separation process that could capture ethylene from a mixture of gases produced by a CO₂ electrolyzer cell. After an extensive literature study and assessing multiple separation techniques, adsorption met the most selection criteria, for example its ability to operate at low driving forces or its ability to be ethylene selective. After the screening of various adsorbents that were ethylene selective based on experimental results or predictions made with Ideal Adsorption Solution Theory (IAST), Active Carbon (AC) was chosen as the adsorbent of choice. AC is chemically and thermally stable, has good regenerability and because of its large commercial availability, the need for material development is obviated.

A preliminary analysis of the mock-up reaction mixture (mole fractions C₂H₄/CO₂/CO/H₂/H₂O : 20/55/15/15/5) was performed and the binary selectivities of most components in the mixture were determined using adsorption isotherm data. From the resulting selectivity data, it was concluded that the C₂H₄/CO₂ pair was the primary impediment towards achieving a ethylene selective system, mainly due to the similar physical properties of both species, e.g. kinetic diameter, polarizability and quadrupole moment.

The behaviour of this binary gas mixture on active carbon was examined using a simple, custom-build experimental set-up. A qualitative assessment of unary breakthrough behaviour and an extensive error analysis of the system was performed to validate the experimental set-up. The binary C₂H₄/CO₂ breakthrough experiments were performed and from the resulting breakthrough data, the selectivity for the adsorbent with respect to ethylene was calculated. In addition, a theoretical model describing adsorption behaviour was developed and the effect of velocity variation due to pressure drop and the adsorption of components was included. After validation using experimental data from literature, the model was used to predict the behaviour of the transient breakthrough experiments. The model was able to predict the qualitative behaviour of the experiments, however the quantitative match between the numerical and experimental results was poor. Most noticeably, CO₂ breakthrough was predicted approximately 30–40 seconds earlier compared to the experiments and C₂H₄ breakthrough was predicted 0–30 seconds late.

The experimental results indicate that separation performance was significantly lower than expected from IAST predictions and in the theoretical model, suggesting that the assumptions of ideality in both models was inappropriate. The deviation of ideality could be explained by competitive adsorption between both species. Additionally it was seen that for increased pressure the selectivity towards ethylene decreased, meaning the relative affinity of CO₂ for AC increased for increasing pressure. From a modelling perspective, two reasons were examined that could explain the mismatch, e.g. model behaviour and input parameters. First a comparison between a constant and variable velocity model showed the superiority of the variable velocity model in predicting breakthrough times when a significant part of the feed is adsorbed. Secondly, inspection of the modelled velocity profile could explain the sharp CO₂

breakthrough front and the broader C_2H_4 front, both validated by the experiments. Comparison of two different sets of isotherm parameters led to the conclusion that their effect on predicting breakthrough behaviour is significant and to obtain a quantitative good match, it is essential to obtain isotherm data of the identical type of adsorbent.

Summarising the results, it is observed that separating ethylene and carbon dioxide is inherently complex and depending on the type of AC, a selectivity of 1.5 to 3.5 in favour of ethylene is reached. This implies that to obtain a stream of 99.9% ethylene either a significant amount of stages would be required, another type of adsorbent could be used in a later stage to remove CO_2 or an additional separation technique could be implemented. However, adsorption using active carbon is a relatively cheap and simple technology to increase the ethylene content in a CO_2 -bearing mixture.

7.2. Recommendations and Outlook

In this work, the foundations have been laid for the development of novel separation process to capture ethylene from a CO_2 bearing stream using active carbon. In order to further develop this concept into an operational separation process the following recommendations are suggested to improve experimental work and theoretical model accuracy plus the subsequent steps towards realisation.

Regarding the experimental set-up the following suggestions are made;

- Implement digital flow controllers for better control of the feed
- Automate the sampling procedure; this way the sampling rate and accuracy can be increased
- Perform experiments under additional conditions, including different pressure ranges, sub-room temperatures and varying feed compositions.
- Increase complexity of the feed mixture by adding carbon monoxide, hydrogen and water.

For additional validation of the theoretical model, the following recommendations are given;

- Measure isotherm equilibria of the specific type of active carbon used in the transient breakthrough experiments and obtain the respective parameter sets.
- Implement digital flow meter in the experimental set-up and verify the velocity profile at the column exit.
- Verify (and improve) the model under more experimental conditions.
- Use the model to estimate the desorption behaviour.

Ultimately, after implementation of the recommendations, the future outlook of this concept could be towards;

- the use of multiple stages, either using multiple beds containing AC or various types of adsorbent, and
- the implementation of this concept in an actual CO_2 -electrolyzer process and capture ethylene continuously.

Bibliography

- [1] IEA (2020), *Global CO2 emissions in 2019*, 2020.
- [2] C. Le Quéré, R. B. Jackson, M. W. Jones, A. J. Smith, S. Abernethy, R. M. Andrew, A. J. De-Gol, D. R. Willis, Y. Shan, J. G. Canadell, P. Friedlingstein, F. Creutzig, and G. P. Peters, “Temporary reduction in daily global CO₂ emissions during the COVID-19 forced confinement”, *Nature Climate Change*, vol. 10, no. 7, pp. 647–653, Jul. 2020.
- [3] L. Ghinea, *Carbon Capture Utilisation and Storage*, 2016.
- [4] C. Fernández-Dacosta, M. Van Der Spek, C. R. Hung, G. D. Oregionni, R. Skagestad, P. Parihar, D. T. Gokak, A. H. Strømman, and A. Ramirez, “Prospective techno-economic and environmental assessment of carbon capture at a refinery and CO₂ utilisation in polyol synthesis”, *Journal of CO₂ Utilization*, vol. 21, pp. 405–422, 2017.
- [5] W. Schakel, G. Oreggioni, B. Singh, A. Strømman, and A. Ramírez, “Assessing the techno-environmental performance of CO₂ utilization via dry reforming of methane for the production of dimethyl ether”, *Journal of CO₂ Utilization*, vol. 16, pp. 138–149, Dec. 2016.
- [6] W. Wang, H. Ning, Z. Yang, Z. Feng, J. Wang, X. Wang, Q. Mao, W. Wu, Q. Zhao, H. Hu, Y. Song, and M. Wu, “Interface-induced controllable synthesis of Cu₂O nanocubes for electroreduction CO₂ to C₂H₄”, *Electrochimica Acta*, vol. 306, pp. 360–365, 2019.
- [7] C. Reller, R. Krause, E. Volkova, B. Schmid, S. Neubauer, A. Rucki, M. Schuster, and G. Schmid, “Selective Electroreduction of CO₂ toward Ethylene on Nano Dendritic Copper Catalysts at High Current Density”, *Advanced Energy Materials*, vol. 7, no. 12, p. 1602114, Jun. 2017.
- [8] J. Albo, M. Perfecto-Irigaray, G. Beobide, and A. Irabien, “Cu/Bi metal-organic framework-based systems for an enhanced electrochemical transformation of CO₂ to alcohols”, *Journal of CO₂ Utilization*, vol. 33, pp. 157–165, Oct. 2019.
- [9] M. Ebaid, K. Jiang, Z. Zhang, W. S. Drisdell, A. T. Bell, and J. K. Cooper, “Production of C₂/C₃ Oxygenates from Planar Copper Nitride-Derived Mesoporous Copper via Electrochemical Reduction of CO₂”, *Chemistry of Materials*, vol. 32, no. 7, pp. 3304–3311, 2020.
- [10] Y. Zheng, A. Vasileff, X. Zhou, Y. Jiao, M. Jaroniec, and S. Z. Qiao, “Understanding the Roadmap for Electrochemical Reduction of CO₂ to Multi-Carbon Oxygenates and Hydrocarbons on Copper-Based Catalysts”, *Journal of the American Chemical Society*, vol. 141, no. 19, pp. 7646–7659, 2019.
- [11] P. De Luna, C. Hahn, D. Higgins, S. A. Jaffer, T. F. Jaramillo, and E. H. Sargent, *What would it take for renewably powered electrosynthesis to displace petrochemical processes?*, Apr. 2019.
- [12] TU Delft E-refinery, *e-Refinery initiative launched*, 2018.
- [13] D. S. Sholl and R. P. Lively, *Seven chemical separations to change the world*, Apr. 2016.
- [14] H. Zimmermann and R. Walzl, “Ethylene in Ullman’s Encyclopedia of Industrial Chemistry”, in *Ullmann’s Encyclopedia of Industrial Chemistry*, Weinheim, Germany: Wiley-VCH Verlag GmbH & Co. KGaA, Apr. 2009.
- [15] R. Krishna, “Screening metal-organic frameworks for mixture separations in fixed-bed adsorbers using a combined selectivity/capacity metric”, *RSC Advances*, vol. 7, no. 57, pp. 35724–35737, Jul. 2017.
- [16] M. Wang, A. S. Joel, C. Ramshaw, D. Eimer, and N. M. Musa, *Process intensification for post-combustion CO₂ capture with chemical absorption: A critical review*, Nov. 2015.
- [17] A. M. Yousef, W. M. El-Maghlany, Y. A. Eldrainy, and A. Attia, “New approach for biogas purification using cryogenic separation and distillation process for CO₂ capture”, *Energy*, vol. 156, pp. 328–351, 2018.

- [18] T. He, Y. Xiao, Q. Zhao, M. Zhou, and G. He, "Ultramicroporous Metal-Organic Framework Qc-5-Cu for Highly Selective Adsorption of CO₂ from C₂H₄ Stream", *Industrial and Engineering Chemistry Research*, vol. 59, no. 7, pp. 3153–3161, 2020.
- [19] J. Hou, P. Liu, M. Jiang, L. Yu, L. Li, and Z. Tang, *Olefin/paraffin separation through membranes: From mechanisms to critical materials*, Oct. 2019.
- [20] Y. Wang, S. B. Peh, and D. Zhao, *Alternatives to Cryogenic Distillation: Advanced Porous Materials in Adsorptive Light Olefin/Paraffin Separations*, Jun. 2019.
- [21] L. Xu, M. Rungta, and W. J. Koros, "Matrimid® derived carbon molecular sieve hollow fiber membranes for ethylene/ethane separation", *Journal of Membrane Science*, vol. 380, no. 1-2, pp. 138–147, 2011.
- [22] S. Achinas, V. Achinas, and G. J. W. Euverink, "A Technological Overview of Biogas Production from Biowaste", *Engineering*, vol. 3, no. 3, pp. 299–307, Jun. 2017.
- [23] D. M. Caicedo-Concha, J. J. Sandoval-Cobo, C.-Q. R. Fernando, L. F. Marmolejo-Rebellón, P. Torres-Lozada, and H. Sonia, "The potential of methane production using aged landfill waste in developing countries: A case of study in Colombia", *Cogent Engineering*, vol. 6, no. 1, D. Pham, Ed., Sep. 2019.
- [24] A. Galadima and O. Muraza, *Revisiting the oxidative coupling of methane to ethylene in the golden period of shale gas: A review*, May 2016.
- [25] D. Salerno, H. Arellano-Garcia, and G. Wozny, "Ethylene separation by feed-splitting from light gases", *Energy*, vol. 36, no. 7, pp. 4518–4523, 2011.
- [26] J. E. Bachman, D. A. Reed, M. T. Kapelewski, G. Chachra, D. Jonnavittula, G. Radaelli, and J. R. Long, "Enabling alternative ethylene production through its selective adsorption in the metal-organic framework Mn₂(M-dobdc)", *Energy and Environmental Science*, vol. 11, no. 9, pp. 2423–2431, 2018.
- [27] J. R. Li, R. J. Kuppler, and H. C. Zhou, "Selective gas adsorption and separation in metal-organic frameworks", *Chemical Society Reviews*, vol. 38, no. 5, pp. 1477–1504, 2009.
- [28] J. E. Bachman, Z. P. Smith, T. Li, T. Xu, and J. R. Long, "Enhanced ethylene separation and plasticization resistance in polymer membranes incorporating metal-organic framework nanocrystals", *Nature Materials*, vol. 15, no. 8, pp. 845–849, 2016.
- [29] A. B. Haan and H. Bosch, *Industrial separation processes: fundamentals*. Walter de Gruyter, 2013.
- [30] M. Wang, A. Lawal, P. Stephenson, J. Sidders, and C. Ramshaw, "Post-combustion CO₂ capture with chemical absorption: A state-of-the-art review", *Chemical Engineering Research and Design*, vol. 89, no. 9, pp. 1609–1624, Sep. 2011.
- [31] C. H. Yu, C. H. Huang, and C. S. Tan, *A review of CO₂ capture by absorption and adsorption*, 2012.
- [32] M. Feng, T. Andrews, and E. Flores, "Hydrocarbon Processing", *Mass Spectrometry Handbook*, pp. 707–723, 2012.
- [33] I. M. Bernhardsen and H. K. Knuutila, *A review of potential amine solvents for CO₂ absorption process: Absorption capacity, cyclic capacity and pKa*, 2017.
- [34] R. Sheldon, *Catalytic reactions in ionic liquids*, Dec. 2001.
- [35] N. V. Plechkova and K. R. Seddon, *Applications of ionic liquids in the chemical industry*, Dec. 2008.
- [36] J. L. Anthony, J. L. Anderson, E. J. Maginn, and J. F. Brennecke, "Anion Effects on Gas Solubility in Ionic Liquids", *The Journal of Physical Chemistry B*, vol. 109, no. 13, pp. 6366–6374, 2005.
- [37] E. D. Bates, R. D. Mayton, I. Ntai, and J. H. Davis, "CO₂ capture by a task-specific ionic liquid", *Journal of the American Chemical Society*, vol. 124, no. 6, pp. 926–927, Feb. 2002.
- [38] D. Camper, J. E. Bara, D. L. Gin, and R. D. Noble, "Room-temperature ionic liquid-amine solutions: Tunable solvents for efficient and reversible capture of CO₂", *Industrial and Engineering Chemistry Research*, vol. 47, no. 21, pp. 8496–8498, Nov. 2008.

- [39] Y. Sun, H. Bi, H. Dou, H. Yang, Z. Huang, B. Wang, R. Deng, and L. Zhang, "A Novel Copper(I)-Based Supported Ionic Liquid Membrane with High Permeability for Ethylene/Ethane Separation", *Industrial and Engineering Chemistry Research*, vol. 56, no. 3, pp. 741–749, 2017.
- [40] M. Kostyanaya, S. Bazhenov, I. Borisov, T. Plisko, and V. Vasilevsky, "Surface Modified Polysulfone Hollow Fiber Membranes for Ethane/Ethylene Separation Using Gas-Liquid Membrane Contactors with Ionic Liquid-Based Absorbent", *Fibers*, vol. 7, no. 1, p. 4, Jan. 2019.
- [41] B. Arman, D. Bonaquist, J. Weber, and M. E. Vincett, *Cryogenic air separation process for producing liquid oxygen*. 2001.
- [42] A. Brunetti, F. Scura, G. Barbieri, and E. Drioli, "Membrane technologies for CO₂ separation", *Journal of Membrane Science*, vol. 359, no. 1-2, pp. 115–125, Sep. 2010.
- [43] C. Song, Q. Liu, S. Deng, H. Li, and Y. Kitamura, *Cryogenic-based CO₂ capture technologies: State-of-the-art developments and current challenges*, 2019.
- [44] K. Nagahama, D. Hoshino, M. Hirata, and H. Konishi, "Binary vapor-liquid equilibria of carbon dioxide-light hydrocarbons at low temperature", *JOURNAL OF CHEMICAL ENGINEERING OF JAPAN*, vol. 7, no. 5, pp. 323–328, Nov. 1974.
- [45] S. Stünkel, O. Litzmann, J. U. Repke, and G. Wozny, "Modeling and simulation of a hybrid separation process for the carbon dioxide removal of the oxidative coupling of methane process", *Computer Aided Chemical Engineering*, vol. 26, pp. 117–122, Jan. 2009.
- [46] A. Dutta, C. W. Chit, I. A. Karimi, and S. Farooq, "Ethylene from natural gas via oxidative coupling of methane and cold energy of LNG", in *Computer Aided Chemical Engineering*, vol. 40, 2017, pp. 1855–1860.
- [47] G. Xu, F. Liang, Y. Yang, Y. Hu, K. Zhang, and W. Liu, "An Improved CO₂ Separation and Purification System Based on Cryogenic Separation and Distillation Theory", *Energies*, vol. 7, no. 5, pp. 3484–3502, May 2014.
- [48] K. Maqsood, A. Ali, A. B. Shariff, and S. Ganguly, "Process intensification using mixed sequential and integrated hybrid cryogenic distillation network for purification of high CO₂ natural gas", *Chemical Engineering Research and Design*, vol. 117, pp. 414–438, 2017.
- [49] C. F. Song, Y. Kitamura, S. H. Li, and K. Ogasawara, "Design of a cryogenic CO₂ capture system based on Stirling coolers", *International Journal of Greenhouse Gas Control*, vol. 7, pp. 107–114, 2012.
- [50] C. Song, Q. Liu, N. Ji, S. Deng, J. Zhao, and Y. Kitamura, "Advanced cryogenic CO₂ capture process based on Stirling coolers by heat integration", *Applied Thermal Engineering*, vol. 114, pp. 887–895, 2017.
- [51] M. J. Tuinier, M. van Sint Annaland, G. J. Kramer, and J. A. Kuipers, "Cryogenic CO₂ capture using dynamically operated packed beds", *Chemical Engineering Science*, vol. 65, no. 1, pp. 114–119, 2010.
- [52] M. J. Tuinier, H. P. Hamers, and M. Van Sint Annaland, "Techno-economic evaluation of cryogenic CO₂ capture-A comparison with absorption and membrane technology", *International Journal of Greenhouse Gas Control*, vol. 5, no. 6, pp. 1559–1565, 2011.
- [53] P. S. Northrop and J. A. Valencia, "The CFZ™ process: A cryogenic method for handling high-CO₂ and H₂S gas reserves and facilitating geosequestration of CO₂ and acid gases", in *Energy Procedia*, vol. 1, Elsevier, Feb. 2009, pp. 171–177.
- [54] M. E. Parker, S. Northrop, J. A. Valencia, R. E. Foglesong, and W. T. Duncan, "CO₂ management at ExxonMobil's LaBarge field, Wyoming, USA", in *Energy Procedia*, vol. 4, Elsevier Ltd, Jan. 2011, pp. 5455–5470.
- [55] W. A. Potts and E. R. Thomas, *Method for separating a multi-component feed stream using distillation and controlled freezing zone*, 1992.
- [56] X. Pan, D. Clodic, and J. Toubassy, "CO₂ capture by antisublimation process and its technical economic analysis", *Greenhouse Gases: Science and Technology*, vol. 3, no. 1, pp. 8–20, Feb. 2013.

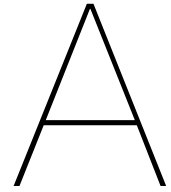
- [57] A. Hart and N. Gnanendran, "Cryogenic CO₂ capture in natural gas", in *Energy Procedia*, vol. 1, Elsevier, Feb. 2009, pp. 697–706.
- [58] D. M. Ruthven, A. Shamsuzzaman, and K. S. Kneabel, *Pressure Swing Adsorption*. Wiley-VCH, 1994.
- [59] H. Patel, "Fixed-bed column adsorption study: a comprehensive review", *Applied Water Science*, vol. 9, no. 3, p. 3, 2019.
- [60] J. C. Abanades, B. Arias, A. Lyngfelt, T. Mattisson, D. E. Wiley, H. Li, M. T. Ho, E. Mangano, and S. Brandani, "Emerging CO₂ capture systems", *International Journal of Greenhouse Gas Control*, vol. 40, pp. 126–166, 2015.
- [61] L. García, Y. A. Poveda, G. Rodríguez, E. Esche, H. R. Godini, G. Wozny, J. U. Repke, and Á. Orjuela, "Adsorption separation of oxidative coupling of methane effluent gases. Mini-plant scale experiments and modeling", *Journal of Natural Gas Science and Engineering*, vol. 61, pp. 106–118, Jan. 2019.
- [62] N. Keller, M.-N. N. Ducamp, D. Robert, and V. Keller, *Ethylene removal and fresh product storage: A challenge at the frontiers of chemistry. Toward an approach by photocatalytic oxidation*, 2013.
- [63] G. Bailén, F. Guillén, S. Castillo, M. Serrano, D. Valero, and D. Martínez-Romero, "Use of activated carbon inside modified atmosphere packages to maintain tomato fruit quality during cold storage", *Journal of Agricultural and Food Chemistry*, vol. 54, no. 6, pp. 2229–2235, 2006.
- [64] D. D. Do, S. Junpirom, and H. D. Do, "A new adsorption-desorption model for water adsorption in activated carbon", *Carbon*, vol. 47, no. 6, pp. 1466–1473, May 2009.
- [65] B. Tummers, *Data Thief III*, 2006.
- [66] P. Ye, Z. Fang, B. Su, H. Xing, Y. Yang, Y. Su, and Q. Ren, "Adsorption of propylene and ethylene on 15 activated carbons", *Journal of Chemical and Engineering Data*, vol. 55, no. 12, pp. 5669–5672, Dec. 2010.
- [67] I. v. Zandvoort, E. J. Ras, R. de Graaf, and R. Krishna, "Using transient breakthrough experiments for screening of adsorbents for separation of C₂H₄/CO₂ mixtures", *Separation and Purification Technology*, vol. 241, 2020.
- [68] K. S. Hwang and W. K. Lee, "The Adsorption and Desorption Breakthrough Behavior of Carbon Monoxide and Carbon Dioxide on Activated Carbon. Effect of Total Pressure and Pressure-Dependent Mass Transfer Coefficients", *Separation Science and Technology*, vol. 29, no. 14, pp. 1857–1891, 1994.
- [69] R. Reich, W. T. Ziegler, and K. A. Rogers, *Erratum: Adsorption of methane, ethane, and ethylene gases and their binary and ternary mixtures and carbon dioxide on activated carbon at 212-301 K and pressures to 35 atmospheres (Industrial & Engineering Chemistry Process Design and Development (1980))*, 1981.
- [70] B. U. Choi, D. K. Choi, Y. W. Lee, B. K. Lee, and S. H. Kim, "Adsorption equilibria of methane, ethane, ethylene, nitrogen, and hydrogen onto activated carbon", *Journal of Chemical and Engineering Data*, vol. 48, no. 3, pp. 603–607, 2003.
- [71] C. A. Grande, F. V. Lopes, A. M. Ribeiro, J. M. Loureiro, and A. E. Rodrigues, "Adsorption of off-gases from steam methane reforming (H₂, CO₂, CH₄, CO and N₂) on activated carbon", *Separation Science and Technology*, vol. 43, no. 6, pp. 1338–1364, 2008.
- [72] A. D. McNaught and A. Wilkinson, *IUPAC. Compendium of Chemical Terminology, 2nd ed. (the "Gold Book")*. 1997.
- [73] B. R. Barnett, M. I. Gonzalez, and J. R. Long, *Recent Progress Towards Light Hydrocarbon Separations Using Metal–Organic Frameworks*, 2019.
- [74] J. Zhou, Y. Zhang, X. Guo, A. Zhang, and X. Fei, "Removal of C₂H₄ from a CO₂ stream by using AgNO₃-modified Y-zeolites", *Industrial and Engineering Chemistry Research*, vol. 45, no. 18, pp. 6236–6242, 2006.

- [75] G. Radaelli, G. Chachra, and D. Jonnavittula, "Low-Energy, Low-Cost Production of Ethylene by Low-Temperature Oxidative Coupling of Methane", Siluria Technologies, Inc., San Francisco, CA (United States), Tech. Rep., 2017.
- [76] A. F. Ismail, K. Chandra Khulbe, T. Matsuura, A. F. Ismail, K. C. Khulbe, and T. Matsuura, "Application of Gas Separation Membranes", in *Gas Separation Membranes*, Springer International Publishing, 2015, pp. 241–287.
- [77] Y. Xu, J. Xu, and C. Yang, "Molecule design of effective C₂H₄/C₂H₆ separation membranes: From 2D nanoporous graphene to 3D AHT zeolite", *Journal of Membrane Science*, vol. 604, p. 118 033, Jun. 2020.
- [78] A. F. Ismail, K. C. Khulbe, and T. Matsuura, *Gas separation membranes: Polymeric and inorganic*. 2015.
- [79] H. Verweij, *Inorganic membranes*, 2. Elsevier Ltd, May 2012, vol. 1, pp. 156–162.
- [80] O. Salinas, X. Ma, E. Litwiller, and I. Pinnau, "High-performance carbon molecular sieve membranes for ethylene/ethane separation derived from an intrinsically microporous polyimide", *Journal of Membrane Science*, vol. 500, pp. 115–123, 2016.
- [81] K. Nymeijer, T. Visser, R. Assen, and M. Wessling, "Olefin-Selective Membranes in Gas-Liquid Membrane Contactors for Olefin/Paraffin Separation", *Industrial and Engineering Chemistry Research*, vol. 43, no. 3, pp. 720–727, 2004.
- [82] J. H. Kim, J. Won, and Y. S. Kang, "Olefin-induced dissolution of silver salts physically dispersed in inert polymers and their application to olefin/paraffin separation", *Journal of Membrane Science*, vol. 241, no. 2, pp. 403–407, 2004.
- [83] C. Liu and N. K. Karns, *Stable facilitated transport membranes for olefin/paraffin separations*, 2019.
- [84] T. Brinkmann, C. Naderipour, J. Pohlmann, J. Wind, T. Wolff, E. Esche, D. Müller, G. Wozny, and B. Hoting, "Pilot scale investigations of the removal of carbon dioxide from hydrocarbon gas streams using poly (ethylene oxide)-poly (butylene terephthalate) PolyActive™ thin film composite membranes", *Journal of Membrane Science*, vol. 489, pp. 237–247, 2015.
- [85] K. Schuldt, J. Pohlmann, S. Shishatskiy, and T. Brinkmann, "Applicability of polyactive™ thin film composite membranes for CO₂ separation from C₂H₄ containing multi-component gas mixtures at pressures up to 30 bar", *Membranes*, vol. 8, no. 2, p. 27, Jun. 2018.
- [86] S. Stünkel, A. Drescher, J. Wind, T. Brinkmann, J.-U. Repke, and G. Wozny, "Carbon dioxide capture for the oxidative coupling of methane process – A case study in mini-plant scale", *Chemical Engineering Research and Design*, vol. 89, no. 8, pp. 1261–1270, Aug. 2011.
- [87] K. Weissermel and H. Arpe, *Industrial Organic Chemistry*, 3rd editio. 1997.
- [88] P. O. Graf and L. Lefferts, "Reactive separation of ethylene from the effluent gas of methane oxidative coupling via alkylation of benzene to ethylbenzene on ZSM-5", *Chemical Engineering Science*, vol. 64, no. 12, pp. 2773–2780, Jun. 2009.
- [89] M. A. Moreira, A. M. Ribeiro, A. F. Ferreira, and A. E. Rodrigues, "Cryogenic pressure temperature swing adsorption process for natural gas upgrade", *Separation and Purification Technology*, vol. 173, pp. 339–356, Feb. 2017.
- [90] M. Héder, "From NASA to EU: The evolution of the TRL scale in Public Sector Innovation", *Innovation Journal*, vol. 22, no. 2, p. 3, 2017.
- [91] K. S. K. Knaebel, "A How "To Guide"for Adsorber Design", *Adsorption Research, Inc. Dublin, Ohio*, p. 23, 2007.
- [92] R. Yang, "Gas Separation by Adsorption Processes", *Chemical Engineering Science*, 1988.
- [93] N. Sue-aok, T. Srihanratana, K. Rangsiwatananon, and S. Hengrasmee, "Study of ethylene adsorption on zeolite NaY modified with group I metal ions", *Applied Surface Science*, vol. 256, no. 12, pp. 3997–4002, 2010.
- [94] A. Julbe and M. Drobek, "Zeolite X: Type", in *Encyclopedia of Membranes*, Springer Berlin Heidelberg, 2014, pp. 1–2.

- [95] I. van Zandvoort, G. P. van Klink, E. de Jong, and J. C. van der Waal, "Selectivity and stability of zeolites [Ca]A and [Ag]A towards ethylene adsorption and desorption from complex gas mixtures", *Microporous and Mesoporous Materials*, vol. 263, pp. 142–149, 2018.
- [96] G. Busca, "Zeolites and Other Structurally Microporous Solids as Acid–Base Materials", in *Heterogeneous Catalytic Materials*, Elsevier, Jan. 2014, pp. 197–249.
- [97] A. L. Myers and J. M. Prausnitz, "Thermodynamics of mixed-gas adsorption", *AIChE Journal*, vol. 11, no. 1, pp. 121–127, Jan. 1965.
- [98] T. E. Osterkamp, H. Murata, T. Akiya, S. Palosaari, J. Korhonen, and N. Araki, "Adsorption isotherms of ethane, ethylene, and carbon dioxide on activated carbon fiber at elevated pressures", vol. 21, no. 3, pp. 315–318, 1988.
- [99] B. U. Choi, D. K. Choi, Y. W. Lee, B. K. Lee, and S. H. Kim, "Adsorption equilibria of methane, ethane, ethylene, nitrogen, and hydrogen onto activated carbon", *Journal of Chemical and Engineering Data*, vol. 48, no. 3, pp. 603–607, 2003.
- [100] F. R. Siperstein and A. L. Myers, "Mixed-Gas Adsorption", vol. 47, no. 5, pp. 1141–1159, 2001.
- [101] G. Calleja, J. Pau, and J. A. Calles, "Pure and Multicomponent Adsorption Equilibrium of Carbon Dioxide, Ethylene, and Propane on ZSM-5 Zeolites with Different Si/Al Ratios", *Journal of Chemical & Engineering Data*, vol. 44, no. 6, pp. 1429–1431, 1999.
- [102] A. M. Plonka, X. Chen, H. Wang, R. Krishna, X. Dong, D. Banerjee, W. R. Woerner, Y. Han, J. Li, and J. B. Parise, "Light Hydrocarbon Adsorption Mechanisms in Two Calcium-Based Microporous Metal Organic Frameworks", *Chemistry of Materials*, vol. 28, no. 6, pp. 1636–1646, 2016.
- [103] K. J. Chen, D. G. Madden, S. Mukherjee, T. Pham, K. A. Forrest, A. Kumar, B. Space, J. Kong, Q. Y. Zhang, and M. J. Zaworotko, "Synergistic sorbent separation for one-step ethylene purification from a four-component mixture", *Science*, vol. 366, no. 6462, pp. 241–246, Oct. 2019.
- [104] H. Hao, Y. Zhao, D. Chen, J. Yu, K. Tan, S. Ma, Y. Chabal, Z. Zhang, J. Dou, Z. Xiao, G. Day, H. Zhou, and T. Lu, "Simultaneous Trapping of C₂H₂ and C₂H₆ from a Ternary Mixture of C₂H₂/C₂H₄/C₂H₆ in a Robust Metal–Organic Framework for the Purification of C₂H₄", *Angewandte Chemie*, vol. 130, no. 49, pp. 16 299–16 303, Dec. 2018.
- [105] Y. Zhang, B. Li, R. Krishna, Z. Wu, D. Ma, Z. Shi, T. Pham, K. Forrest, B. Space, and S. Ma, "Highly selective adsorption of ethylene over ethane in a MOF featuring the combination of open metal site and π -complexation", *Chemical Communications*, vol. 51, no. 13, pp. 2714–2717, Jan. 2015.
- [106] H. Yang, Y. Wang, R. Krishna, X. Jia, Y. Wang, A. N. Hong, C. Dang, H. E. Castillo, X. Bu, and P. Feng, "Pore-Space-Partition-Enabled Exceptional Ethane Uptake and Ethane-Selective Ethane–Ethylene Separation", *Journal of the American Chemical Society*, vol. 142, no. 5, pp. 2222–2227, Feb. 2020.
- [107] B. Li, Y. Zhang, R. Krishna, K. Yao, Y. Han, Z. Wu, D. Ma, Z. Shi, T. Pham, B. Space, J. Liu, P. K. Thallapally, J. Liu, M. Chrzanowski, and S. Ma, "Introduction of π -complexation into porous aromatic framework for highly selective adsorption of ethylene over ethane", *Journal of the American Chemical Society*, vol. 136, no. 24, pp. 8654–8660, Jun. 2014.
- [108] M. A. Al-Ghouti and D. A. Da'ana, *Guidelines for the use and interpretation of adsorption isotherm models: A review*, 2020.
- [109] Z. A. Allothman, "A review: Fundamental aspects of silicate mesoporous materials", *Materials*, vol. 5, no. 12, pp. 2874–2902, 2012.
- [110] P. A. Monson, *Understanding adsorption/desorption hysteresis for fluids in mesoporous materials using simple molecular models and classical density functional theory*, Sep. 2012.
- [111] N. Ayawei, A. N. Ebelegi, and D. Wankasi, *Modelling and Interpretation of Adsorption Isotherms*, 2017.
- [112] Y. Park, D. K. Moon, Y. H. Kim, H. Ahn, and C. H. Lee, "Adsorption isotherms of CO₂, CO, N₂, CH₄, Ar and H₂ on activated carbon and zeolite LiX up to 1.0 MPa", *Adsorption*, vol. 20, no. 4, pp. 631–647, 2014.

- [113] S. Hosseinpour, S. Fatemi, Y. Mortazavi, M. Gholamhoseini, and M. T. Ravanchi, "Performance of Cax Zeolite for separation of C₂H₆, C₂H₄, and CH₄ by adsorption process; capacity, selectivity, and dynamic adsorption measurements", *Separation Science and Technology*, vol. 46, no. 2, pp. 349–355, 2011.
- [114] A. Al-Hajjaj, B. Zamora, A. A. Shah, E. Reguera, D. V. Bavykin, and F. C. Walsh, "On the application of standard isotherms to hydrogen adsorption in microporous materials", *International Journal of Hydrogen Energy*, vol. 36, no. 22, pp. 14 464–14 476, 2011.
- [115] G. Yue, H. Wu, J. Yue, M. Li, C. Zeng, and W. Liang, "Adsorption measurement and dual-site Langmuir model II: Modeling and prediction of carbon dioxide storage in coal seam", *Energy Exploration and Exploitation*, vol. 37, no. 4, pp. 1268–1285, Jul. 2019.
- [116] V. K. Singh and E. A. Kumar, "Measurement of CO₂ adsorption kinetics on activated carbons suitable for gas storage systems", *Greenhouse Gases: Science and Technology*, vol. 7, no. 1, pp. 182–201, Feb. 2017.
- [117] K. V. Kumar, "Comparative analysis of linear and non-linear method of estimating the sorption isotherm parameters for malachite green onto activated carbon", *Journal of Hazardous Materials*, vol. 136, no. 2, pp. 197–202, 2006.
- [118] F. V. Lopes, C. A. Grande, A. M. Ribeiro, J. M. Loureiro, O. Evaggelos, V. Nikolakis, and A. E. Rodrigues, "Adsorption of H₂, CO₂, CH₄, CO, N₂ and H₂O in activated carbon and zeolite for hydrogen production", *Separation Science and Technology*, vol. 44, no. 5, pp. 1045–1073, 2009.
- [119] K. S. Walton and D. S. Sholl, "Predicting multicomponent adsorption: 50 years of the ideal adsorbed solution theory", *AIChE Journal*, vol. 61, no. 9, pp. 2757–2762, 2015.
- [120] I. van Zandvoort, J. K. van der Waal, E. J. Ras, R. de Graaf, and R. Krishna, "Highlighting non-idealities in C₂H₄/CO₂ mixture adsorption in 5A zeolite", *Separation and Purification Technology*, vol. 227, 2019.
- [121] N. F. Cessford, N. A. Seaton, and T. Düren, "Evaluation of ideal adsorbed solution theory as a tool for the design of metal-organic framework materials", *Industrial and Engineering Chemistry Research*, vol. 51, no. 13, pp. 4911–4921, Apr. 2012.
- [122] Q. Cen, M. Fang, Z. Wang, and Z. Luo, "Effect of water on CO₂ adsorption with activated carbon", *ICMREE 2013 - Proceedings: 2013 International Conference on Materials for Renewable Energy and Environment*, vol. 3, pp. 885–888, 2013.
- [123] M. I. Stewart, "Dehydration", in *Surface Production Operations*, 3rd editio, Elsevier, Jan. 2014, pp. 279–373.
- [124] O. F. Baquero, "Design of an Activaed Carbon Columns plant for Studying Micro-Pollutants Removal", *Engineering and Technology*, pp. 110–130, 2000.
- [125] A. Gabelman, "Adsorption basics: Part 1", *Chemical Engineering Progress*, vol. 113, no. 8, pp. 1–6, 2017.
- [126] O. Levenspiel, "Flow Through Packed Beds", in *Engineering Flow and Heat Exchange*, 3rd editio, 2014, ch. Chapter 6, pp. 133–151.
- [127] G. Towler and R. K. Sinnott, *Chemical Engineering Design - Principles, Practice and Economics of Plant and Process Design (2nd Edition)*. 2013.
- [128] EVISA, *Instrument Database: Varian Inc. - CP-4900 Micro-GC*, 2010.
- [129] L. Janssen and M. Warmoeskerke, *Transport Phenomena Data Companion*, 3rd editio. 2006, p. 91.
- [130] R. Verma, H. N. Nagendra, S. Kasthuriengan, N. C. Shivaprakash, and U. Behera, "Thermal conductivity studies on activated carbon based cryopanel", *IOP Conference Series: Materials Science and Engineering*, vol. 502, no. 1, 2019.
- [131] I. B. L. Ltd., *AISI 310 Stainless Steel vs. AISI 316 Stainless Steel - Material Properties Database*, 2020.

- [132] J. Blumm, A. Lindemann, B. Niedrig, and R. Campbell, "Measurement of selected thermophysical properties of the NPL certified reference material stainless steel 310", in *International Journal of Thermophysics*, vol. 28, 2007, pp. 674–682.
- [133] S. C. Chapra and R. P. Canale, *Numerical methods for engineers, second edition*, Second Edi. 2006.
- [134] D. Garcia, *Simpson's rule for numerical integration*, 2020.
- [135] N. Al-Janabi, R. Vakili, P. Kalumpasut, P. Gorgojo, F. R. Siperstein, X. Fan, and P. McCloskey, "Velocity variation effect in fixed bed columns: A case study of CO₂ capture using porous solid adsorbents", *AIChE Journal*, vol. 64, no. 6, pp. 2189–2197, 2018.
- [136] F. Dekking and C. Kraaikamp, *A Modern Introduction to Probability and Statistics*, 1st. Springer London, 2005.
- [137] B. P. Bering and V. V. Serpinskii, "Simultaneous Adsorption of Ethylene and Propylene on Active Carbon", *Doklady Akad. Nauk S. SSR*, vol. 85, no. 1065-8, 1952.
- [138] R. Krishna, "Screening metal-organic frameworks for mixture separations in fixed-bed adsorbents using a combined selectivity/capacity metric", *RSC Advances*, vol. 7, no. 57, pp. 35 724–35 737, 2017.
- [139] B. Babu and S. Gupta, "Modeling And Simulation Of Fixed Bed Adsorption Column: Effect Of Velocity Variation", *i-manager's Journal on Future Engineering and Technology*, vol. 1, no. 1, pp. 60–66, 2005.
- [140] J. D. Seader, W. D. Seider, D. R. Lewin, L. Bouille, and A. Rycroft, *Separation Process Principles, 3rd Edition*. 2006.
- [141] P. N. Dwivedi and S. N. Upadhyay, "Particle-Fluid Mass Transfer in Fixed and Fluidized Beds", *Industrial and Engineering Chemistry Process Design and Development*, vol. 16, no. 2, pp. 157–165, 1977.
- [142] F. J. Gutiérrez Ortiz, M. Barragán Rodríguez, and R. T. Yang, "Modeling of fixed-bed columns for gas physical adsorption", *Chemical Engineering Journal*, vol. 378, 2019.
- [143] M. E. Kinaci, T. Lichtenegger, and S. Schneiderbauer, "A CFD-DEM model for the simulation of direct reduction of iron-ore in fluidized beds", *Chemical Engineering Science*, vol. 227, no. May, 2020.
- [144] S. M. Walas, *Chemical Process Equipment Selection and Design*. 1990.

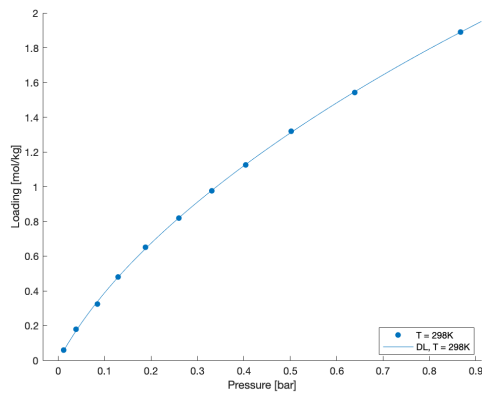


Active Carbon Isotherm Data

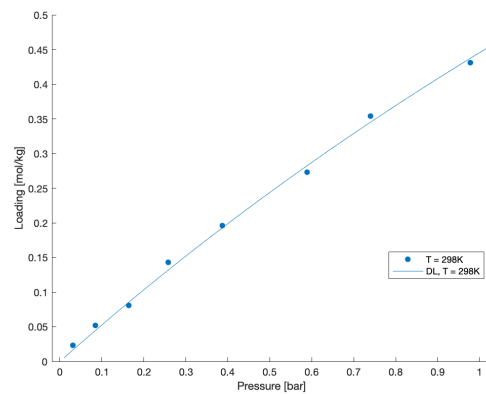
A.1. Hwang et al CO₂/CO

Table A.1: Parameters fits for dualsite Langmuir model for CO₂ and CO on NORIT B4 activated carbon.

Isotherm model	Component	Site A				Site B				nSTD [%]
		q_{sat} [mol/kg]	$B_{A,0}$ [1/bar]	E_a [J/mol]	μ [-]	q_{sat} [mol/kg]	$B_{A,0}$ [1/bar]	E_a [J/mol]	μ [-]	
DS Langmuir	CO ₂	6.5	7.16e-5	22e3	-	0.5	1.59e-3	20e3	-	3
	CO	1.1	5.57e-6	15e3	-	2.5	7.85e-5	20e3	-	17



(a) CO₂ isotherm. Fit by dual site Langmuir model (DL)



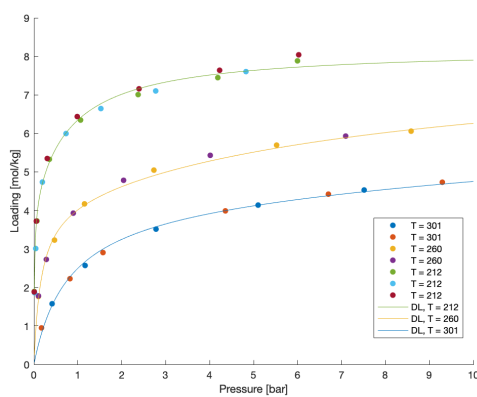
(b) CO isotherm. Fit by dual site Langmuir-Freundlich (SIPS) model (DLF)

Figure A.1: Isotherm data for CO₂ and CO based on data of Hwang et al [68]. Various data sets are represented by different colours.

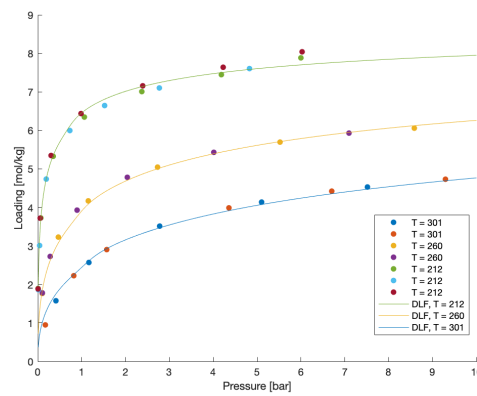
A.2. Reich et al C₂H₄/CO₂

Table A.2: Parameters fits for dualsite Langmuir and Langmuir Freundlich model for C₂H₄ and CO₂ on Pittsburgh Chemical Company activated carbon.

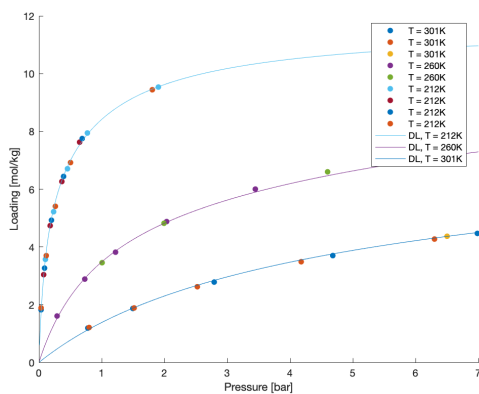
Isotherm model	Component	Site A				Site B				nSTD [%]
		q_{sat} [mol/kg]	$B_{A,0}$ [1/bar]	E_a [J/mol]	μ [-]	q_{sat} [mol/kg]	$B_{A,0}$ [1/bar]	E_a [J/mol]	μ [-]	
DS Langmuir	C ₂ H ₄	4.2	7.44e-5	24e3	-	4.0	3.21e-6	23e3	-	3.3
	CO ₂	5.9	5.63e-5	21e3	-	5.8	7.51e-7	25e3	-	3.2
SIPS	C ₂ H ₄	8.9	4.11e-3	11e3	0.47	0.2	1.48e-4	20e3	1	5.6
	CO ₂	10.8	7.89e-5	18e3	0.76	0.4	2.33e-4	24e3	1	2.1



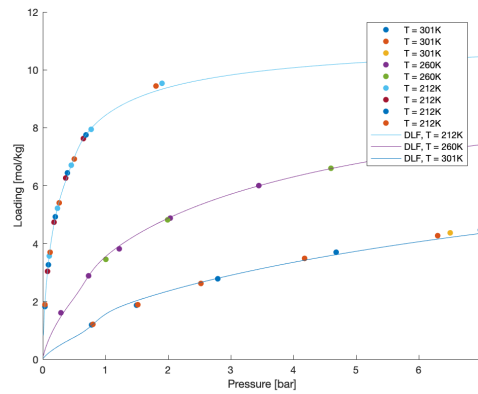
(a) C₂H₄ isotherm. Fit by dual site Langmuir model (DL)



(b) C₂H₄ isotherm. Fit by dual site Langmuir-Freundlich (SIPS) model (DLF)



(c) CO₂ isotherm. Fit by dual site Langmuir model (DL)



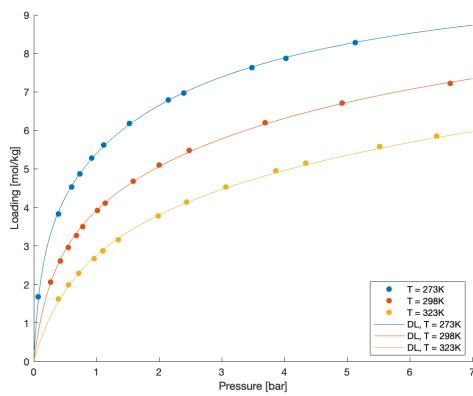
(d) CO₂ isotherm. Fit by dual site Langmuir-Freundlich (SIPS) model (DLF)

Figure A.2: Isotherm data for C₂H₄ and CO₂ based on data of Reich et al [69]. Various data sets are represented by different colours.

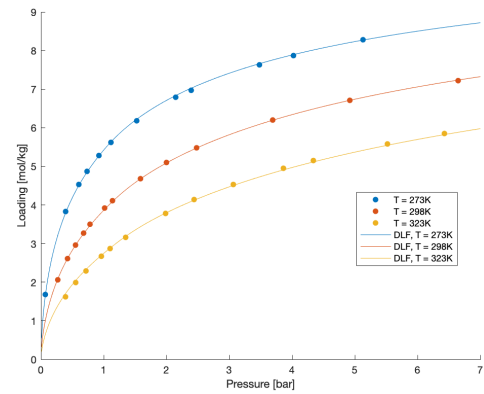
A.3. Osterkamp C₂H₄/CO₂

Table A.3: Parameters fits for dualsite Langmuir and Langmuir Freundlich model for C₂H₄ and CO₂ on KF-1500 activated carbon.

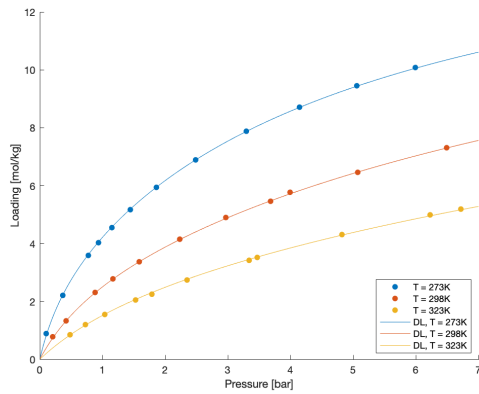
Isotherm model	Component	Site A				Site B				nSTD [%]
		q_{sat} [mol/kg]	$B_{A,0}$ [1/bar]	E_a [J/mol]	μ [-]	q_{sat} [mol/kg]	$B_{A,0}$ [1/bar]	E_a [J/mol]	μ [-]	
DS Langmuir	C ₂ H ₄	4.0	8.78e-5	26e3	-	6.5	1.34e-5	23e3	-	0.9
	CO ₂	2.8	1.5e-4	22e3	-	13.9	8.32e-6	23e3	-	1.8
DS SIPS	C ₂ H ₄	11.6	1.08e-3	15e3	0.62	0.060	9.66e-5	20e3	1	0.8
	CO ₂	18.8	1.28e-4	17e3	0.77	0.05	1.10e-3	20e3	1	0.9



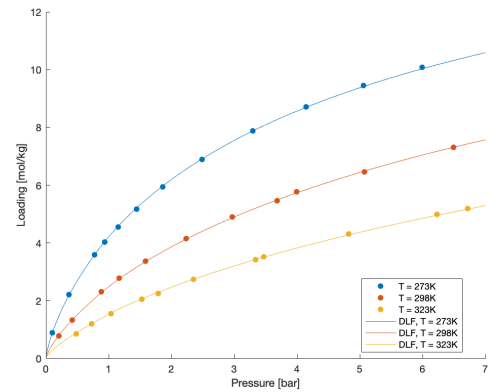
(a) C₂H₄ isotherm. Fit by dual site Langmuir model (DL)



(b) C₂H₄ isotherm. Fit by dual site Langmuir-Freundlich (SIPS) model (DLF)



(c) CO₂ isotherm. Fit by dual site Langmuir model (DL)



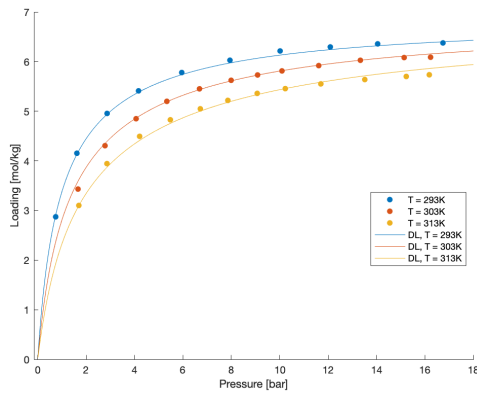
(d) CO₂ isotherm. Fit by dual site Langmuir-Freundlich (SIPS) model (DLF)

Figure A.3: Isotherm data for C₂H₄ and CO₂ based on data of Osterkamp et al [98]. Various data sets are represented by different colours.

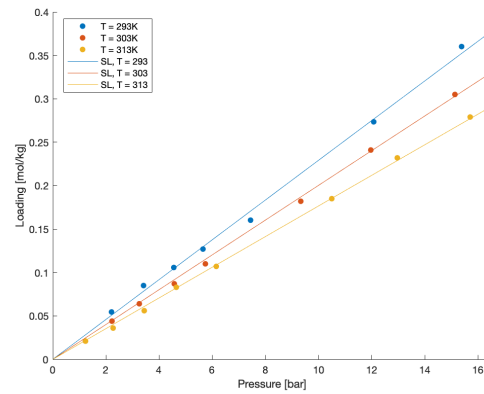
A.4. Choi et al C₂H₄/H₂

Table A.4: Parameters fits for single and dualsite Langmuir model for C₂H₄ and H₂ on Calgon Company activated carbon.

Isotherm model	Component	Site A				Site B				nSTD [%]
		q_{sat} [mol/kg]	$B_{A,0}$ [1/bar]	E_a [J/mol]	μ [-]	q_{sat} [mol/kg]	$B_{A,0}$ [1/bar]	E_a [J/mol]	μ [-]	
DS Langmuir	C ₂ H ₄	2.1	2.06e-8	41e3	-	4.7	1.37e-4	22e3	-	0.2
SS Langmuir	H ₂	111.5	3.5e-6	10e3	-					9.9 (meh)



(a) C₂H₄ isotherm. Fit by dual site Langmuir model (DL)



(b) CO isotherm. Fit by single site Langmuir-Freundlich (SIPS) model (SLF)

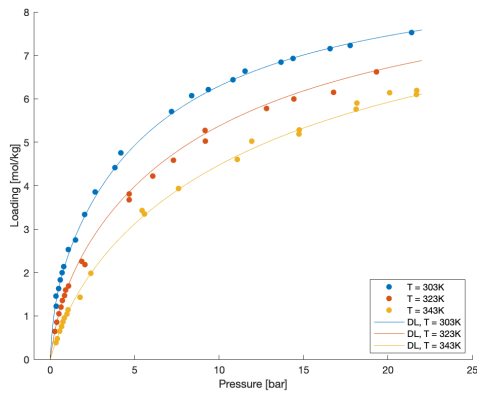
Figure A.4: Isotherm data for CO₂ and CO based on data of Choi et al [99]. Various data sets are represented by different colours.

A.5. Grande et al CO₂/CO/H₂

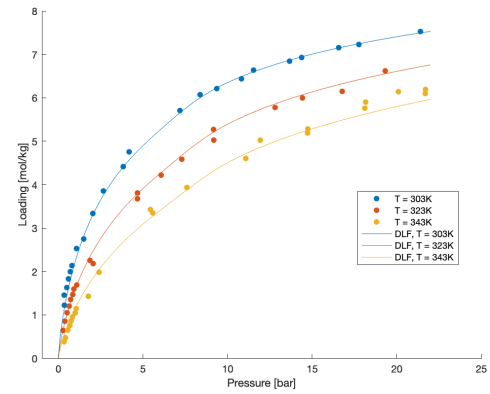
Table A.5: Parameters fits for dualsite Langmuir and Langmuir-Freundlich model for CO₂, CO and H₂ on *commercially* activated carbon.

Isotherm model	Component	Site A				Site B				nSTD [%]
		q_{sat} [mol/kg]	$B_{A,0}$ [1/bar]	E_a [J/mol]	μ [-]	q_{sat} [mol/kg]	$B_{A,0}$ [1/bar]	E_a [J/mol]	μ [-]	
DS Langmuir	CO ₂	7.8	1.14e-4	18e3	-	1.5	7.3e-8	45e3	-	1.3
	CO	2.0	4.34e-7	21e3	-	4.0	7.14e-5	21e3	-	4.7
	H ₂ ⁱ	5.5	1.6e-3	2.9e3	-					31
SIPS	CO ₂	9.4	3.38e-4	17e3	0.77	0.28	5.16e-11	19e3	1	7.7
	CO	2.7	5.06e-5	23e3	1.01	2.8	8.19e-7	20e3	1	1.0
	H ₂ ⁱ	1.6	3.1e-3	3.7e3	1.18					4.8

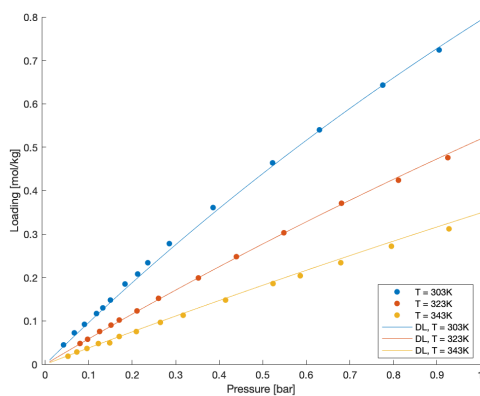
ⁱ Parameter estimation of H₂ data was unreliable, since isotherm data was extracted from graphical data.



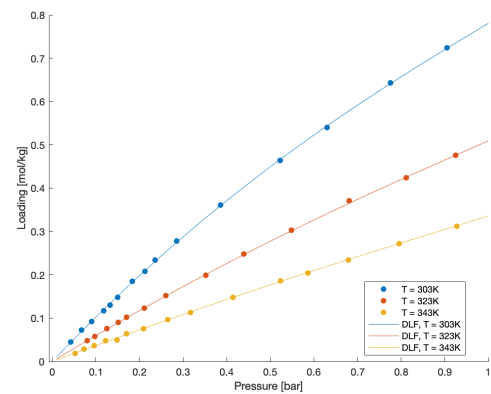
(a) CO₂ isotherm. Fit by dual site Langmuir model (DL)



(b) CO₂ isotherm. Fit by dual site Langmuir-Freundlich (SIPS) model (DLF)



(c) CO isotherm. Fit by dual site Langmuir model (DL)



(d) CO isotherm. Fit by dual site Langmuir-Freundlich (SIPS) model (DLF)

Figure A.5: Continued on the next page

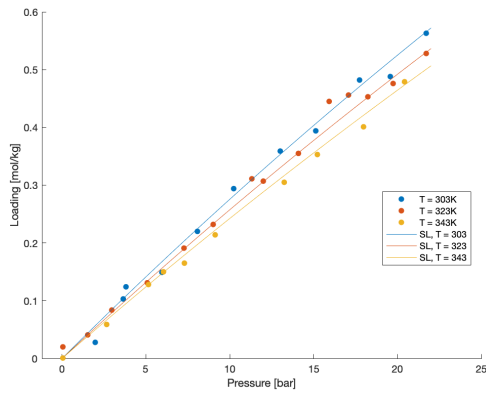
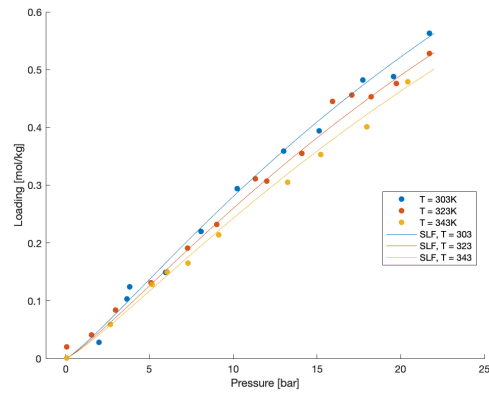
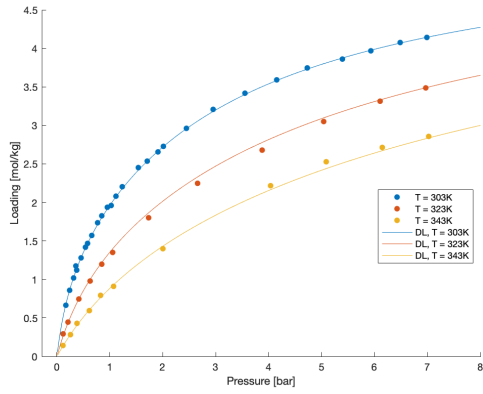
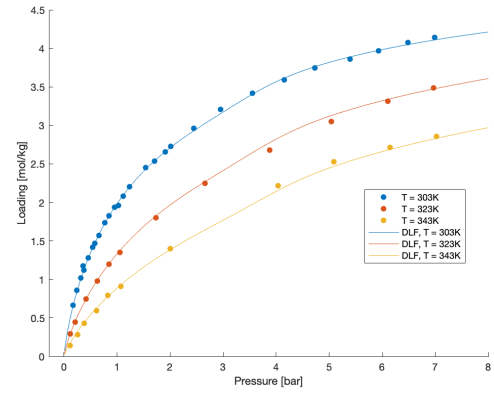
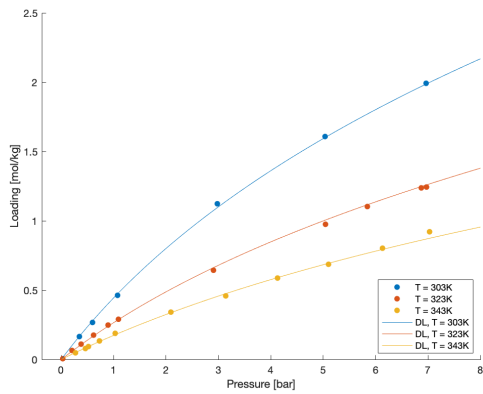
(e) H₂ isotherm. Fit by dual site Langmuir model (DL)(f) H₂ isotherm. Fit by dual site Langmuir-Freundlich (SIPS) model (DLF)

Figure A.5a: Isotherm data for C₂H₄ and CO₂ based on data of Grande et al [71]. Various data sets are represented by different colours.

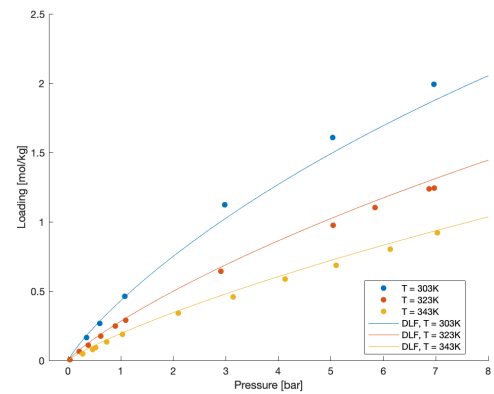
A.6. Lopes et al CO₂/CO/H₂

Table A.6: Parameters fits for dualsite Langmuir and Langmuir-Freundlich model for CO₂, CO and H₂ on *commercially* activated carbon.

Isotherm model	Component	Site A				Site B				nSTD [%]
		q_{sat} [mol/kg]	$B_{A,0}$ [1/bar]	E_a [J/mol]	μ [-]	q_{sat} [mol/kg]	$B_{A,0}$ [1/bar]	E_a [J/mol]	μ [-]	
DS Langmuir	CO ₂	4.5	2.92e-5	23e3	-	1.1	1.03e-6	38e3	-	2.3
	CO	7.0	2.15e-8	35e3	-	1.6	3.13e-4	16e3	-	8.8
	H ₂	0.62	9.29e-5	14e3	-	0.97	9.01e-5	14e3	-	21
DS SIPS	CO ₂	5.2	4.91e-5	24e3	0.82	0.22	2.07e-8	19e3	1	5.4
	CO	8.6	4.32e-5	18e3	0.86	2.74e-4	3.2e-4	20e3	1	69
SS SIPS	H ₂	14.5	9.45e-6	14e3	1.00					39

(a) CO₂ isotherm. Fit by dual site Langmuir model (DL)(b) CO₂ isotherm. Fit by dual site Langmuir-Freundlich (SIPS) model (DLF)

(c) CO isotherm. Fit by dual site Langmuir model (DL)



(d) CO isotherm. Fit by dual site Langmuir-Freundlich (SIPS) model (DLF)

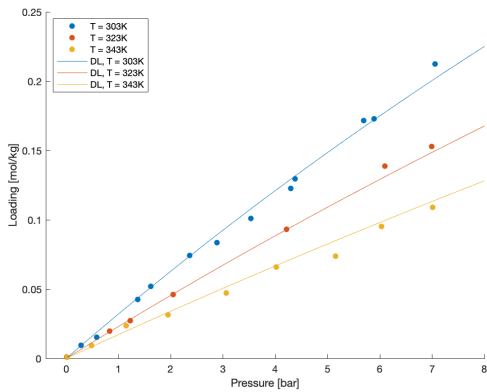
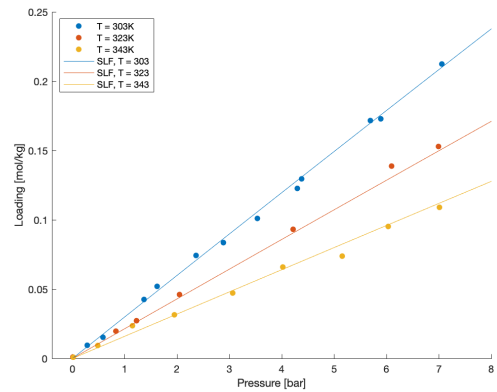
(e) H₂ isotherm. Fit by dual site Langmuir model (DL)(f) H₂ isotherm. Fit by single site Langmuir-Freundlich (SIPS) model (SLF)

Figure A.6: Isotherm data for CO₂, CO and H₂ based on data of Lopes et al [118]. Various data sets are represented by different colours.

A.7. Park et al CO₂/CO/N₂/H₂

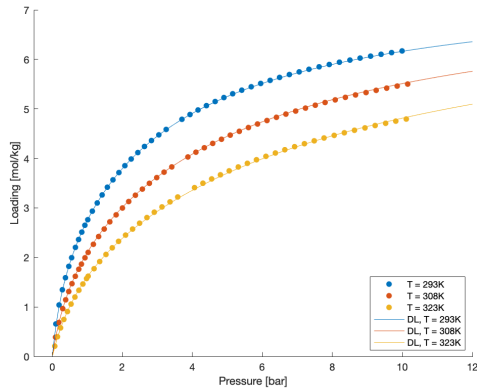
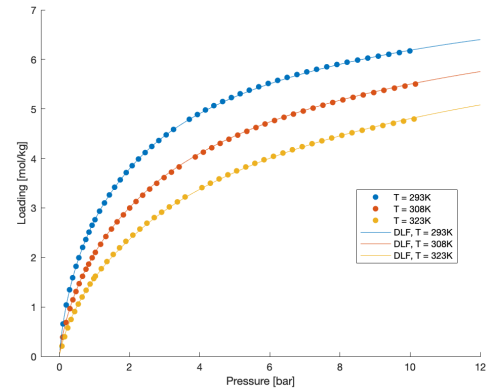
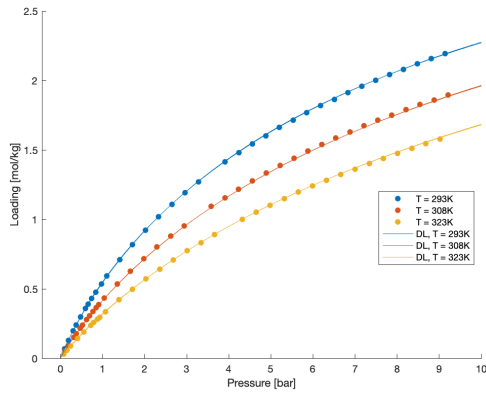
Table A.7: Parameters fits for dualsite Langmuir and single- and dualsite Langmuir-Freundlich model for CO₂, CO, N₂ and H₂ on Kuraray Chemical Company activated carbon.

Isotherm model	Component	Site A				Site B				nSTD [%]
		q_{sat} [mol/kg]	$B_{A,0}$ [1/bar]	E_a [J/mol]	μ [-]	q_{sat} [mol/kg]	$B_{A,0}$ [1/bar]	E_a [J/mol]	μ [-]	
DS Langmuir	CO ₂	5.9	8.17e-6	26e3	-	1.72	1.56e-4	24e3	-	2.5
	CO	3.6	1.41e-4	16e3	-	0.41	1.63e-4	21e3	-	1.4
	N ₂	3.7	1.27e-4	15e3	-	0.65	2.56e-4	18e3	-	0.4
	H ₂	0.54	1.75e-4	14e3	-	2.3	2.74e-5	15e3	-	18.4
DS SIPS	CO ₂	8.3	1.6e-4	19e3	0.75	4.10e-3	3.84e-7	20e3	1	3.5
	CO	4.0	2.71e-4	15e3	0.92	3.6e-3	0.59	18e3	1	4.4
	N ₂	4.1	2.83e-4	15e3	0.92	7.54e-4	0.71	18e3	1	8.1
SS SIPS	H ₂	18.8	1.78e-5	13e3	0.88					7.9

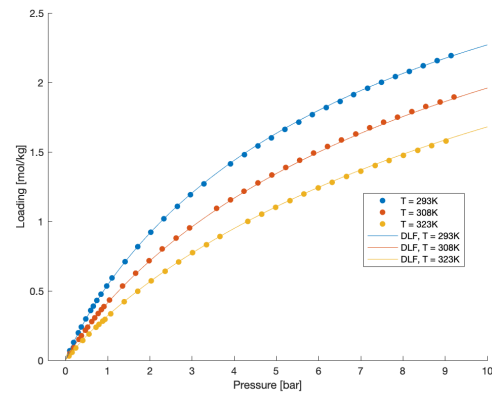
A.8. Al-Janabi et al CO₂/N₂

Table A.8: Parameters fits for dualsite Langmuir model for CO₂ and N₂. Used for the validation of the numerical model [135].

Isotherm model	Component	Site A				Site B				nSTD [%]
		q_{sat} [mol/kg]	$B_{A,0}$ [1/bar]	E_a [J/mol]	μ [-]	q_{sat} [mol/kg]	$B_{A,0}$ [1/bar]	E_a [J/mol]	μ [-]	
DS Langmuir	CO ₂	7.1	1.53e-4	17.8e3	-	0.74	2.1e-3	21.6e3	-	1.61
	N ₂	4.69	6.79e-5	15.4e3	-	0.56	6.97e-4	17.7e3	-	0.62

(a) CO₂ isotherm. Fit by dual site Langmuir model (DL)(b) CO₂ isotherm. Fit by dual site Langmuir-Freundlich (SIPS) model (DLF)

(c) CO isotherm. Fit by dual site Langmuir model (DL)



(d) CO isotherm. Fit by dual site Langmuir-Freundlich (SIPS) model (DLF)

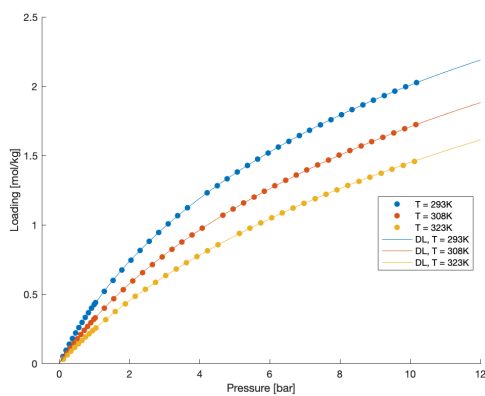
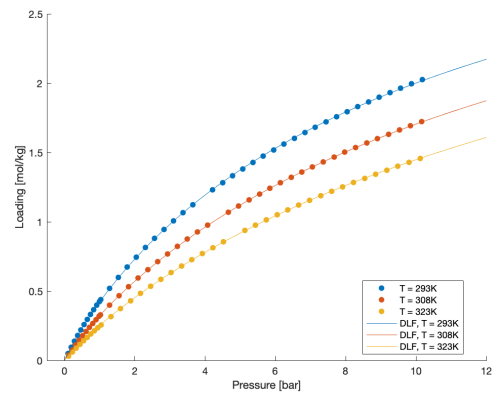
(e) N₂ isotherm. Fit by dual site Langmuir model (DL)(f) N₂ isotherm. Fit by single site Langmuir-Freundlich (SIPS) model (SLF)

Figure A.7: Continued on the next page

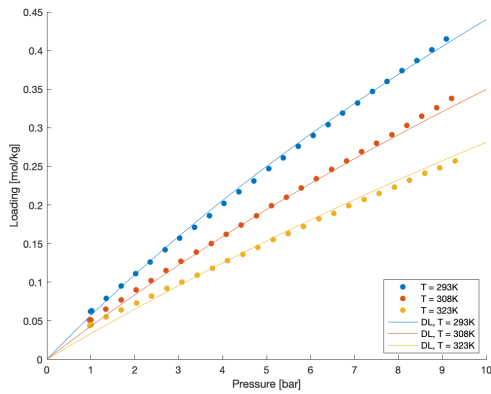
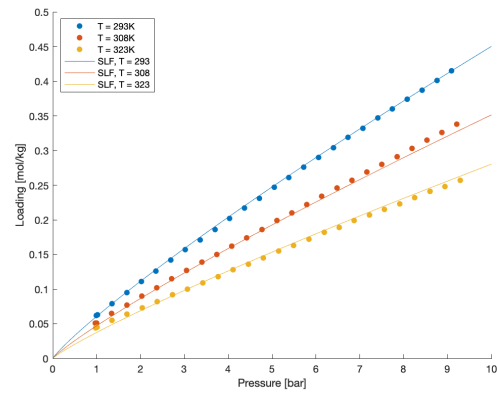
(g) H₂ isotherm. Fit by dual site Langmuir model (DL)(h) H₂ isotherm. Fit by single site Langmuir-Freundlich (SIPS) model (SLF)

Figure A.7a: Isotherm data for CO₂, CO, N₂ and H₂ based on data of Park et al [112]. Various data sets are represented by different colours.

B

System error analysis of microGC

After calibration of each component the Varian CP-4900 micro gas chromatograph the system error was evaluated and the standard deviation was determined from this analysis.

B.1. Procedure

A 20 mL syringe was filled with approximately 10 mL N₂ and 10 mL CO₂ gas and left for 3 hours to diffuse into an homogeneous mixture. After homogenisation this syringe was connected to the mGC and not disconnected until the end of the experiment, to prevent any contamination of air. For each run the valve between the syringe and adapter was opened, 1-2 mL gas was pushed into the mGC and the valve was closed again. This was repeated for twelve runs.

B.2. Results

The results are given in [Table B.1](#). From this data the normalised standard deviation per component is calculated using [Equation B.1](#), resulting in: $\sigma_{N_2} = 1.42\%$ and $\sigma_{CO_2} = 1.37\%$. The summed error over the full volume range (nSTD) is found by summing in quadrature, via [Equation B.2](#).

	Run 1	Run 2	Run 3	Run 4	Run 5	Run 6
N ₂	51.19	52.63	51.33	52.13	51.44	50.98
CO ₂	49.93	50.15	50.12	50.88	50.42	49.42
	Run 7	Run 8	Run 9	Run 10	Run 11	Run 12
N ₂	50.22	50.41	51.52	51.41	52.03	50.47
CO ₂	48.89	49.12	50.65	51.01	50.65	49.89

Table B.1: Result of twelve identical measurements of the same gas mixture on the Varian CP-4900 micro-GC

$$\sigma_i = 100 \sqrt{\frac{1}{N-1} \sum_{i=1}^N \left(\frac{y_i - \bar{y}}{y_i} \right)^2} \quad (\text{B.1})$$

$$\text{nSTD} = \sqrt{\sigma_{N_2}^2 + \sigma_{CO_2}^2} \quad (\text{B.2})$$

C

Experimental Set-up

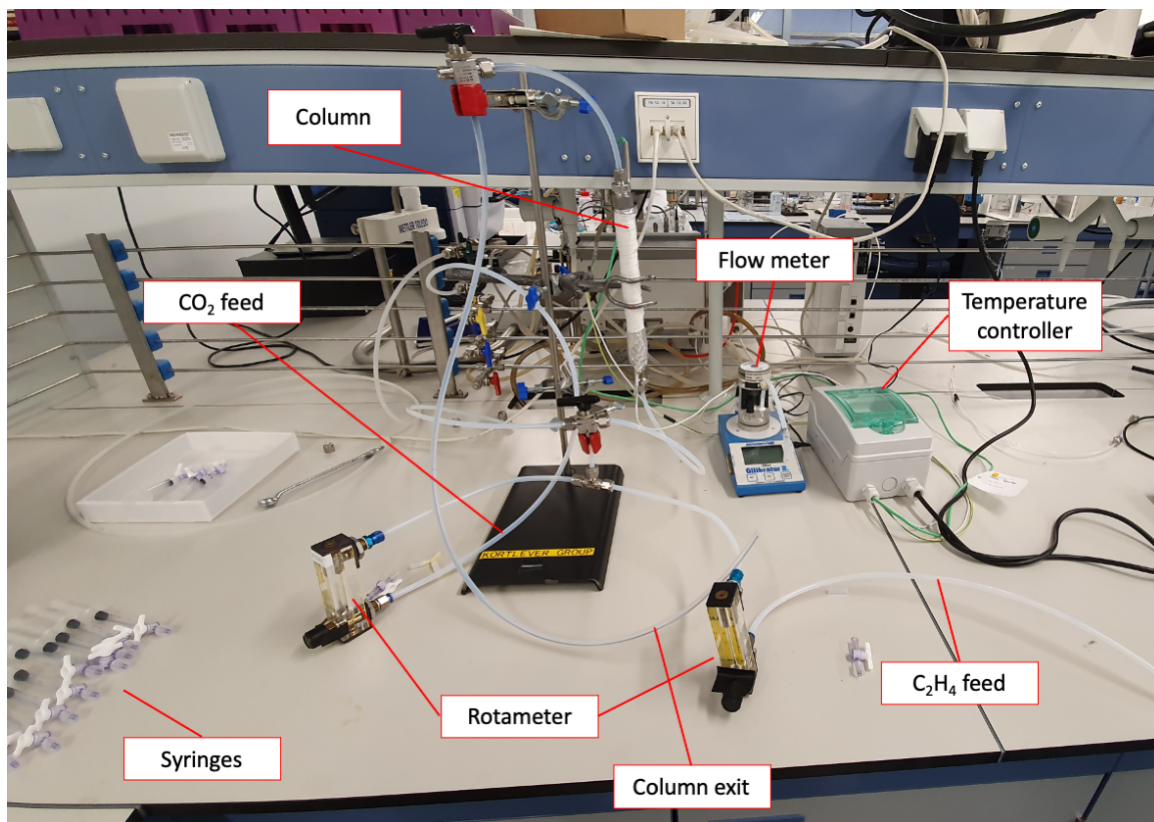


Figure C.1: Overview of the experimental set-up used for the transient breakthrough experiments